BIOPHYSICAL AND FUNCTIONAL CHARACTERIZATION OF WHEAT METALLOTHIONEIN AT MOLECULAR LEVEL

by
FİLİZ YEŞİLIRMAK

Submitted to the Graduate School of Engineering and Natural Sciences
in partial fulfillment of
the requirements for the degree of
Doctor of Philosophy

Sabanci University
Spring 2008

BIOPHYSICAL AND FUNCTIONAL CHARACTERIZATION OF WHEAT METALLOTHIONEIN AT MOLECULAR LEVEL

APPROVED BY:

Prof. Dr. Zehra Sayers Gökhan …….

(Dissertation Supervisor)

Assoc. Prof. Dr. Hikmet Budak …….

(Dissertation Co-Supervisor)

Assist. Prof. Dr. Alpay Taralp …….

Prof. Dr. İsmail Çakmak …….

Prof. Dr. Beki Kan …….

DATE OF APPROVAL: ……

ABSTRACT

Metallothioneins (MTs) are small, cysteine-rich proteins with high binding capacity for metals including Zn, Cu and Cd. MTs exist in a wide range of organisms and are classified in one super-family according to the distribution of cysteine motifs in their sequences. Plant Type 1 MTs are low molecular weight (7-8 kDa) aromatic residue lacking metal-binding proteins. They have two metal-binding domains separated by a conserved specifically long spacer region of about 30-45 amino acids. Recent studies indicate that all members of this family do not have a single unifying function; while some MTs participate in metal homeostasis others play a role in detoxification of heavy metals. Despite the large literature on MT sequences and functional roles, lack of direct biochemical and biophysical data on purified proteins hinders a comprehensive understanding of sequence, structure, metal-binding and function relationships in MTs from different sources.

Due to their aggregation propensity, sensitivity to oxidation, proteolytic cleavage especially in the spacer region and difficulties in quantification, standard methods could not be directly used for purification of plant MTs. A Type 1 MT from *Triticum durum,* dMT, was expressed in *E. coli* cells as a fusion protein with GST (Bilecen et al., 2005). In the present study structure-function relationship of dMT is investigated using the fusion protein GSTdMT as a model system. The procedure developed for GSTdMT purification required strict anaerobic conditions and critical parameters including concentration of Cd and specific reducing agents, as well as choice of buffers was optimized.

The purified GSTdMT was characterized by size exclusion chromatography, SDS- and native-PAGE, UV-vis absorption spectrophotometry, inductively coupled plasma optical emission spectroscopy (ICP-OES), dynamic light scattering (DLS), circular dichroism (CD), Extended X-ray Absorption Fine Structure (EXAFS) and small-angle solution X-ray scattering (SAXS).

Size exclusion chromatography revealed a stable dimeric form of GSTdMT in solution. Purified GSTdMT solutions were monodisperse and homogeneous and thus suitable for structural and functional studies. The Cd binding ability of GSTdMT was initially characterized by UV-vis absorption spectroscopy and through the ICP-OES measurements the Cd^{2+} binding ratio was found to 3.5 Cd^{2+}/protein. This finding was further confirmed by EXAFS measurement which strongly indicated Cd-S coordination with four sulphurs.

SAXS measurements revealed that GSTdMT has an elongated shape with a radius of gyration of 3.57 nm. *ab initio* models resulted in a structure in which two GST molecules form an electron dense region at one end of the dimer and the two dMT molecules extend from this region. dMT structure appears to be independent of GST in the GSTdMT fusion. The combination of SAXS results with biochemical data lead to the proposal of a hairpin like model for dMT structure.

Results show that the metal content and structure of dMT in the fusion protein are preserved, thus biologically relevant structural parameters can be determined using the GSTdMT construct.

In a previous study (Bilecen et al., 2005) the predicted structure for the spacer region had shown similarity with that of a family that includes DNA binding proteins. In this thesis DNA binding possibility of dMT protein was examined through the whole genome PCR-based screening method. It was found that application of this method resulted in several artifacts and in our hands the method could not be used for investigation of DNA binding possibility of any protein.

In part of this work response of *Triticum durum* cv. Balcalı-85 to environmental Cd was investigated. Balcalı-85 was subjected to increasing Cd concentrations (e.g., 0, 2, 5, 10, and 20 μM Cd). As a result, reduction in dry weight matter was observed both in roots and shoot. Also, it was found that Balcalı-85 has high capacity to retain Cd in roots. These studies were carried out as a part of an investigation which will focus on the correlation between *mt-d* gene expression and Cd response.

In addition, southern blot analysis revealed that the *mt-d* gene, having 2 exons and a non-coding intron region, has a single copy in *T. durum* genome.

ÖZET

Metallotioninler (MT'ler), sistin bakımından zengin, düşük molekül ağırlıklı Zn, Cu ve Cd gibi metallere yüksek bağlanma kapasitesi olan proteinlerdir. MT'ler hemen hemen tüm organizmalarda bulunurlar ve gen sekanslarındaki sistin motiflerinin dağılımına göre bir familya içerisinde sınıflandırılırlar. Bitki Tip 1 MT'leri, düşük molekül ağırlıklı (7-8 kDa), aromatik grupları olmayan metal bağlayan proteinlerdir. Yaklaşık 30-45 amino asitten oluşan oldukça uzun evrimsel korunmuş bir köprü bölgesi ile birleştirilmiş iki metal bağlama bölgesine sahiptiler. Son zamanlardaki çalışmalar göstermiştir ki bu familyanın tüm üyeleri bir tip işlevde rol oynamaz. Aksine bazı MT'ler metal dengesini korumada işlev görürken diğerleri ağır metallerin detoksifikasyonunda rol oynarlar. MT sekansları ve fonksiyonel rolleri hakkında çok geniş literatür olmasına rağmen, saflaştırılmış proteinler üzerine doğrudan biyokimyasal ve biyofiziksel verilerin olamaması farklı kaynaklardan gelen MT'lerin sekans, yapı, metal bağlama ve fonksiyon ilişkilerinin kapsamlı bir şekilde ortaya çıkarılmasını engellemektedir.

Oligomer oluşturma eğilimleri, oksitlenme hassasiyetleri, özellikle köprü bölgesinden kırılmaları ve derişim belirlemedeki zorluklar nedeniyle bitki MT'lerinin saflaştırılmasında standart yöntemler doğrudan uygulanamazlar. *Triticum durum'*dan bir Tip 1 MT'ni, dMT, *E. coli* bakterisinde GST ile füzyon proteini şeklinde sentezlettirilmiştir (Bilecen 2005). Bu doktora tezi çalışmasında GSTdMT füzyon proteini bir model sistem olarak kullanılarak dMT'nin yapı ve fonksiyon ilişkisi araştırılmıştır. GSTdMT saflaştırılması için anaerobik ortamda Cd konsantrasyonu, özel indirgeyici ajanlar ve tampon seçimi gibi kiritik parametreler optimize edilerek yeni bir süreç geliştirilmiştir.

Saflaştırılan GSTdMT büyüklük ayırmalı kromofotografi (SEC), SDS ve nativ PAGE, UV-vis absorpsiyon spektrofotometresi, ICP-OES emisyon spektrofotometresi, dinamik ışık saçılması (DLS), sirküler dikroizm (CD), EXAFS ve X-ışınları küçük açı saçılma (SAXS) yöntemleri kullanılarak karakterize edilmiştir.

SEC ile dengeli dimer formunda GSTdMT proteini ayrıştırılmıştır. Saflaştırılan GSTdMT solüsyonları tek tip yapı içermeleri ve homojen olmaları açısından yapısal ve fonksiyonel calışmalar için uygundurlar. GSTdMT'nin Cd bağlayabilme özelliği UV-vis absorpsiyon spektrofotometresi ile belirlenmiş ve ICP-OES ölçümleri yoluyla Cd^{2+} bağlanma oranı 3.5 Cd^{2+}/protein olarak bulunmuştur. Bu bulgu aynı zamanda Cd-S koordinasyonunun dört süllfür ile gerçekleştiğini gösteren EXAFS ölçümü ile doğrulanmıştır.

SAXS ölçümleri GSTdMT nin eylemsizlik yarıçapı 3.57 nm olan uzun ve asimetrik bir şekle sahip olduğunu göstermistir. *ab initio* modelleri bir uçta iki dimer GST molekülünün oluşturduğu bir elektron yoğun bölge ve bu bölgeden uzanan iki dMT molekülünden oluşan bir yapı ile sonuçlanmıştır. dMT yapısının GSTdMT füzyonundaki GST den bağımsız olduğu ortaya çıkmıştır. SAXS sonuçlarının biyokimyasal verilerle birleşimi dMT yapısı için saç firketesi benzeri bir modelin varlığını ortaya çıkarmıştır.

Sonuçlar füzyon protein içerisinde dMT metal içeriğinin ve yapısının korunduğunu göstermiştir. Bundan dolayı GSTdMT biyolojik olarak anlamlı yapısal parametrelerin belirlenmesinde kullanılabilinir.

Bir önceki çalışmada (Bilecen 2005) köprü bölgesi için tahmin edilen yapının DNA'ya bağlanan proteinleri içeren bir familya ile benzerlik gösterdiği bulundu. Bu tezde dMT'nin DNA bağlanma ihtimali "Whole genome PCR" yöntemi ile araştırılmıştır. Bu yöntemin uygulamasında birçok sorunun oluşabileceği bulunmuştur ve her hangi bir proteinin DNA bağlanma ihtimalinin araştırılmasında kullanılamayacağı bulunmuştur.

Bu çalışmanın diğer kısmında of *Triticum durum* cvs. Balcalı-85 bitkisinin çevresel Cd'a olan tepkisi araştırılmıştır. Balcalı-85 artan Cd konsantrasyonlarına tabii tutulmuştur (0, 2, 5, 10, and 20 μM Cd). Sonuç olarak kök ve yeşil aksanda kuru ağırlığın azalması gözlemlenilmiştir. Ayrıca Balcalı-85'in köklerinde çok fazla Cd tutma kapasitesinde olduğu bulunmuştur. Bu çalışma *mt-d* geni ve Cd tepkisi arasındaki bağlantıyı bulma araştırmasının bir parçası olarak yapılmıştır.

Ayrıca, southern blot analizi ile 2 ekson ve 1 kodlamayan introndan oluşan *mt-d* geninin *T. durum* genomunda sadece bir kopya olarak bulunduğu gösterilmiştir.

To my husband with all my heart…

ACKNOWLEDGEMENTS

It is a pleasure to express my gratitude to all who made this thesis possible.

I would like to express my special thanks to my supervisor and my mentor Zehra Sayers for her patience, understanding, support, and guidance throughout of this thesis. She has been the major driving force in my studies, and it has been an invaluable experience being her PhD student and working with her. Without her continual support and guidance, this thesis would not have been possible.

I want to express my appreciation to my co-supervisor, Hikmet Budak for his helpful advice, encouragement, sincere interest and support throughout the course of this study.

I would generously like to thank each member of my committee members of my thesis, Alpay Taralp, İsmail Çakmak and Beki Kan for their critical suggestions and excellent remarks on my thesis.

I am grateful to my friends for their continuous guidance, emotional and academic support. Special thanks to Filiz Çollak, Gizem Dinler Doğanay, Burcu Köktürk, Özge Cebeci, Elif Damla Arısan, Bahar Soğutmaz Özdemir, Gözde Korkmaz, and Gürkan Yardımcı.

I would like to give my special thanks to plant physiology lab members who helped me through my plant physiology experiments. Special thanks to Atilla Yazıcı, Özgür Gökmen, Yusuf Tutuş and Veli Bayır for their friendship and help.

I am also grateful to Sedef Tunca Gedik, Dilek Telci, Fahriye Ertuğrul, Neslihan Ergen, Onur Gökçe, and Alper Küçükural for their friendship and help to this study.

Throughout my life my parents, Şahizer and Türker Dede, have always have been with me. I would like to thank you for all their love, encouragement and support to every step of my life. Thank you for always being there, and for loving me regardless.

Last, but certainly not least, I would like to thank my husband, Sebahattin Yeşilirmak, for his encouragement, endless love, patience and for his believe in me all this time. By using words, it is impossible to express my love and appreciation to him.

Filiz Yeşilırmak
March 2008, İstanbul

TABLE OF CONTENTS

1. INTRODUCTION..... 1

2. OVERVIEW..... 4

2.1 Metallothioneins (MTs)..... 4

2. 1.1 Classification..... 4

2. 1.2 Mammalian MTs..... 5

2.1.2.1 Structure of Mammalian MTs..... 8

2.1.2.2 Function of Mammalian MTs..... 11

2. 1.3. Plant MTs..... 13

2.1.3.1 Classification of Plant MTs..... 13

2.1.3.2 Localization of Plant MTs..... 14

2.1.3.3 Isolation and Metal binding Characteristics of Plant MTs..... 16

2.1.3.4 Structure of Plant MTs..... 16

2.1.3.5 Function of Plant MTs..... 20

3 MATERIALS and METHODS..... 23

3.1 MATERIALS..... 23

3. 1.1 Chemicals..... 23

3. 1.2 Primers..... 23

3. 1.3 Enzymes..... 23

3. 1.4 Cells..…… 24

3. 1.5 Buffers and Solutions..…….... 24

3. 1.6 Culture Media..……..... 24

3.1.6.1 Liquid Medium..……..... 24

3.1.6.2 Solid Medium..…….... 24

3. 1.7 Plant Material..…….... 24

3. 1.8 Equipments..…….... 24

3.2 METHODS..……..... 25

3. 2.1 Nucleic acid Methods..…….... 25

3.2.1.1 Genomic DNA Isolation from Plant..……..... 25

3.2.1.2 Total RNA Isolation from Plants..……. 25

3.2.1.3 Separation of DNA by Agarose gel..……. 26

3.2.1.4 Separation of DNA by Polyacrylamide gel..……. 26

3.2.1.5 Determination of Nucleic acid Concentrations …… 26

3.2.1.6 cDNA Synthesis…..……..... 27

3.2.1.7 Preparation of the Radioactively labeled cDNA Probe.....…… 27

3.2.1.8 Southern Blotting..……..... 27

3.2.1.9 Blotting, Hybridization and Detection..……. 27

3.2.1.10 Autoradiography ……..…….. 28

3.2.1.11 Whole Genome PCR…..…… 28

3.2.1.11.1 Preparation of DNA for Whole Genome PCR..…….. 28

3.2.1.11.2 Protein-DNA Interaction..……... 29

3.2.1.11.3 PCR Amplification of Linker-ligated DNA …….. 29

3. 2.2 Protein Analysis. ……..... 30

3.2.2.1 Bacterial cell Growth …… 30

3.2.2.2 Expression of GSTdMT ……... 30

3.2.2.3 Purification of GSTdMT Recombinant Protein ……..... 30

3.2.2.4 Purification of dMT Protein …… 31

3.2.2.5 SDS Polyacrylamide gel Electrophoresis (PAGE) ……... 31

3.2.2.6 Native-PAGE ……... 32

3.2.2.7 Coomassie Blue Staining ..……... 32

3.2.2.8 Silver Staining ……... 32

3.2.2.9 Western Blotting ..……...……... 32

3.2.2.10 Determination of Protein Concentration ……... 33

3.2.2.11 Dynamic Light Scattering …… 33

3.2.2.12 Small angle X-ray Scattering (SAXS) …….. 34

3.2.2.13 Extended X-ray Absorption Fine Structure (EXAFS)…… 36

3.2.2.14 Inductively Coupled Plasma Optical Emission Spectroscopy (ICP-OES) …… 37

3. 2.3 Plant Methods ..…… 37

3.2.3.1 Plant Material ……..... 37

3.2.3.2 Plant Growth Conditions and Cadmium Treatments..……..... 37

3.2.3.3 Cadmium Concentration and Content …… 38

4. RESULTS ……..... 39

4.1 Purification of Homogeneous GSTdMT Protein …….. 39

4. 1.1 Calibration of the Column …… 39

4. 1.2 Optimization of GSTdMT Purification …… 41

4.1.2.1 Determination of the Storage Conditions for GSTdMT …….. 62

4.1.2.2 Reversibility of Oligomerization of GSTdMT ……. 67

4. 1.3 Determination of Cd Binding Ratio for GSTdMT…….. 70

4. 1.4 UV-Vis Spectrophotometric Characterization of GSTdMT...…….... 70

4. 1.5 Secondary Structure Analysis of GSTdMT ..…… 72

4.2 Purification of dMT …….. 73

4. 2.1 Calibration of Column …… 73

4. 2.2 Size Exclusion Chromatography of dMT…….. 75

4.3 Structural Studies …… 80

4. 3.1 Structural Analysis of GSTdMT Using SAXS..…… 80

4. 3.2 EXAFS Analysis on GSTdMT ……. 88

4.4 Functional Studies ……. 90

4. 4.1 cDNA Synthesis ……... 90

4. 4.2 Southern Blotting of *mt-d* gene……..... 91

4. 4.3 Plant Growth and Cadmium Treatments of Balcalı-85 93

4. 4.4 Investigation of DNA binding of GSTdMT..…… 95

5 DISCUSSION ……... 109

5.1 Purification of Homogeneous GSTdMT and dMT Protein …….. 109

5.2 Biophysical Characterization of GSTdMT …… 113

5.3 Structural Analysis of GSTdMT and dMT…… 114

5.4 Functional Studies ……. 117

6 CONCLUSION ……... 119

7 REFERENCES ……..... 121

APPENDIX A …… 131

APPENDIX B ……. 133

APPENDIX C ……. 135

LIST OF FIGURES

Figure 2.1: Schematic representation of Cd-thiolate clusters in mammalian MT based on NMR and X-ray spectroscopy data..……..... 8

Figure 2.2: Crystal structure of Cd_5, Zn_2-MT-2 from rat liver and NMR structure of sea urchin of Cd_7-MTA. ……..... 10

Figure 2.3: Comparison of Cu_8-MT crystal structure (cyan tube) with Ag_7-MT NMR model (green tube) (A) and Cu_7-MT NMR model (red tube) (B)…….

Figure 2.4: Schematic representation of MT redox cycle…… 12

Figure 2.5: An assumed hairpin structure model of metallothionein protein associated with metal ions…… 17

Figure 2.6: The proposed hypothetical structures of metal-thiolate clusters in MT3…….. 19

Figure 3.1: Difference between the intensity, volume and number size distribution differences of two sizes of particles; 5nm and 50nm……... 34

Figure 4.1: Elution profile of calibration proteins from the size exclusion column HiLoad® 26/60 Superdex 75……... 40

Figure 4.2: Calibration curve of HiLoad® 26/60 Superdex 75 size exclusion column…….. 40

Figure 4.3: Experimental strategy of the purification of GSTdMT…..... 42

Figure 4.4: Elution profile of the GSTdMT from GST affinity chromatography using the PBS buffer system with 0.2 mM $CdCl_2$…… 43

Figure 4.5: Size exclusion chromatography elution profile of AI using the PBS buffer system with 0.2 mM $CdCl_2$……... 43

Figure 4.6: Size exclusion chromatography elution profile of AII using the PBS buffer system with 0.2 mM $CdCl_2$……. 44

Figure 4.7: SDS-PAGE analysis of GSTdMT purification using the PBS buffer system with 0.2 mM $CdCl_2$…….. 44

Figure 4.8: Native-PAGE analysis of fractions from GSTdMT purification using the PBS buffer system with 0.2 mM $CdCl_2$……. 45

Figure 4.9: Intensity distribution of scattered light from top peak fraction of GSTdMT fusion protein purified using the PBS buffer system…….. 45

Figure 4.10: Elution profile of the GST from GST affinity column with the PBS buffer system…… 46

Figure 4.11: Native-PAGE analysis of GST purified from GST affinity column using the PBS buffer system…… 46

Figure 4.12: Size exclusion chromatography elution profile AI using the PBS buffer system with 0.1 mM $CdCl_2$……... 47

Figure 4.13: Size exclusion chromatography elution profile of AII from GST affinity column using the PBS buffer system with 0.1 mM $CdCl_2$…….. 47

Figure 4.14: SDS-PAGE analysis of purified GSTdMT using the PBS buffer system with 0.1 mM $CdCl_2$……..... 48

Figure 4.15: Native-PAGE analysis of purified GSTdMT using the PBS buffer system with 0.1 mM $CdCl_2$…….. 48

Figure 4.16: Size exclusion chromatography elution profile of AII using PBS as buffer system with 0.1 mM $CdCl_2$ and 1mM DTT…….. 49

Figure 4.17: Native-PAGE analysis of purified GSTdMT using the PBS buffer system with 0.1 mM $CdCl_2$ and 1mM DTT……. 49

Figure 4.18: Elution profile of the GST from GST affinity column using Buffer A with 1mM DTT…… 50

Figure 4.19: Size exclusion chromatography elution profile of GST affinity column using Buffer A with 1mM DTT…….. 51

Figure 4.20: SDS-PAGE analysis of GST purified using Buffer A with 1mM DTT…….. 51

Figure 4.21: Native-PAGE analysis of GST purified using Buffer A with 1mM DTT. Lane 1-5, fractions from pool GII of size exclusion column……. 51

Figure 4.22: Elution profile of the GSTdMT from GST affinity column using Buffer A system with 1mM DTT without $CdCl_2$……. 52

Figure 4.23: Size exclusion chromatography elution profile of pool AI from GST affinity column when using Buffer A with 1mM DTT without $CdCl_2$…… 52

Figure 4.24: SDS-PAGE analysis of purified GSTdMT using Buffer A with 1mM DTT without $CdCl_2$…… 53

Figure 4.25: Size exclusion chromatography elution profiles of GST affinity column using Buffer A with 0.1mM $CdCl_2$ and 0.1mM TCEP……..... 54

Figure 4.26: Native-PAGE analysis of purified fusion GSTdMT using Buffer A with 0.1mM $CdCl_2$ and 0.1mM TCEP…… 54

Figure 4.27: Size exclusion chromatography elution profile of Pool AI using Buffer A with 1 mM DTT and 0.1mM $CdCl_2$ only in lysis……. 55

Figure 4.28: SDS-PAGE analysis of purified GSTdMT using Buffer A with 1 mM DTT and 0.1mM $CdCl_2$ only in lysis…… 55

Figure 4.29: Native-PAGE analysis of purified GSTdMT using Buffer A system with 1 mM DTT and 0.1mM $CdCl_2$ only in lysis……. 56

Figure 4.30: Western blot analysis of GSTdMT using Buffer A with 1 mM DTT and 0.1mM $CdCl_2$ only in lysis…… 56

Figure 4.31: Intensity distribution of the scattered light from a fraction of GSTdMT from peak GII after freezing and thawing……... 57

Figure 4.32: Intensity distribution of the scattered light measurement from a fraction of GSTdMT from peak GI after freezing and thawing…….. 57

Figure 4.33: Elution profile of the GST from GST affinity chromatography using Buffer B with 1 mM DTT…… 58

Figure 4.34: Size exclusion chromatography elution profile for GST of pool AI using HEPES as Buffer B with 1 mM DTT……. 58

Figure 4.35: SDS-PAGE analysis of GST purification using Buffer B with 1 mM DTT……..... 59

Figure 4.36: Native-PAGE analysis of GST purified using Buffer B with 1 mM DTT……..... 59

Figure 4.37: Elution profile of the GSTdMT from GST affinity chromatography using Buffer B with 1 mM DTT and 0.1 mM $CdCl_2$ only in lysis buffer…… 60

Figure 4.38: Size exclusion column elution profile of Pool AI using Buffer B with 1 mM DTT and 0.1mM $CdCl_2$ only in lysis buffer…….. 60

Figure 4.39: SDS-PAGE analysis of fractions from GSTdMT purification using Buffer B with 1 mM DTT and 0.1mM $CdCl_2$ only in lysis buffer …….. 61

Figure 4.40: Native-PAGE analysis of purified GSTdMT using Buffer B with 1 mM DTT and 0.1mM $CdCl_2$ only in lysis buffer……. 61

Figure 4.41: Intensity distribution of scattered light from GSTdMT purified using Buffer B with 1 mM DTT and 0.1mM $CdCl_2$ only in lysis buffer……. 61

Figure 4.42: Electrophoretic analysis of GST fractions purified in Buffer B and stored for three days at different temperatures……..... 63

Figure 4.43: Electrophoretic analysis of GST fractions purified in Buffer B and stored for six days at different temperatures. …….. 63

Figure 4.44: Dynamic light scattering measurement of the GST (lane 2 in Native-PAGE analysis) stored for three days at -20^{o}C. …….. 64

Figure 4.45: Dynamic light scattering measurement of the GST (lane 3 in Native-PAGE analysis) stored for three days at 4^{o}C..……. 64

Figure 4.46: Dynamic light scattering measurement of the GST (lane 2 in Native-PAGE analysis) stored for six days at-20^{o}C..…….. 64

Figure 4.47: Dynamic light scattering measurement of the GST (lane 3 in Native-PAGE analysis) stored for six days at 4^{o}C. ..……... 65

Figure 4.48: Dynamic light scattering measurement of the GST (lane 1 in Native-PAGE analysis) stored for three days at -80^{o}C. ..…… 65

Figure 4.49: Dynamic light scattering measurement of the GST (lane 1 in Native-PAGE analysis) stored for six days at-80^{o}C. ..……

Figure 4.50: Native-PAGE analysis of purified GSTdMT fractions stored for six days in different conditions using Buffer B with 1 mM DTT and 0.1mM $CdCl_2$ only in lysis…….. 66

Figure 4.51: Dynamic light scattering measurement of the GSTdMT (lane 1 in Native-PAGE analysis) stored for six days at -80^{o}C…….. 66

Figure 4.52: Dynamic light scattering measurement of the GSTdMT (lane 2 in Native-PAGE analysis) stored for six days at -20^{o}C..……..... 67

Figure 4.53: Dynamic light scattering measurement of the GSTdMT (lane 3 in Native-PAGE analysis) stored for six days at 4^{o}C..……..... 67

Figure 4.54: Native-PAGE analysis of concentrated GSTdMT fractions. …….. 68

Figure 4.55: Dynamic light scattering measurement of concentrated GSTdMT…. 68

Figure 4.56: Dynamic light scattering measurement of concentrated GSTdMT stored for 6 days at 4^{o}C…… 69

Figure 4.57: Dynamic light scattering measurement of ½ diluted GSTdMT…….. 69

Figure 4.58: Dynamic light scattering measurement of ¼ diluted GSTdMT…….. 69

Figure 4.59: Absorbance spectrum of GSTdMT compared with that of GST at similar protein concentration……... 71

Figure 4.60: Concentration dependence of 250 nm band of GSTdMT at the concentrations of 4.62 mg/ml and 2.35 mg/ml…… 71

Figure 4.61: Comparison of GST and GSTdMT CD spectra. GST (blue solid line) GSTdMT (pink solid line)…….. 73

Figure 4.62: Size exclusion chromatography elution profiles of calibration proteins……. 74

Figure 4.63: Calibration curve for HiLoad® 16/60 Superdex 75 size exclusion column…….. 74

Figure 4.64: Size exclusion chromatography elution profile of dMT ……..…….. 75

Figure 4.65: Silver stained 16% Tris-tricine analysis of purified dMT……... 75

Figure 4.66: Silver stained 10% Native-PAGE analysis of purified dMT……..... 76

Figure 4.67: Dynamic light scattering measurements of dMT stored at 4^{o}C…….. 77

Figure 4.68: Dynamic light scattering measurement of dMT stored at 80^{o}C…….. 78

Figure 4.69: Absorption spectrum of purified dMT…… 79

Figure 4.70: CD spectrum of purified dMT……. 79

Figure 4.71: SAXS curves for GSTdMT……. 80

Figure 4.72: SAXS curves for BSA (A) and GST (B)……..……... 81

Figure 4.73: SAXS curves for GSTdMT samples at different concentrations; (1) at 2.4 mg/ml, (2) at 4.6 mg/ml in Buffer B…….. 82

Figure 4.74: Guinier plots for GSTdMT (at 2.4 mg/ml) (A) and that for GST (at 2.15 mg/ml) (B) in Buffer B……..……...…….. 83

Figure 4.75: Correlation between Rg and GSTdMT concentration……. 84

Figure 4.76: Analysis of SAXS data for GST using GNOM algorithm…….. 85

Figure 4.77: Analysis of SAXS data for GSTdMT using GNOM algorithm…….. 86

Figure 4.78: Shape model for GSTdMT developed using GASBOR…….. 87

Figure 4.79: Shape model for GSTdMT developed using DAMMIN……. 88

Figure 4.80: The normalized K-edge X-ray absorption spectrum of Cd4-GSTdMT…….. 89

Figure 4.81: Fourier transform spectra of GSTdMT. χ; EXAFS signal, k; photoelectron wavenumber, R; interatomic distance, FT; Fourier transform…….. 90

Figure 4.82: Agarose gel analysis of RT-PCR showing cDNA for *d-mt*……. 90

Figure 4.83: Agarose gel analysis of the Triticum species digested with *Eco*RI, *Bam*HI and double digestion with *Eco*RI and *Bam*HI, respectively…… 91

Figure 4.84: Southern blot analysis of the Triticum species digested with *Eco*RI, *Bam*HI and double digestion with *Eco*RI and *Bam*HI, respectively……... 92

Figure 4.85: Agarose gel analysis of the Triticum species digested with *Eco*RI, *Bam*HI, respectively…… 92

Figure 4.86: Southern blot analysis of the Triticum species digested with *Eco*RI, *Bam*HI, respectively……. 92

Figure 4.87: Shoot and root growth of the durum wheat cultivar Balcalı-85 with increasing Cd application …… 93

Figure 4.88: Effect of increasing Cd application on shoot and root dry weight…….. 94

Figure 4.89: Effect of increasing Cd application on root Cd uptake……... 94

Figure 4.90: Effect of increasing Cd application on shoot Cd uptake……. 94

Figure 4.91: Experimental strategy of Whole Genome PCR……... 96

Figure 4.92: 1.5% Agarose gel analysis of digested and sonicated Balcalı-85 genomic DNA…….. 97

Figure 4.93: 1.5% Agarose gel analysis of ligation and TaqI digestion products... 97

Figure 4.94: 1.5% Agarose gel analysis of PCR products in control experiments for WGPCR.....……... 98

Figure 4.95: 1.5% Agarose gel analysis of PCR products of the 1st round (on the left) and 2nd round (on the right) of WGPRC experiments…….. 99

Figure 4.96: 1.5% Agarose gel analysis of PCR products of the 1st round (on the left) and 2nd round (on the right) of WGPRC experiments in the presence of poly-dIdC……. 99

Figure 4.97: 1% Agarose gel analysis of samples from washing steps of WGPRC experiments……..... 99

Figure 4.98: 7% Nondenaturing PAGE (on the left) and 1% Agarose gel analysis (on the right) of PCR products of the 1st round……

Figure 4.99: 7% Nondenaturing PAGE (on the left) and 1% Agarose gel analysis (on the right) of PCR products of the 2nd round amplification ……... 101

Figure 4.100: 7% Nondenaturing PAGE analysis of PCR products of the 1st and 2nd round PCR…….. 102

Figure 4.101: 7% Nondenaturing PAGE analysis of PCR products of the 1st, 2nd and 3rd rounds…….. 103

Figure 4.102: 7% Nondenaturing PAGE analysis of PCR products of the 1st and 2nd rounds with primer fd1 at 55°C and 60°C…… 104

Figure 4.103: 7% Nondenaturing PAGE analysis of PCR products of the 1st and 2nd rounds with 0.5 μM primer fd1 at 55°C……. 104

Figure 4.104: 7% Nondenaturing PAGE analysis of PCR products of the 1st, 2nd and 3rd rounds……... 105

Figure 4.105: 7% Nondenaturing PAGE analysis of PCR products of the 1st, 2nd, 3rd and 4th rounds……..…….. 106

Figure 4.106: 7% Nondenaturing PAGE analysis of PCR products of the 1st, 2nd and 3rd rounds of amplifications with products of WGPCR experiments using 1 μM primer fd1…….. 107

Figure 4.107: 7% Nondenaturing PAGE analysis samples from washing steps…. 107

Figure 4.108: 7% Nondenaturing PAGE analysis of PCR products of the 1st, 2nd and 3rd rounds……... 108

Figure 4.109: 7% Nondenaturing PAGE analysis samples from washing steps … 108

Figure 5.1: Possible Cd binding schemes of dMT…… 116

LIST OF TABLES

Table 2.1: Metallothionein families and subfamilies…… 7

Table 2.2: Four types of plant MT according to the Cys motifs in their N- and C-terminal domains…….. 15

Table 4.1: Protein samples used for column calibration and their molecular weights and elution volumes. ……... 39

Table 4.2: Comparison of yields of GSTdMT and GST purification……..... 62

Table 4.3: Absorption values for pooled, concentrated and diluted GSTdMT……. 68

Table 4.4: Cd/GSTdMT binding ratio for GSTdMT peak fractions from size exclusion column pool GII…… 70

Table 4.5: UV-vis absorbance values, concentrations and Cd^{2+}/GSTdMT determined by ICP-OES…… 71

Table 4.6: Comparison of the ellipticity of GST and GSTdMT ……..... 73

Table 4.7: Protein samples used for column calibration and their molecular weights and elution volumes……..... 74

Table 4.8: Ellipticity values of purified dMT at 222 and 208 nm..……... 79

Table 4.9: Calculated molecular mass (MM) for GSTdMT and GSTdMT…….. 82

Table 4.10: Primers designed for *mt* gene identification on *T. durum* genomic DNA…….. 91

Table 4.11: Linkers and primers designed for Whole Genome PCR…… 97

Table 4.12: Absorption values of amplified and nonamplified forms of poly-dIdC. 100

Table 4.13: Linkers and primers designed for Whole Genome PCR……..... 103

ABBREVIATIONS

Ag: Silver

Ar: Argon

As: Arsenic

bp: base pair

BSA: Bovine serum albumin

Cd: Cadmium

cDNA: Complementary DNA

CTAB: Cetyltrimethylammonium bromide

Cu: Copper

Cys: Cystein

Da: Dalton

DLS: Dynamic Light Scattering

dNTP: Deoxyribonucleotide triphosphate

DTT: Dithiothreitol

EDTA: Etilendiamin tetraasetikasit

EtBr: Ethidium Bromide

EtOH: Ethanol

EXAFS: Extended x-ray absorption fine structure

Fe: Iron

FPLC: Fast perfusion liquid chromatography

Glu: Glutamate

GSH: reduced glutathione

GSSG: oxidized glutathione

GST: Glutathione S-transferase

GST: Glutathione *S*-transferase

H_2O_2: Hydrogen peroxide

HEPES: 4-(2-hydroxyethyl)-1-piperazineethanesulfonicacid

Hg: Mercury

His: Histidine

I(0): The forward scattering

ICP-OES: Inductively coupled plasma optical emission spectroscopy

IPTG: Isopropyl-B-D-thiogalactoside

kDa: Kilodalton

Lys: Lysine

mg: milligram

mRNA: Messenger Ribo nucleic acid

MT: Metallothionein

***mt-d*:** Metallothionein gene from *Triticum durum*

OD: Optical density

***p(r)*:**Distance distribution function

PAGE: Polyacrylamide gel electrophoresis

pGEXdMT: *mt-d* gene inserted into pGEX-4-T2 vector

PMSF: Phenylmethanesulphonylfluoride

R_g: Radius of gyration

ROS: Reactive oxygen species

S: Sulphur

SAXS: Small angle X-ray scattering

SDS: Sodium dodecyl sulfate

SSC: sodium chloride/sodium citrate

TEMED: Tetramethylethylenediamine

Zn: Zinc

µg: microgram

µl: micro liter

Chapter 1

INTRODUCTION

Metallothioneins (MTs) are a group of low molecular weight (6-8 kDa) cystein (Cys) rich polypeptides that can bind metal ions including copper (Cu), cadmium (Cd), zinc (Zn), silver (Ag), mercury (Hg) through the thiol groups of their Cys residues that are localized in the N- and C-termini of the protein in specific motifs. Aromatic amino acids are usually absent. All Cys residues occur in the reduced form and are coordinated to the metal ions through mercaptide bonds, giving rise to spectroscopic features characteristic of metal-thiolate clusters. MTs have been widely found in diverse organisms including mammals, plants, and fungi as well as some prokaryotes (Vasak and Hasler, 2000).

Classification of the members of the MT family has been based on the phylogenetic relationships and the distribution patterns of Cys residues along the MT sequences; 15 subfamilies have been identified (Binz and Kagi, 1999). Plant MT proteins have been historically divided into four major types on the basis of the arrangement of Cys residues and Cys free spacer regions (Cobbet and Goldsbrough, 2002). Plant Type 1 MTs have two Cys rich metal binding domains which are separated by a spacer region containing 30-45 amino acids whereas, this region has only 2-10 amino acids in mammalian MTs. Plant MTs are different from mammalian MTs also in terms amino acid sequences, charge and total Cys content.

Several functional roles including heavy metal detoxification, homeostasis of essential metals, free radical scavenging, regulation of metalloenzyme and transcription factors and more recently metabolic regulation by Zn donation have been reported for mammalian MTs (Vasak, 2005). The function of plant MT proteins is still not completely understood. Metal binding propensity of purified plant recombinant MTs

(Kille et al., 1991; Evans et al., 1992; Murphy et al., 1997; Mir et al., 2004; Bilecen et al., 2005) and up-regulation of the *mt* genes upon exposure of plants to heavy metals (Guo et al., 2003) have lead to the conclusion that plant MTs play a role in maintaining metal ion homeostasis and detoxification of heavy metals. Involvement of plant MTs in metal chaperoning, scavenging of reactive oxygen species (Akashi et al., 2004, Wong et al., 2004), stress response such as wounding (Choi et al., 1996), pathogen infection (Butt et al., 1998), senescence (Buchanan-Wollaston, 1994; Yu et al., 1998; Guo et al., 2003) and fruit ripening (Cobbett and Goldsbrough, 2002) have also been reported.

The 3D structure of MTs originating from mammalian and fungal sources has been extensively investigated using Nuclear magnetic resonance (NMR) and X-ray crystallography (Vasak and Hasler, 2000). Both techniques revealed a monomeric dumbbell shape in accordance with clustering of the Cys motifs. In this structure, a total of seven metal ions are located in two separate metal-thiolate clusters with ($Metal_3Cys_9$) and ($Metal_4Cys_{11}$) domains providing the $Metal_7Cys_{20}$ stoichiometry. The two metal binding domains are connected with a flexible spacer region (Klaasen and Chodhuri, 1999). The protein appears to be lacking a well defined secondary structure and it is considered to be an oxidatively unstable random coil which folds through metal binding (Rigby and Stillman, 2004; Duncan et al., 2006).

In contrast to their mammalian counterparts there is no direct structural work on plant MTs. Two different models have been proposed for plant holo-MT structure; the hairpin (Kille et al., 1991; Domenech et al., 2006; Freisinger, 2007; Peroza and Freisinger, 2007) and the dumbbell model (Zhu et al., 2000; Bilecen et al., 2005).

In the previous study by Bilecen et al., (2005) a novel gene, from *Triticum durum,* encoding a Type 1 MT protein, dMT, was isolated and expressed in *E. coli* cells as a fusion protein with glutathione S-transferase (GST). The work presented in this thesis mainly aims to investigate the possible structure and related functional roles of dMT.

Specific goals of this work can be summarized as;

(1) Determining optimum conditions for producing homogeneous and monodisperse recombinant GSTdMT solutions at high protein concentration for structural studies. These studies were expected to guide the way for establishing a purification procedure for dMT and lead to information about the structure of dMT.

(2) Studies at genomic level to determine the copy number of the *mt* gene in durum wheat for comparison with known plant mt gene families for assignment of functional roles.

(3) Investigating physiological responses to Cd in *T. durum* cv. Balcalı-85 in order to be able correlate these with *mt-d* gene expression if time permitted.

(4) Investigating the possibility for an interaction between durum DNA and GSTdMT.

The structure of this thesis is organized such that this introductory section is followed by an overview of the current status of research on MTs. Chapter 3 explains materials and methods utilized in this study in a detailed fashion. Results are presented in Chapter 4 and are discussed in Chapter 5 in the light of current literature. Chapter 6 involves a brief synopsis and conclusions of this study along with future perspectives.

Chapter 2

OVERVIEW

2.1 Metallothioneins (MTs)

Metallothioneins (MTs) constitute a superfamily of low molecular weight cysteine (Cys) rich proteins. Cys residues have the capacity to bind to a variety of metal ions, most commonly Zn^{+2}, Cu^{+2} and Cd^{+2}, by mercaptide bonds and the biochemical, biophysical and functional properties of MTs are largely dependent on the bound metal ion. MT was first isolated from horse (equine) renal cortex in 1957 by Margoshes and Valle (Vasak and Kagi, 1994) when they purified a Cd/binding protein, and since then MTs represent the major group of naturally-Cd-containing biomolecules. More than 200 metallothioneins have been identified in a wide range of organisms including plants, animals, and fungi, and even in some prokaryotes (Rauser, 1999; Cobbett and Goldsbrough, 2002; Zhou et al., 2005).

2.1.1 Classification

According to the first established classification by Fowler et al., in 1987, MT superfamily was divided into three classes. Class I MTs include proteins which show a Cys distribution similar to mammalian MTs and are widespread in vertebrates. Class II MTs are those that do not show the typical Cys distribution and are present in plants, fungi and nonvertebrates. Class III MTs include enzymatically synthesized Cys-rich polypeptides; cadystins and phytochelatins. The latter are enzymatically synthesized peptides with a poly $(\gamma\text{-Glu-Cys})_n$-glycine structure.

This subdivision has become insufficient as the number of new MT sequences increased. Thus the second classification was performed by Binz and Kagi in 1999 (also

in http://www.expasy.ch/cgi-bin/lists?metallo.txt) according to the phylogenetic relationships and the distribution patterns of Cys residues along the MT sequences. This system subdivides the MT superfamily into families, subfamilies, subgroups and isolated isoforms and alleles. As a result, MTs have currently been grouped into 15 families (Binz and Kagi, 1999). Family 15 contains the plant MTs and has been further classified by Cobbet and Goldsbrough into 4 Types (1, 2, 3 and 4) depending on the distribution of their Cys residues and a Cys-devoid regions (called spacers) characteristic of plant MTs (Cobbet and Goldsbrough, 2002) (Table 2.1).

2.1.2 Mammalian MTs

Mammalian MTs contain 61 to 68 amino acids, in which 20 are Cys and no aromatic amino acids are observed. The number and position of Cys residues are highly conserved and Cys-X-Cys, Cys-X-Y-Cys (X and Y represent non-cysteine amino acids), and Cys-Cys sequences are the most common motifs. All Cys residues appear to be associated with 7 equivalents of divalent metal ions or 12 monovalent metal ions by mercaptide bonds; metals are coordinated reversibly without forming covalent bonds. MTs have molecular weights of about 6000 to 7000 Da. The mammalian MT amino acid sequence displays two cysteine-rich domains; α-domain or C-terminal is the more stable, contains eleven Cys residues associated with four divalent metals and β-domain or N- terminal is the more reactive, with nine Cys incorporating three divalent metals. Mammalian MTs predominantly bind Zn, but in the case of high levels of Cu or Cd, Zn can be readily displaced (Coyle et al., 2002; Zimeri et al., 2005; Vasak and Kagi, 1994; Kang, 2006).

There are four major isoforms of mammalian MTs which differ in amino acid residues other than Cys and also in their charge properties. MT1 and MT2 are expressed in all mammalian cells, but the highest expression is in liver, while expression of MT3 and MT4 is more limited. MT3 is expressed mainly in the brain and very low levels in pancreas and intestine. MT4 is only expressed in epithelial cells in skin and it is not very known (Vasak and Kagi, 1994; Haq et al., 2003).

Table 2.1: Metallothionein families and subfamilies (Modified from Binz and Kagi, 1999 and Cobbett and Goldsbrough, 2002)

Family	Sequence pattern	Example
1.Vertebrate	K-x(1,2)-C-C-x-C-C-P-x(2)-C	***M.musculus*** **MT1** MDPNCSCTTGGSCACAGSCKCKECKCTSCKKCCSCCPVGCAKCAQGCVCKGSSEKCRCCA
2.Molluscan	C-x-C-x(3)-C-T-G-x(3)-C-x-C-x(3)-C-x-C-K	***M.edulis*** **10MTIV** MPAPCNCIETNVCICDTGCSGEGCRCGDACKCSGADCKCSGCKVVCKCSGSCACEGGCTGPSTCKCAPGCSCK
3.Crustacean	P-[GD]-P-C-C-x(3,4)-C-x-C	***H.americanus*** **MTH** MPGPCCKDKCECAEGGCKTGCKCTSCRCAPCEKCTSGCKCPSKDECAKTCSKPCKCCP
4.Echinoderms	P-D-x-K-C-V-C-C-x(5)-C-x-C-x(4)- C-C-x(4)-C-C-x(4,6)-C-C	***S.purpuratus*** **SpMTA** MPDVKCVCCKEGKECACFGQDCCKTGECCKDGTCCGICTNAACKCANGCKCGSGCSCTEGNCAC
5.Diptera	C-G-x(2)-C-x-C-x(2)-Q-x(5)-C-x-C-x(2)D-C-x-C	***D.melanogaster*** **MTNB** MVCKGCGTNCQCSAQKCGDNCACNKDCQCVCKNGPKDQCCSNK
6.Nematoda	K-C-C-x(3)-C-C	***C.elegans*** **MT1** MACKCDCKNKQCKCGDKCECSGDKCCEKYCCEEASEKKCCPAGCKGDCKCANCHCAEQKQCGDKTHQHQGTAAAH
7.Ciliate	---	***T.termophila*** **MTT1** MDKVNSCCCGVNAKPCCTDPNSGCCCVSKTDNCCKSDTKECCTGTGEGCKCVNCKCCKPQANCCCGVNAKPCCFDPNSGCCCVSKTNNCCKSDTKECCTGTGEGCKCTSCQCCKPVQQGCCCGDKAKACCTDPNSGCCCSNKANKCCDATSKQECQTCQCCK
8.Fungal 1	C-G-C-S-x(4)-C-x-C-x(3,4)-C-x-C-S-x-C	***N.crassa*** **MT** MGDCGCSGASSCNCGSGCSCSNCGSK
9.Fungal 2	---	***C.glabrata*** **MT2** MANDCKCPNGCSCPNCANGGCQCGDKCECKKQSCHGCGEQCKCGSHGSSCHGSCGCGDKCECK
10.Fungal 3	---	***C.glabrata*** **MT2** MPEQVNCQYDCHCSNCACENTCNCCAKPACACTNSASNECSCQTCKCQTCKC
11.Fungal 4	C-X-K-C-x-C-x(2)-C-K-C	***Y.lipolitica*** **MT3** MEFTTAMLGASLISTTSTQSKHNLVNNCCCSSSTSESSMPASCACTKCGCKTCKC
12.Fungal 5	---	***S.cerevisiae*** **CUP1** MFSELINFQNEGHECQCQCGSCKNNEQCQKSCSCPTGCNSDDKCPCGNKSEETKKSCCSGK

13.Fungal 6	---	***S.cerevisiae* CRS5** TVKICDCEGECCKDSCHCGSTCLPSCSGGEKCKCDHSTGSPQCKSCGEKCKCETTCTCEKSKCNCEKC
14.Procaryota	K-C-A-C-x(2)-C-L-C	**Synechococcus sp SmtA** MTTVTQMKCACPHCLCIVSLNDAIMVDGKPYCSEVCANGTCKENSGCGHAGCGCGSA
15.Plant		
15.1.Plant MTs Type 1	C-X-C(3)-C-X-C(3)-C-X-C-spacer-C-X-C(3)-C-X-C(3)- C-X-C	***Pisum sativum* MT** MSGCGCGSSCNCGDSCKCNKRSSGLSYSEMETTETVILGVGPAKIQFEGAEMSAASEDGGCKCGDNCTCDPCNCK
15.2.Plant MTs Type 2	C-C(3)-C-X-C(3)-C-X-C(3)-C-X-X-C-spacer-C-X-C(3)-C-X-C(3)-C-X-C	***L.esculetum* MT** MSCCGGNCGCGSSCKCGNGCGGCKMYPDMSYTESSTTTETLVLGVGPEKTSFGAMEMGESPVAENGCKCGSDCKCNPCTCSK
15.3.Plant MTs Type 3	C(2)-C-X-C-spacer-C-X-C(3)-C-X-C(2)-C-X-C	***A.thaliana* MT3** MSSNCGSCDCADKTQCVKKGTSYTFDIVETQESYKEAMIMDVGAEENNANCKCKCGSSCSCVNCTCCPN
15.4.Plant MTs Type 4 or Ec	C-x(3)-C-X-C(3)-C-x(5)-C-X-C(17)-C-X-C(3)-C-X-C(3)-C-X-C(15)-C-X-C(3)-C-X-C(2)-C-X(3,5)	***T.aestium* MT** MGCNDKCGCAVPCPGGTGCRCTS…ARSGAAAGEHTTCGCGEHCGCNPCACGREGTPSGRANRRANCSCGAACNCASCGSATA
99. Phytochelatins and nonprotein MTs		

2.1.2.1 Structure of Mammalian MTs

Three-dimensional structures of several mammalian MTs were investigated by NMR and X-ray crystallography. Both techniques revealed a monomeric dumbbell shape in accordance with clustering of the Cys motifs. Seven metal ions are located in two separate metal-thiolate clusters. A three-metal cluster ($Metal_3Cys_9$) with three bridges is located in β-domain and a four-metal cluster ($Metal_4Cys_{11}$) with five bridges is in the α-domain providing the $Metal_7Cys_{20}$ stoichiometry (Figure 2.1) (Klaasen and Chodhuri, 1999). In both clusters, metals ions are tetrahedrally coordinated by bridging and terminal thiolate ligands. The two metal binding domains are connected with a flexible hinge region composed of a conserved Lys-Lys segment. The order of metal binding begins with the α-domain and after saturation continues with the β-domain. In the case of metal releasing the β-domain comes first, indicating that the three-metal cluster is more labile, i.e. metallation and demetallation taking place rapidly, whereas the metal is bound more tightly to the four-metal cluster (Fischer and Davie, 1998; Vasak and Hasler, 2000; Romero-Isart and Vasak, 2002).

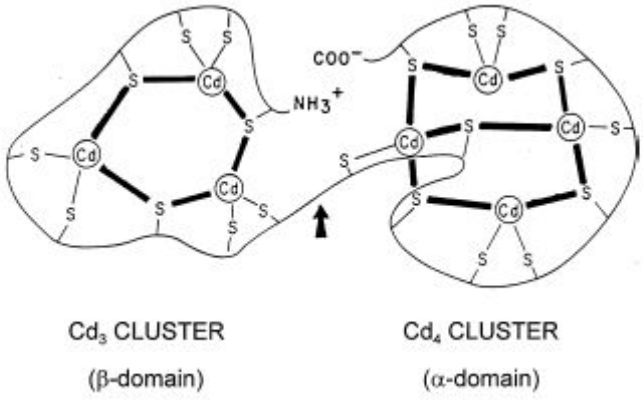

Figure 2.1: Schematic representation of Cd-thiolate clusters in mammalian MT based on NMR and X-ray spectroscopy data. Three bridging and six terminal Cys ligands are placed in the β-domain (Cd_3 cluster) and four bridging and six terminal ligands in the α-domain (Cd_4 cluster) (Klaassen and Choudhuri, 1999).

According to far-UV CD spectra the metal-free form (apoMT) was estimated to contain 55% disordered structure, 6% α-helix, 18% β-sheet and 26% β-turn, which indicated a predominantly disordered structure and it was interpreted as an oxidatively unstable random coil. But, when metal ions bind to apoMT, the polypeptide chain

rapidly folds resulting in the formation of two metal-thiolate clusters (Vasak and Kagi, 1994; Duncan et al., 2006).

The first three-dimensional (3D) MT structure was that of MT-2 from rat liver determined by NMR and X-ray crystallography (Figure 2.2) (Robbins et al., 1991). The crystal structure of rat Cd_5, Zn_2-MT-2 and the solution NMR structures of Cd_7-MT-2 from rabbit, rat and human sources demonstrated similar metal-thiolate cluster structures (Vasak 2005; Peterson et al., 1996; Bertini et al., 2000).

The invertebrate, sea urchin MT isoform A (MTA) is an evolutionary-distant MT, it has 64 amino acids and contains same number of Cys motifs and metal ions as the mammalian MTs, but there is no sequence homology relationship. The structure of Cd bound MTA was determined by NMR and two metal-thiolate clusters in each of the globular domains; Cd_4Cys_{11} cluster in α-domain and Cd_3Cys_9 cluster in β-domain was observed (Figure 2.2). Although this structure looks like the known mammalian MT structure, it is considerably dissimilar in terms of the Cys-metal coordination bonds connectivity pattern and the polypeptide backbone local folding. It is suggested that the existence of similar metal-thiolate clusters even in evolutionary-distant MT shows the functional role (Riek et al., 1999; Vasak and Kagi, 1994).

The only reported 3D structure of Cu^+ containing MT is yeast MT with 53 amino acids. The yeast MT differs in the number of Cys residues (12) and metal content from the structurally well characterized mammalian MTs. The NMR solution structure for yeast MT was determined for the native Cu-containing form and for the Ag^+ derivative and both showed that Cu^+ or Ag^+ ions are bound in a single cluster of Cu_7-Cys_8. However, due to the possibility of Ag^+ and Cu^+ having different coordination properties, a new NMR study of Cu_7-MT from the same species was performed and as a result a highly improved structure was obtained with the seven Cu^+ ions. Lately the crystal structure was determined for Cu-MT from yeast and found that eight rather than seven Cu atoms were coordinated to all 10 Cys and arranged in a Cu_8-thiolate cluster. This Cu_8-MT X-ray structure was different from that of Ag_7-MT NMR structure and similar, but not identical, to that of Cu_7-MT NMR structure (Figure 2.3). Besides the different structure of the metal cluster, the main differences were the cysteine topology and the conformation of some portions of the backbone (Calderone et al., 2005).

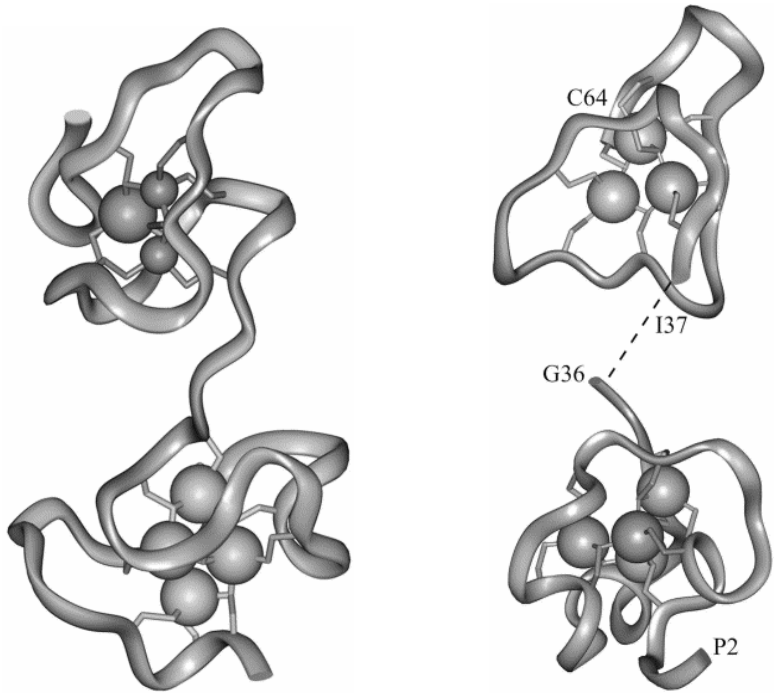

Figure 2.2: Crystal structure of Cd_5, Zn_2-MT-2 from rat liver and NMR structure of sea urchin of Cd_7-MTA (Robbins et al., 1991 and Riek et al., 1999).

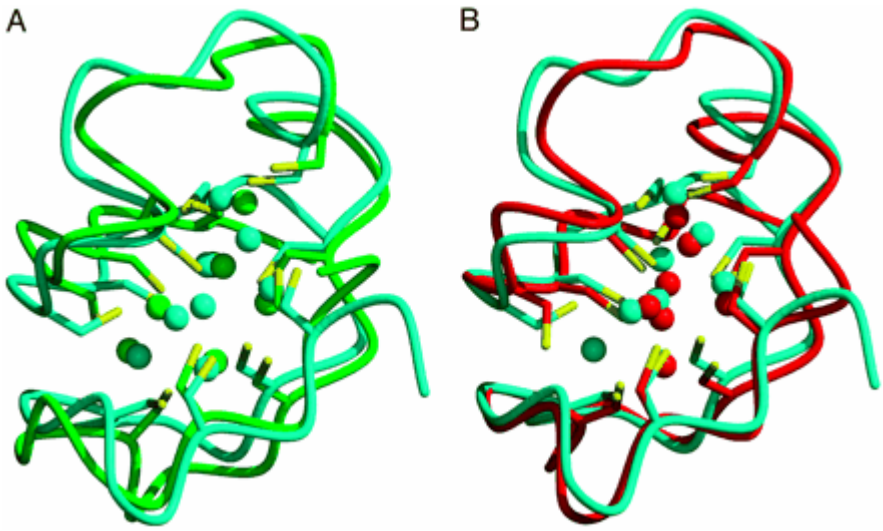

Figure 2.3: Comparison of Cu_8-MT crystal structure (cyan tube) with Ag_7-MT NMR model (green tube) (A) and Cu_7-MT NMR model (red tube) (B). The Cu_8-MT copper atoms are represented as cyan spheres and the Ag_7-MT and Cu_7-MT NMR models are represented as green and red spheres, respectively. The cysteine side chains are also displayed (Calderone et al., 2005).

2.1.2.2 Function of Mammalian MTs

Mammalian MTs have been extensively studied; they are expressed differentially in various tissues, in several developmental stages and in response to metals, steroids and stress. However, it has not been possible to assign an essential or critical biological function for mammalian MTs. Many studies have implicated three major biological functions these are: (1) detoxification of heavy metals such as Cd, Hg and As (2) homeostasis of essential metals including Zn and Cu and (3) protection against oxidative stress (Klaassen and Choudhuri, 1999). More recently metabolic regulation by Zn donation, sequestration and redox control have also been suggested (Vasak, 2005).

It is known that mammalian MTs can provide protection against Cd toxicity. This role has been investigated using mice and various cell lines, and it was found that cells expressing excess amount of MT are resistant to Cd toxicity, while cells that cannot synthesize any MT are sensitive to Cd. In addition, studies using transgenic and knockout mouse also showed the protection role of MT towards Cd toxicity. Studies with MT-null mice demonstrated that MT was needed for the protection of kidney and liver from Cd toxicity. However, it has been thought that protection from Cd toxicity is a property of MTs rather than having an evolutionary conserved function (Palmiter, 1998; Klaassen and Choudhuri, 1999; Kang, 2006).

A widely considered but still discussed functional role includes zinc donation to specific storage sites or to proteins. MT has high affinity to Zn due to the large number of free sulfhydryl (SH) groups. Although Zn-binding occurs with high affinity, these highly reactive sulfhydryl groups can undergo exchange reactions permitting transfer of Zn to other proteins. A recent and significant development in MT research is the finding of the redox regulation of Zn/ S (sulfur) interaction. Zn in biology is redox inert in contrast to Cu and iron (Fe). It is suggested that, MT/thionein act as a control device for the concentration of available Zn. MT binds Zn more tightly than other zinc proteins. Accordingly, Zn cannot move freely from this tight binding site in MT. When the environment becomes oxidized, the bound Zn is released through oxidation of the thiolate cluster, which has low redox potential and this leads to the formation of MT-disulfide or thionin (if all metals are released). When environment becomes reduced in

the case of increase in GSH/GSSG (reduced/oxidized glutathione) ratio, MT-disulfide or thionin is reduced to MT-thiol or thionein and this is enhanced by selenium catalyst or other unidentified catalytic agents. In the presence of Zn, MT is quickly reconstituted. This process represents MT redox cycle as shown in Figure 2.4 (Vasak and Hasler, 2000; Palmiter 1998; Klaassen and Choudhuri, 1999; Maret, 2000; Kang, 2006).

Several in vitro studies showed that, Zn_7-MTs and apoMT affect the activity of zinc dependent proteins and zinc finger transcription factors by transferring or removing Zn. For example, it was shown that, there is a fast Zn exchange between MT and the Zn cluster in the Gal4 transcription factor (Maret et al 1997). These studies indicate that, even though metal-thiolate clusters have thermodynamic stability, such metal exchange reactions do occur. Furthermore, recent studies showed that a cellular oxidant reduced and oxidized glutathione facilitate intermolecular metal transfer by oxidizing Cys residues of metal clusters. Therefore, recently it has been suggested that MTs might function as a zinc chaperon for synthesis of metalloproteins and metal dependent transcription factors. The binding stability of Zn makes MT serve as a reservoir for Zn. This recent consideration of the redox regulation of MT provides a mechanism for function of MT, including homeostasis of essential metals, detoxification of toxic metals, and protection from oxidative stress (Vasak and Hasler, 2000; Palmiter 1998; Klaassen and Choudhuri, 1999; Maret, 2000; Kang, 2006).

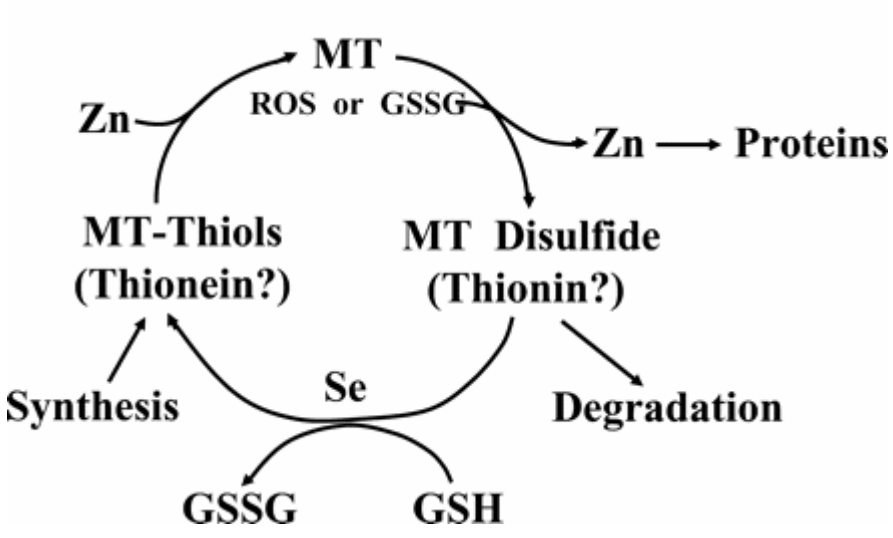

Figure 2.4: Schematic representation of MT redox cycle (Kang, 2006)

Another proposed function is that MTs can protect against oxidative damage. As mentioned above, the multiple Cys residues in metal-thiolate clusters are readily oxidized *in vitro* during oxidative stress, therefore they can serve as scavengers of harmful radicals. It was shown that MT containing zinc and/or cadmium can scavenge hydroxyl and superoxide radicals (Thornalley et al., 1985). In a recent study the role of MT as a free radical scavenger has been demonstrated using a cell-free system (Cai et al., 2000). In another study it was demonstrated that, yeast cells that cannot synthesize MT and are also lacking superoxide dismutase were more sensitive to oxidative stress (Tamai et al., 1993). Moreover, oxidative stress agents' chloroform, turpentine, diethyl methane, and H_2O_2 can also induce expression of MT1 and MT2 isoforms *in vivo*. Further studies have shown that MT is about 800 times more potent than GSH in preventing hydroxyl radical (Palmiter, 1998; Klaassen and Choudhuri, 1999).

2.1.3 Plant MTs

The first identified plant MT was the wheat EcMT protein in 1987 by Lane et al, and since then more than 140 putative MT genes have been recorded in various species, which accounts for about half of all recorded MTs (Zhou et al., 2006). The plant MTs generally contain two cysteine-rich domains as in the case of Class I MTs. In most plant MTs these two domains are separated by spacer region containing 30-45 amino acids whereas in mammalian MTs this region has only 2-10 amino acids. Plant MTs are different from their mammalian counterparts also in terms amino acid sequences, charge and total Cys content.

2.1.3.1 Classification of Plant MTs

Plant MTs belong to Class II according to the early classifications (Fowler et al., 1987) and constitute Family 15 according to Binz and Kagi (1999). These have been further classified into 4 Types depending on the distribution of their Cys residues and Cys-devoid regions (called spacers) characteristic of plant MTs (Table 2.2). Type 1 MTs contain a total of six Cys-X-Cys motifs (X represents a noncysteine amino acid) equally distributed among two domains which are separated by about 40 amino acids. Type 2 MTs contain total fourteen Cys residues and a spacer region of about 40 amino acid residues. One Cys-Cys, two Cys-X-Cys and one Cys-X-X-Cys motifs are present

in the N-terminal domain, and three Cys-X-Cys motifs are present in the C-terminal domain. Type 3 MTs contain only four Cys residues in the N-terminal domain and three Cys-X-Cys motifs in the C-terminal domain. As Type 1 and Type 2, the two domains are separated by about 40 amino acids. Finally, Type 4 MTs are different from others by having three Cys-rich domains containing 5 or 6 conserved Cys residues and are separated by 10 to 15 residues. They also contain additional 8 to 10 amino acids in N-terminal domain (Rauser, 1999; Cobbet and Goldsbrough, 2002).

Several plant species have genes encoding all these four types of MTs indicating their evolution precedes the division of monocotyledonous and dicotyledonous, and this bring the possibility that flowering plants also contain all of four types of MTs (Cobbet and Goldsbrough, 2002).

2.1.3.2 Localization of Plant MTs

The exact cellular localization of plant MTs is not known and information from expression studies indicates that many MT genes are expressed at very high levels in different plant tissues. Transcripts of plant MTs are detected in roots, stems, leaves, flowers, fruits and seeds under different conditions (Rauser, 1999). According to RNA expression studies in various plant species, Type 1 MT genes are expressed more richly in roots, whereas Type 2 MT genes are in leaves. In Type 3 MT, expression is detected in leaves or in fruits as they ripen. Expression of Type 4 MT is restricted to developing seeds and regulated by absisic acid (Cobbet and Goldsbrough, 2002).

Recently, the organ specificity has been reported for MT genes in many plant species. For instance, the rice *OsMT-II-1a* genes were highly expressed in developing seeds (Zhou et al., 2005) while another rice *ricMT* gene was highly expressed in stem nodes (Yu et al., 1998). Also, in Arabidopsis and *Vicia faba* expression of MT is predominant in trichomes (Garcia-Hernandez et al., 1998; Foley and Singh, 1994).

Table 2.2: Four types of plant MT according to the Cys motifs in their N- and C- terminal domains. Conserved Cys residues are marked with star. The protein sequences are predicted from gene sequences in Arabidopsis (At), *Brassica napus* (Bn), rice (Os), pea (Ps), alfalfa (Ms), *Brassica oleracea* (Bo), petunia (Ph), *Silene vulgaris* (Sv), banana (Ma), kiwifruit (Ad), cotton (Gh), *Picea glauca* (Pg), maize (Zm), and wheat (Ta) (Cobbet and Goldsbrough, 2002).

Type1	* *	* * * *					* * *	* * *
AtMT1a	MADSN**C**G**C**GS	S**C**K**C**GDS**C**S**C**	EKNY.....	.....	.....	.....NKEC	DN**C**S**C**GSN**C**S	**C**GSN**C**N**C**
AtMT1C	MAGSN**C**G**C**GS	S**C**K**C**GDS**C**S**C**	EKNY.....	.....	.....	.....NKEC	DN**C**S**C**GSN**C**S	**C**GSS**C**N**C**
BnMT1	MAGSN**C**G**C**GS	G**C**K**C**GDS**C**S**C**	EKNY.....	.....	.....	.....NTEC	DN**C**S**C**GSN**C**S	**C**GDS**C**S**C**
OsMT1a	MS...**C**S**C**GS	S**C**S**C**GSN**C**S**C**	GKKYPDLEEK	SSSTKATVVL	GVAPEKKOOF	EAAAESGETA	HG**C**S**C**GSS**C**R	**C**NP.**C**N**C**
PsMT1	MSG..**C**G**C**GS	S**C**N**C**GDS**C**K**C**	NKRSSGLSYS	EMETTETVIL	GVGPAKIOFE	GAEMSAASED	GG**C**K**C**GDN**C**T	**C**DP.**C**N**C**K
MsMT1	MSG..**C**N**C**GS	S**C**N**C**GDS**C**K**C**	NKRSSGLSYS	EMETTETVIL	GVGPAKIHFE	GAEMGVAAKD	GG**C**K**C**GDS**C**T	**C**DP.**C**N**C**K

Type 2	** * *	* * *	*				* *	* * * *	
AtMT2a	MS**CC**GGN**C**G**C**	GSG**C**K**C**GNG**C**	GG**C**KMYPDLG	FSGETTTTET	FVLGVAPAMK	NOYEASGESN	NAENDA**C**K**C**G	SD**C**K**C**DP**C**T**C**	K
BoMT2	MS**CC**GGN**C**G**C**	GSG**C**K**C**GNG**C**	GG**C**KMYPDLG	FSGETTTTET	FVLGVAPTMK	NOHEASGEGV	.AENDA**C**K**C**G	SD**C**K**C**DP**C**T**C**	E
AtMT2b	MS**CC**GGS**C**G**C**	GSA**C**K**C**GNG**C**	GG**C**KRYPDL.	...ENTATET	LVLGVAPAMN	SOYEASGETF	VAENDA**C**K**C**G	SD**C**K**C**NP**C**T**C**	K
PhMT2	MS**CC**GGN**C**G**C**	GSG**C**K**C**GNG**C**	GG**C**KMYPDLS	YT.ESTTTET	LILGVGPEKT	SFGSMEMGES	PAEN.G**C**K**C**G	SD**C**K**C**DP**C**T**C**	SK
SvMT2	MS**CC**NGN**C**G**C**	GSA**C**K**C**GSG**C**	GG**C**KMFPDFA	E..GSSGSAS	LVLGVAP.MA	SYFDAEMEMG	VATENG**C**K**C**G	DN**C**Q**C**DP**C**T**C**	K
OsMT2	MS**CC**GGN**C**G**C**	GSS**C**Q**C**GNG**C**	GG**C**K.YSEVE	PTTTTTFLAD	ATNKGSGAAS	GGSEMGAENG	SCGCNT**C**K**C**G	TS**C**G**C**SC**C**N**C**	N

Type 3	* * *	*				* * *	* * *
AtMT3	MSSN**C**GS**C**D**C**	ADKTQ**C**VKKG	TSYTFDIVET	QESYKEAMIM	DVGAEENNAN	CK**C**K**C**GSS**C**S	**C**VN**C**T**C**CPN
MaMT3	MS.T**C**GN**C**D**C**	VDKSQ**C**VKKG	NSYGIDIVET	EKSYVDEVIV	AAEAAEHDG.	.K**C**K**C**GAA**C**A	**C**TD**C**K**C**GN
AdMT3	MSDK**C**GN**C**D**C**	ADSSQ**C**VKKG	NS..IDIVET	DKSYIEDVVM	GVPAAESGG.	.K**C**K**C**GTS**C**P	**C**VN**C**T**C**D
OsMT3	MSDK**C**GN**C**D**C**	ADKSQ**C**VKKG	TSYGVVIVEA	EKSHFEEV..	.AAGEENGG.	..**C**K**C**GTS**C**S	**C**TD**C**K**C**GK
GhMT3	MSDR**C**GN**C**D**C**	ADRSQ**C**TK.G	NSNTM.IIET	EKSYINTAVM	DAPAENDG..	.K**C**K**C**GTG**C**S	**C**TD**C**T**C**GH
PgMT3	MSSD**C**GN**C**D**C**	ADKSQ**C**TKKG	FQID.GIVET	SYEMGHGGD.	..VSLEND..	..**C**K**C**GPN**C**Q	**C**GT**C**T**C**HT

Type 4		* * *	* *	*	* * * *	*	* *	* * *	
AtMT4a	MADTGKGSSV	AG**C**NDS**C**G**C**P	SP**C**PGGNS**C**R	**C**RM..R.EAS	AGDQGHMV**C**P	**C**GEH**C**G**C**NP**C**	N**C**PKTQTQTS	AKG....**C**T**C**	GEG**C**T**C**AS**C**A	T
AtMT4b	MADTGKGSAS	AS**C**NDR**C**G**C**P	SP**C**PGGES**C**R	**C**KM..MSEAS	GGDQEHNT**C**P	**C**CEH**C**G**C**NP**C**	N**C**PKTQTQTS	AKG....**C**T**C**	GEG**C**T**C**AT**C**A	A
PhMT4	MADL.RGSS.	AI**C**DER**C**G**C**P	SF**C**FGGVA**C**R	**C**ASGGAATAG	GGDMEHKK**C**P	**C**GEH**C**G**C**NP**C**	T**C**PKSEGTTA	GSGK.AH**C**K**C**	GFG**C**T**C**VQ**C**A	S
ZmMT4	MG.....	...DDK**C**G**C**A	VP**C**PGGKD**C**R	**C**TS...G..S	GGQREHTT**C**G	**C**GEH**C**E**C**SP**C**	T**C**GRATMPSG	RENRRAN**C**S**C**	GAS**C**N**C**AS**C**A	SA
TaMT4	MG.....	..**C**DDK**C**G**C**A	VP**C**PGGTG**C**R	**C**TS...ARSG	AAAGEHTT**C**G	**C**GEH**C**G**C**NP**C**	A**C**GREGTPSG	RANRRAN**C**S**C**	GAA**C**N**C**AS**C**G	SATA
QaMT4	MG.....	..**C**DDK**C**G**C**A	VP**C**PGGTG**C**R	**C**AS...S.AR	SGGGDHTT**C**S	**C**GDH**C**G**C**NP**C**	R**C**GRESQPTG	RENRRAG**C**S**C**	GDS**C**T**C**AS**C**G	STTTTAPAAT T

2.1.3.3 Isolation and Metal binding Characteristics of Plant MTs

Although MT genes have been investigated in many plants, purification of the MT proteins from plant tissues has proven to be very difficult due to instability of the proteins in the presence of oxygen and their susceptibility to proteolysis especially within the long spacer region (Kille et al., 1991).

Several plant MTs have been expressed as recombinant proteins in *E. coli* and *A. thaliana* to examine metal binding properties of these proteins. Ec protein is the first characterized plant MT and is found to associate with Zn at approximately 5mol/mol protein (Lane et al., 1987). An MT gene from pea, $PsMT_A$ was overexpressed in *E. coli* via a heat inducible expression vector and the recombinant protein was found to bind Cd (Kille et al., 1991). Another Type 1 $PsMT_A$ coupled to GST fusion protein was expressed in *E. coli* bound Cu, Cd and Zn with the highest affinity for Cu (Tommey et al., 1991). Moreover, expressing $PsMT_A$ as GST fusion in *E. coli* resulted in accumulation of Cu (Evans et al., 1992) and a similar experiment using fava bean Type 1 and Type 2 MTs resulted in binding of Cu and Cd, and weakly Zn (Foley et al., 1997). Arabidopsis MT1 and MT2 genes were expressed in MT-deficient strains of yeast and Synechococcos and they complemented these mutations restoring tolerance to Cu and Zn (Zhou and Goldsbrough, 1994; Robinson et al., 1996). A new procedure was used to purify Arabidopsis MT1, MT2 and MT3 proteins from plant extracts based on the size, SH content and affinity for Cu with copper- and thiol-affinity chromatography in which proteins were first stripped of Cu. Incubation of purified proteins with Cu revealed Cu/protein ratios of 8.4, 7.3, and 5.5 for MT1, MT2 and MT3, respectively (Murphy et al., 1997). A Type 2 MT, QsMT from *Quercus suber* was expressed in *E. coli* in the presence of Zn, Cd and Cu and was found to have high binding capacity for Cd ions (Mir et al., 2004).

2.1.3.4 Structure of Plant MTs

In contrast to comprehensive information on the structure of mammalian MTs, there is hardly any data on plant MT structure. Similarly, the role/structure of the spacer region in holo-MT is unknown. The general speculation about the existence of long

spacer region is that it may be essential for the conformational organization of Cys rich domains upon metal binding (Robinson et al., 1993).

Two different models have been proposed for plant holo-MT structure; hairpin and dumbbell model. In hairpin model two Cys-rich domains interact with each other to form a single cluster and the spacer region does not participate in metal binding. This model was proposed for pea MT (Kille et al., 1991) and recently for QsMT from *Q. suber* (Domenech et al., 2006). In the dumbbell model there are two metal clusters for each two Cys-rich domains and it was proposed for a kiwi Type 3 MT (Zhu et al., 2000) and for durum wheat Type 1 MT (Bilecen et al., 2005).

In 1991 for the first time, an MT from pea, $PsMT_A$ was overexpressed in *E. coli* in the presence of Cd. The Cd/$PsMT_A$ ratio was found to be between 5.6 to 6.1. In this study it was shown, for the first time, that binding of Cd was able to protect the spacer region of protein from proteolytic degradation. In the proposed hairpin model it was suggested that residues 2-21 and 56-75 and two Cys rich metal binding domains of holo-PsMTA were folded together by binding of Cd which is called hairpin model (Figure 2.5) (Kille et al., 1991).

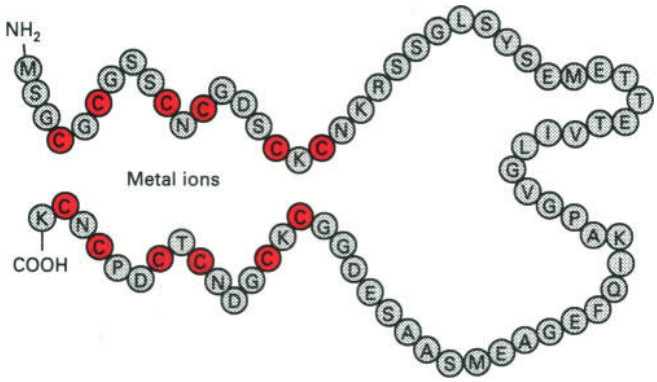

Figure 2.5: An assumed hairpin structure model of metallothionein protein associated with metal ions (Kille et al., 1991).

Several Type 3 MTs have been characterized in more detail in terms of metal binding. The purified GST-MT3-A fusion protein from oil palm, *Elaeis guineensis* was found to have similar metal binding properties to Type 1 and 2 products. The type 1 gene from pea (*PsMTA*) and type 2 gene from *Arabidopsis* (*MT2*) expressed as GST

fusion proteins in *E. coli* each bind Zn with strong affinities and it was found that the half of dissociation pH value of Zn from GST/MT3-A was found as 5.1 which was close to values obtained from PsMTA and MT2 indicating that GST-MT3-A bound Zn with strong affinity. It was suggested that the identical arrangement of Cys residues in the C-terminal domains could be the explanation for this similarity (Abdullah et al., 2002).

Several studies have shown that the metal content of plant MTs is lower than that of mammalian MTs. A Type 2 QsMT from *Q. suber* having 14 Cys residues bound Zn with a major Zn_4-QsMT and two minor Zn_3-QsMT and Zn_5-QsMT similar to pea Type 1 $PsMT_A$ (Tommey et al., 1991) and these values were lower as compared to mammalian Zn_7-MT1 having18 Cys residues (Mir et al., 2004).

In a recent study a Type 3 MT, MT3, and its two mutant forms have been characterized from *Musa acuminata* (banana) for metal binding properties. The existence of a weaker metal ion coordination site and lower metal content compared to mammalian MTs were shown. To find the involvement of a histidine residue in metal binding two mutants in which the histidine (His) residue at position 46 was changed to a Cys, MT3_H46C, and to Ala, MT3_H46A, were constructed. In the presence of Zn, wild type MT3 and two mutants MT3_H46A and MT3_H46C yielded different species of $Zn_{3.0}$MT3, $Zn_{2.9}$MT3_H46A and $Zn_{4.0}$MT3_H46C and incubation with Cd^{2+} resulted in $Cd_{4.3}$MT3, $Cd_{4.1}$MT3_H46A and $Cd_{4.3}$MT3_H46C. Thus, Zn binding was enhanced by the addition of Cys residue, but, for Cd binding no difference between wild type and MT3_H46C mutant form was observed. It was also found that all 10 Cys residues in MT3 and 11 Cys residues in MT3_H46C were involved in metal binding. The half-dissociation pH values of Zn^{2+} and Cd^{2+} ions were found similar to the previously found values of 5.6 Zn^{2+}MT1 and 4.0 Cd^{2+}MT1 from pea MT1GST fusion protein (Tommey et al., 1991). The half-dissociation pH values indicate overall pH stability of metal binding and this stability in MT3 was lower than mammalian MTs and Type 4 MTs. In this study different metal-thiolate cluster structures were proposed as shown in Figure 2.6. Column (A) shows the involvement of 11^{th} residue in the formation of metal-thiolate cluster structures whereas column (B) shows structures without 11^{th} residue. (A.1) shows the structure of metal binding with the involvement of His residue and might be seen in Zn_3MT3. Also Zn_3MT3 with Zn_3MT3_H46A might have a structure as

in (B.1). Confirmations as in (A.2) might be considered in Zn_4MT3, Zn_4MT3_H46C, Cd_4MT3 and Cd_4MT3_H46C and for (B.2) Zn_4MT3, Cd_4MT3 and Cd_4MT3_H46A. By releasing some of steric strains from (A.2), an alternative arrangement was obtained in (A.3) and showed a metal-thiolate cluster similar to M_4Cys_{11} cluster of mammalian MTs or to $M_4Cys_9His_2$ of bacterial MT. It is also suggested that Cd^{2+} ion was better occupying the bridging position between the two clusters due to its ionic radius (Freisinger, 2007).

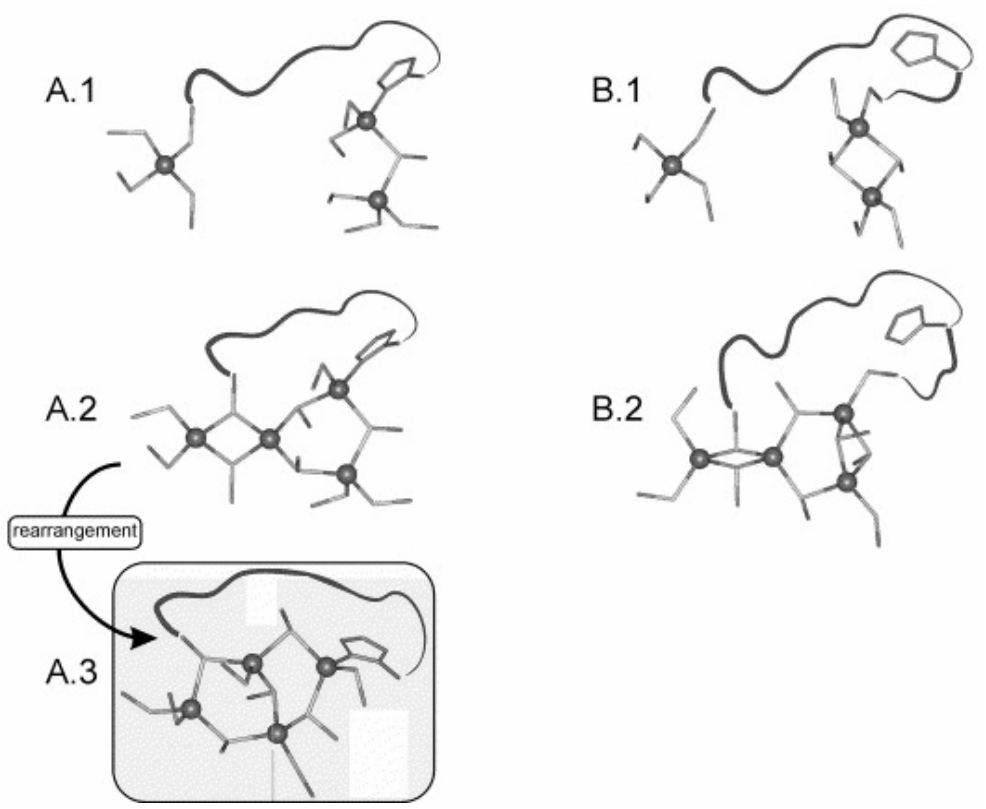

Figure 2.6: The proposed hypothetical structures of metal-thiolate clusters in MT3. Column (A) represents the participation of 11th residue in of metal-thiolate cluster whereas column (B) shows structures without 11th residue; the involvement of His residue (A.1), the involvement of Cys residue (A.2), and an alternative arrangement (A.3) (Freisinger, 2007).

A recent study was directed towards understanding the role of spacer region in folding of QsMT and structural differences between Zn- and Cd-QsMT proteins using Raman and infrared spectroscopy. QsMT has one spacer region separated by two Cys-rich domains with 8 and 6 Cys residues respectively and has an additional His residue.

The average metal ion content of QsMT were found to be higher in Cd-QsMT than Zn-QsMT which was Cd_6QsMT and Zn_4QsMT, therefore it was suggested that QsMT has distinct Zn^{2+} and Cd^{2+} binding potential and resulted in different metal cluster structures; a more compact structure and a reduced protein volume for Zn_4-QsMT compared to Cd_6-QsMT. As a result the observation was that Zn-QsMT folded with four Zn^{2+} ions without participation of His residue in metal binding, whereas the main structure in Cd-QsMT was composed of six Cd^{2+} ions and His residue in the spacer region. For the secondary structure it was found that Zn- and Cd-QsMT were composed of mainly β-sheets, probably in spacer region and β-turns in Cys-rich domains. This high percentage of β-sheets in the secondary structure is fairly rare among MTs (Domenech et al., 2007).

Recently, it was shown that wheat Ec was able to bind six Zn^{2+} ions in two metal-thiolate clusters (Peroza and Ferisinger, 2007; Leszczyszyn et al., 2007). Also it was observed that two conserved His residues participated in metal binding either directly or by preservation of hydrogen bonding within the cluster (Leszczyszyn et al., 2007).

2.1.3.5 Function of Plant MTs

Plant MTs display variation in terms of sequence, especially in metal binding Cys residues, and this indicates that functions of various plant MTs are also diverse (Cobbet and Goldsbrough, 2002).

Identification MT proteins in plants is difficult due to the instability of these proteins in the presence of oxygen. The function of plant MT proteins is still not completely understood, and most of the information comes from mRNA expression studies. The suggested roles for plant MTs, similar to their mammalian counterparts, are maintaining metal ion homeostasis, detoxification of toxic metals, and protection against oxidative stress (Cobbet and Goldsbrough, 2002; Wong et al., 2004; Akashi et al., 2004).

Plant MT proteins have the capacity of binding metal ions and some plant MT genes are induced by metals. These results suggest that MTs play an important role in

metal tolerance and homeostasis in plants. Studies have shown that MT was induced by various metal ions, mostly Cu and to a lesser extent Cd and Zn. However, MT expression in response to metal ions shows variation in different plant species and tissues and in terms of types of MT. In general the literature suggests that MTs are involved in Cu tolerance and homeostasis. For example, in *Arabidopsis* Cu treatment resulted in induction of MT gene expression and limited induction with Cd and Zn were observed (Zhou and Goldsbrough, 1994). Furthermore, in *Triticum aestivum* it was shown that five different MT genes; *wali*1 to *wali*5 were induced by aluminum stress and their expression was reduced when the Al was removed (Snowden and Gardner, 1993). In contrast, in *Vicia faba* MT transcript level was not induced by Cu treatment as well as Cd, Fe and Zn (Foley et al., 1997). Moreover, *Mimulus guttatus* MT was repressed by Cu treatment (De Miranda et al., 1990).

According to the transcript levels plant MTs are suggested to play different roles at different stages of plant development. For example in rice a serial analysis of gene expression (SAGE) study has shown that MT genes represent 3% of all transcripts in two-week-old seedlings (Matsumura et al., 1999).

A number of studies show that expression of MT genes is induced during senescence (Cobbet and Goldsbrough, 2002). Senescence involves relocation of released nutrients including metal ions to other organs from senescing cells and this process is also related to oxidative stress. Because senescence involves degradation of protein, lipid and nucleic acids these processes result in significant metabolic changes. These degradative processes, particularly for lipids, often result in increased production of reactive oxygen species (ROS). An MT gene in *Brassica napus* was induced at high level during leaf senescence (Buchanan-Wollaston, 1994). In rice, high transcript level of Type 2 ricMT was found in senescing stems (Yu et al., 1998). In a study associated with the senescence related genes in Arabidopsis it was shown that MT1 accumulated during natural leaf senescence (Miller et al., 1999). Another study in Arabidopsis revealed that expression of MT genes was highly induced by Cu especially in trichomes and increased during senescence (Guo et al., 2003). In Arabidopsis a LSC54 MT gene shown previously to increase during leaf senescence was also induced in response to increase in ROS (Navabpour et al., 2003). It has been proposed that MT proteins may serve as metal chelators for transferring released metal ions from senescing cells to

developing cells or seeds for protection from toxic effects of metal ions or they may be involved in scavenging the ROS generated during senescence (Cobbet and Goldsbrough, 2002; Mir et al., 2004).

Recently increasing evidence suggests an alternative role for plant MTs as ROS scavengers as observed in animals (Akashi et al., 2004; Wong et al., 2004). Induction of MTs are strongly induced by oxidative stress (Tate et al., 2002; Mir et al., 2004), this may be due to MTs role in scavenging reactive oxygen species (ROS). The expression of a watermelon Type 2 CLMT2 gene was induced by drought/high light stress in the leaves and the recombinant CLMT2 protein showed a high activity for scavenging hydroxyl radicals (Akashi et al., 2004). In rice MT OsMT2b was also shown to be a ROS scavenger and down regulation of its expression was involved in defense signaling in response to resistance (Wong et al., 2004). MT expression was induced in *T. tubifex* when it was exposed to the pesticide chitosan which causes chemical stress in relation with oxidative stress (Mosleh et al., 2007). A recent study shows a Type 1 Ch1MT1 expression was induced by several abiotic stresses, salts, a ROS inducer and metal ions (Zn and Cu) and improved the ability of MT to scavenge ROS (Nishiuchi et al., 2007).

Plant MT gene expression is regulated also by other stress factors such as wounding (Choi et al., 1996) and pathogen infection (Butt et al., 1998). Generally plants undergo oxidative stress associated with generation of ROS when exposed to wounding or pathogen infection. These conditions induce expression of some MTs suggesting that these may be a part of the general stress response (Cobbet and Goldsbrough, 2002).

Recently several studies revealed that plant MTs may have a role during developmental processes. It was shown that in rice the *OsMT-II-1a* gene expression was highly abundant in developing seeds and 2-day glumes after pollination. This result suggested that seed development and pollination might be mediated partly by *OsMT-II-1a* gene expression (Zhou et al., 2005). In *Zea mays* a Type 2 MT *MZm3-4* gene was expressed only in male reproductive organs during microsporogenesis (Charbonnel-Campaa et al., 2000).

Chapter 3

MATERIALS and METHODS

3.1 MATERIALS

3.1.1 Chemicals

All chemicals were supplied by Aldrich (Germany), GE-Biosciences (Sweden), Amresco (USA), Applichem (Germany), BioRad (USA), Fermentas (Germany), Fluka (Switzerland), Invitrogen (Germany), Merck (Germany), Riedel de Häen (Germany) Roche (Germany), Promega (USA), Qiagen (Germany) and Sigma (USA). All chemicals are listed in Appendix A.

3.1.2 Primers

Primers were designed according to Kinzler and Vogelstein (1989), Watson et al., (2000) and synthesized by Iontek (Turkey) and SeqLab (Germany).

3.1.3 Enzymes

Restriction enzymes *Eco*RI, *Hind* III, *Bam*HI and *Tag*I were purchased from Promega and Fermentas. T4 DNA Ligase was supplied by Fermentas and Taq Polymerase was supplied by Fermentas. Omniscript Reverse Transcriptase (QIAGEN) was used in production of cDNA. Shrimp Alkaline Phosphatase and Klenow fragment were supplied by Fermentas.

3.1.4 Cells

E.coli strains BL21 (DE3).

3.1.5 Buffers and Solutions

All buffers and solutions used in recombinant DNA manipulations, except those provided with commercial kits, were prepared according to Sambrook et al., (2001). Buffers and their compositions are presented in Appendix B.

3.1.6 Culture Media

3.1.6.1 Liquid Medium

LB (Luria-Bertani) Broth from SIGMA was used to prepare liquid culture media for bacterial growth. The standard components of LB broth are 10 g/L Tryptone (pancreatic digest of casein), 5 g/L Yeast extract and 5 g/L NaCl. For preparing 1 liter LB broth 20 g powder is suspended in 1 L of distilled water.

3.1.6.2 Solid Medium

LB (Luria-Bertani) Agar from SIGMA was used for the preparation of solid culture media for bacterial growth. The standard components of LB agar are 10 g/L Tryptone (pancreatic digest of casein), 5 g/L Yeast extract, 5 g/L NaCl and 15 g/L Agar. For preparing 1 liter LB agar 40 g powder is suspended in 1 L of distilled water.

3.1.7 Plant Material

Expression studies were carried using *Triticum durum* Balcalı-85 cultivar.

3.1.8 Equipments

List of all the equipments used during this study are presented in Appendix C.

3.2 METHODS

3.2.1 Nucleic acid Methods

3.2.1.1 Genomic DNA Isolation from Plant

Genomic DNA was isolated from plants using a modified CTAB procedure. 2 gram plant material was mixed with 8.3 ml solution consisting of 8.08 ml prewarmed CTAB (cetyltrimethylammonium bromide) extraction buffer, 0.17 ml 2-mercaptoethanol to give a final concentration of 2% and 100 µg/ml proteinase K and incubated at 55^{o}C for 60 minutes. 6.7 ml phenol:chloroform:isoamylalcohol (PCI) (25:24:1) was added and vortexed briefly. After centrifugation at 13000g for 10 minutes at room temperature, the supernatant was transferred to a new tube, mixed with 6.7 ml PCI and centrifuged again. This extraction was repeated 3 times. DNA was precipitated by the addition of the 2/3 volume of isopropanol and incubating for at least 30 minutes at -20^{o}C. DNA was collected by centrifugation at 13000*g* for 20 minutes at 4°C. The pellet was resuspended in 1.3 ml TE buffer. 13.3 µl of RNaseA (from 10 mg/ml stock) was added and incubated at 37°C for 30 minutes. To extract DNA 1.3 ml CI was added and centrifuged at 13000g for 10 minutes at room temperature. The supernatant was transferred to a new tube and precipitated with ½ volume of NH_4Ac and 2 volumes of 100% ethanol and incubated for at least 30 minutes at -20^{o}C. Genomic DNA was collected by centrifugation at 13000*g* for 20 minutes at 4°C. The pellet was washed twice with 70% ethanol and air-dried. The genomic DNA was dissolved in 330 µl ml of TE buffer and incubated at 65°C for 1 hour and then centrifuged at 16000g for 10 minutes at 4°C. The supernatant was transferred to a clean tube and stored at 4°C.

3.2.1.2 Total RNA Isolation from Plants

200 mg leaf or root tissue was ground with 1.5 ml Trizol reagent inside a mortar until it became liquid. 1 ml of the liquid was taken into an eppendorf tube, which was

kept on ice while processing the other samples. After processing all the samples, they were incubated at room temperature for 10 minutes. After addition of 0.4 ml chloroform from a regular stock bottle, tubes were shaken and incubated at room temperature for a further 5 minutes. After centrifugation at 13400g for 15 minutes at 4^{o}C, the upper layer containing the total RNA was transferred to a fresh tube. To precipitate RNA 0.5 ml isopropanol was added and samples were incubated at room temperature for 10 minutes. Total RNA pellet was collected by centrifugation at 13400g for 10 minutes at 4^{o}C and washed with 1ml 75% ethanol. Then mixed by vortexing and centrifuged at 5400g for 5 minutes at 4^{o}C. After drying at room temperature for about 10 minutes, total RNA was resuspended in 20-50 µl formamide. In order to enhance dissolving, the sample was incubated at 55^{o}C for up to an hour. RNA samples were stored at -80°C.

3.2.1.3 Separation of DNA by Agarose gel

For the separation of high molecular weight DNA, 1% agarose gels containing 0.1 µg/ml ethidium bromide in 1xTAE was used. The samples were prepared by mixing with 6x loading buffer. Gels were run at 100 mV constant current for 30 minutes. Size of DNA fragments were estimated using MassRuler DNA Ladder Mix.

3.2.1.4 Separation of DNA by Polyacrylamide gel

For the separation of low molecular weight DNA fragments 7% nondenaturing polyacrylamide gel was used. Gel was prepared by mixing 6.8 ml distilled water, 2.4 ml 5xTBE, 2.8 ml acrylamide-bisacrylamide (29:1), 200 µl 10% ammonium peroxodisulfate and 10 µl TEMED. Gels were run at 25 mA constant current for about 1 hour and were stained in 1xTBE buffer containing 0.1 µg/ml ethidium bromide for 15 min at room temperature with shaking.

3.2.1.5 Determination of Nucleic acid Concentrations

RNA concentration was determined by measuring the absorption (A) of the samples at 260 nm and calculating the concentration (C) according to the formula: C(µg /µl) = A_{260} x 40 x Dilution Factor.

DNA concentration was determined by measuring the absorption (A) of the samples at 260 nm and calculating the concentration (C) according to the formula: C(µg /µl) = A_{260} x 50 x Dilution Factor.

3.2.1.6 cDNA Synthesis

Reverse transcription of 2 µg of total RNA was performed according to the manufacturer's instructions of Omniscript Reverse Transcriptase kit (QIAGEN). The cDNA was stored at -20°C.

3.2.1.7 Preparation of the Radioactively labeled cDNA Probe

The dMT cDNA was used as probe for both Southern blotting and labeled with ^{32}P-dATP by 5'end labeling. For labeling reaction 2 µg cDNA and 6000Ci/mmol ^{32}P γ-ATP isotope, 10x T4 polynucleotide kinase buffer, T4 polynucleotide kinase enzyme and dH_2O were used and incubated at 37^{o}C for 1 hour.

3.2.1.8 Southern Blotting

15 µg aliquots of genomic DNA were digested overnight with EcoRI or BamHI at 37^{o}C. Digested DNA samples were denatured at 95^{o}C for 5 min and separated by electrophoresis on a 1% agarose gel in 1x TAE buffer containing 0.2 µg final concentration of EtBr at 50 volt for about 4 hours at 4^{o}C. After visualization on UV, the gel was cut and rinsed with dH_2O to remove EtBr. Before blotting the gel was washed for 10 minutes in depurination solution (250 mM HCl), which depurinates the DNA fragments thus allowing more efficient transfer from the gel to membrane, then the DNA gel was washed in denaturation solution (1.5 M NaCl, 0.5 M NaOH) for 25 minutes and finally neutralized with 1.5 M NaCl, 0.5 M Tris-HCl pH 7.5 for 30 minutes. Finally the gel was placed into the transfer buffer of 10x sodium chloride/sodium citrate solution (SSC).

3.2.1.9 Blotting, Hybridization and Detection

The DNA was transferred by downward capillary blotting on to a Whatman Nytran SPC (super positive charge) nylon membrane. A 4-6 stack of paper towel and 4 pieces of whatman 3MM paper, the same size as the nylon membrane, was placed on a tray at the bottom of the 10x SSC soaked nylon membrane. The gel was placed on top of the nylon membrane under 2 more pieces of wet whatman 3MM paper. 2 larger pieces of whatman 3MM paper as a wick were soaked in 10x SSC transfer buffer and stacked on the top under a weight as the entire sandwich and left overnight to transfer. The membrane was first baked at 80^{o}C for 30 min and exposed to ultraviolet radiation for 5 minutes to covalently crosslink the DNA to the membrane. The blot was then soaked in rotating at 60ºC in pre-hybridization buffer for 30 minutes.

3.2.1.10 Autoradiography

After hybridization, blots were washed twice in low stringency buffer; 2x SSC, 0.1% SDS (2-5ml/cm^2) for 15 minutes at 60ºC for Southern blotting and at 65ºC for Northern blotting followed by high stringency washes with 1x SSC, 0.1%SDS for 15 minutes each at again 60ºC or 65ºC. Finally, the blot was exposed to Kodak BioMax MS film for 16 hours to 2 days at -80ºC with Cronex intensifying screens.

3.2.1.11 Whole Genome PCR

3.2.1.11.1 Preparation of DNA for Whole Genome PCR

Total 4 µg *T. durum* cv. Balcalı 85 genomic DNA was digested with Taq I enzyme and sonicated 25 minutes to get average sizes of 300 bp. Sonicated DNA was subjected to Klenow reaction to fill in the sticky ends created by Taq I. DNA fragments in 100 µl reaction mixture containing 10x Klenow buffer and 10 mM dNTP mix were incubated for 1 hour at 37^{o}C. In order to prevent self ligation of blunt ends DNA was dephosphorylated by SAP (Shrimp Alkaline Phosphatase) and incubated at 37^{o}C for 30 minutes. DNA was then extracted with phenol:chloroform:isoamylalcohol (25:24:1) and precipitated with ethanol. DNA was ligated to 15 µg each of linkers using T4 DNA ligase in 100 µl ligase buffer containing 10x T4 ligase buffer, 50% PEG-4000 and

incubated at 16^{o}C for overnight. To prevent self ligation of linkers the ligation mixture was digested with *Taq*I enzyme at 37^{o}C for 2 hours. After restriction digestion linker-ligated DNA was precipitated with ethanol and resuspended in 10 µl dH_2O.

3.2.1.11.2 Protein-DNA Interaction

Protein was bound to Glutathione Sepharose 4 Fast Flow (GE-Biosciences) following the manufacturer's instructions. 1 ml of slurry of Glutathione Sepharose beads were centrifuged at 500g for 5 minutes to get rid of EtOH and were washed with 5 volumes of dH_2O and protein binding buffer. The GSTdMT protein was added to Glutathione Sepharose beads and incubated for 30 minutes by shaking. In order to remove unbound proteins the protein-bound beads were washed with protein binding buffer.

For DNA-protein interaction linker-ligated genomic DNA was mixed with GSTdMT bound glutathione beads and with 200 µl of DNA binding buffer pH 7.5; 50 mM Hepes, 120 mM NaCl, 5 mM $MgCl_2$, 50% glycerol and 1 mM DTT. The mixture was rotated at room temperature for 1 hour before centrifugation at 16000g for 10 minutes. Bound DNA was then eluted by the addition of 200 µl elution buffer pH 8.0; 20 mM HEPES and 1mM NaCl. The mixture was rotated for 30 minutes at room temperature before centrifugation at 16000g for 10 minutes. The eluate was precipitated with ethanol and resuspended with 10 µl dH_2O before being used as a PCR template.

3.2.1.11.3 PCR Amplification of Linker-ligated DNA

For amplification of recovered DNA fragments, a 50 µl of PCR reaction was prepared using 2 µl of template, 1 µl of dNTPs (10 mM each), 5 µl of each primer (1 µM), 5 µl 10 x PCR buffer, 4 µl of $MgCl_2$ (25 mM), 1 µl of Taq polymerase and the volume was completed with dH_2O. The amplification was carried out in an Eppendorf cycler with the following conditions: 95°C x 5 min, 30 x {95°C x 1 min, Tm x 1.5 min, 72°C x 1 min}, 72°C x 7 min. The annealing temperature and time was adjusted according to primer pairs used.

3.2.2 Protein Analysis

3.2.2.1 Bacterial Cell Growth

Cells were grown overnight in LB Broth (Luria Bertani) medium prior to any application. LB Agar (Miller's LB agar) solid medium was used as selective and unselective solid medium for the growth of bacteria.

3.2.2.2 Expression of GSTdMT

E.coli BL21 (DE3) cells transformed with recombinant pGEX-*dmt* were grown overnight by using LB broth medium with 100 μg/ml ampicillin at 37^{o}C. The next day 1.5 Liter LB containing 0.1mM $CdCl_2$ and 100 μg/ml ampicillin were inoculated with fresh overnight culture at 1:50 ratio and grown at 37^{o}C. When optical density at 600 nm reached to 1, expression of GSTdMT protein was induced by adding IPTG (isopropyl-B-D-thiogalactoside) at a final concentration of 0.7 mM. After growing for further 6 hours, cells were pelleted at 8275g for 25 minutes using a Sorvall centrifuge with SLA-3000 rotor. Pellets were washed with HEPES binding buffer containing 20 mM HEPES, 100 mM NaCl, 2.5 mM $MgCl_2$ and 0.1 mM $CdCl_2$ in a glove bag filled with argon and stored at –80^{o}C.

3.2.2.3 Purification of GSTdMT Recombinant Protein

All buffers were degassed and purged with argon (Ar) prior to using and all procedures were carried out in Ar environment. The cell pellet was resuspended in 76 ml HEPES binding buffer pH 8.0 containing 0.1mM $CdCl_2$, 1 mM DTT, 0.5 mM PMSF and 2 tablets of EDTA-free protease inhibitor cocktail under argon filled glove box and the cells were lysed by sonication (Fisher Bioblock Scientific) at 8 sn pulse and 9 sn stop for 10 minutes at 4^{o}C under Ar flow. 20% Triton X-100 was added to a final concentration of 1% and the suspension was mixed gently for 45 minutes at 4^{o}C to facilitate solubilization of proteins. After clearing by centrifugation at 4^{o}C at 20000g for 1 hour, the supernatant from the cell lysate was loaded onto a 5 mL GSTrap$^{(R)}$ FF prepacked affinity column (GE-Biosciences) which was previously equilibrated with HEPES binding buffer using a peristaltic pump with a constant flow rate of 1

mL/minute. The bound fusion protein was eluted with elution buffer pH 8.0 containing 50 mM Tris- HCl, 100 mM NaCl, 20 mM reduced Glutathione, 1 mM DTT, 0.5 mM PMSF and the EDTA-free protease inhibitor cocktail. Fractions from the affinity column were pooled and dialyzed against HEPES binding buffer with 1 mM DTT and 0.5 mM PMSF at 4^{o}C. After dialysis the fusion protein was applied to a HiLoad $^{(R)}$ 26/60 Superdex 75 column previously equilibrated with HEPES binding buffer containing 1 mM DTT and protein was eluted at a flow rate of 1.5 mL/min with HEPES binding buffer containing 1 mM DTT. Chromatography was carried out using the AKTA FPLC System (GE-Biosciences) and the absorbance of the eluate was monitored at 280 nm. Fractions of 500 µl were collected and they were analyzed by SDS-PAGE.

3.2.2.4 Purification of dMT Protein

The purification procedure of dMT protein was based on Capdevilla et al with some modifications but largely was same as GSTdMT protein purification until binding of lysate to the GSTrap FF affinity column. Instead the supernatant was used to purify the GSTdMT fusion proteins by batch affinity chromatography with Gluthatione-Sepharose-4B at a volume ratio of 1:10 matrix:sample. The mixture was incubated with gentle agitation for 30 minutes at 4^{o}C and then centrifuged at 4^{o}C at 500 g for 5 minutes. After three washes with Binding buffer; 50 mM Tris-HCl pH 7.5, 2.5 mM $MgCl_2$, 100 mM NaCl containing 1mM DTT; mixing 10 minutes then centrifugation at 500g for 5 minutes, 10 U/mg thrombin was poured into 10 ml beads and protein mixture and digestion carried out overnight at 4^{o}C. After centrifugation at 500g for 5 minutes the GST portion remained bound to beads but dMT part was eluted together with thrombin. Total 10 ml eluate was then five-fold concentrated using Concentrator with a cutoff of 10kD at 15000g for 33 minutes and then fractionated using HiLoad® 16/60 Superdex-75 size exclusion column with Binding buffer and 1mM DTT, 1 ml/min.

3.2.2.5 SDS Polyacrylamide Gel Electrophoresis (PAGE)

SDS-PAGE was used to separate protein samples. Protein samples (50 ng) were heated at 100^{o}C for 10 minutes in 2x SDS-PAGE sample buffer, and loaded onto 12% SDS polyacrylamide gels with a 5% stacking gel. Gels were run at 80 V constant

voltage in 1x SDS running buffer until the bands passed to resolving gel and electrophoresis was completed at 120 V.

3.2.2.6 Native-PAGE

The protein samples were analyzed on 10% native-polyacrylamide gels which were prepared without a stacking layer. Buffers used were the same as those used in denaturing gels except that SDS was omitted from all. Sample buffer did not contain SDS and samples were not boiled to avoid denaturing. Gels were run at 80 V constant voltage in 1x Native-PAGE running buffer until the bands passed to resolving gel and electrophoresis was completed at 120V.

3.2.2.7 Coomassie Blue Staining

For visualization, SDS- and Native-PAGE gels were stained with Coomassie blue staining solution and then destained in destaining solution.

3.2.2.8 Silver Staining

For visualization, SDS- and Native-PAGE gels were stained with silver staining plus kit (BioRad).

3.2.2.9 Western Blotting

SDS-PAGE was used to separate protein samples. Protein samples (50 ng) were heated at 100^{o}C for 10 minutes in 2x SDS-PAGE sample buffer and loaded onto 12% SDS polyacrylamide gels with a 5% stacking gel. After electrophoresis for approximately 1 hour at 25 Amps, proteins were transferred to PVDF membrane in transfer buffer using Novex western transfer apparatus at 25V overnight at 4^{o}C. The transfer sandwich consisted of three pre-soaked blotting pads, then a piece of 3MM Whatman paper, the gel, the PVDF membrane, another piece of 3MM Whatman paper, and the other three pre-soaked blotting pads. After overnight transfer, PVDF membrane was incubated in blocking solution for 1 hour at room temperature with shaking. Then membrane was washed with PBS-T for 15 minutes at room temperature with shaking.

Followed by incubation with anti-GST HRP conjugate at a dilution of 1/10.000 in 10 ml fresh blocking solution for 1 hour at room temperature on an orbital shaker. Membrane was then washed three times with PBS-T for 15 minutes at room temperature and proteins were visualized using ECL advance western blotting detection systems (GE-Biosciences).

3.2.2.10 Determination of Protein Concentration

In order to calculate the protein concentration, absorption at 280 nm was measured and calculation was done according to the calculated GSTdMT coefficient of 1.232.

3.2.2.11 Dynamic Light Scattering

Dynamic Light Scattering (also known as PCS - Photon Correlation Spectroscopy) measures Brownian motion and provides information about the size of the particles in a solution. Particles are illuminated with a laser and the intensity fluctuations in the scattered light are analyzed. In practice, particles suspended in a liquid are never stationary; they move due to Brownian motion. Brownian motion is the movement of particles due to the random collision with the molecules of the liquid that surrounds the particle. An important feature of Brownian motion for DLS is that small particles move quickly and large particles move more slowly.

The fundamental size distribution generated by DLS is an intensity distribution; this can be converted, using Mie theory, to a volume distribution. This volume distribution can also be further converted to a number distribution. However, number distributions are of limited use as small errors in gathering data for the correlation function. A very simple way of describing the difference between the intensity, volume and number distributions is to consider a sample that contains only two sizes of particles (5nm and 50nm) but with equal numbers of each size particle. The first graph in Figure 3.1 shows the result as a number distribution. As expected the two peaks are of the same size (1:1) as there are equal numbers of particles. The second graph shows the result of the volume distribution. The area of the peak for the 50nm particles is 1000 times larger the peak for the 5nm (1:1000 ratio). This is because the volume of a 50nm particle is

1000 times larger that the 5nm particle. The third graph shows the result of an intensity distribution. The area of the peak for the 50nm particles is now 1,000,000 times larger the peak for the 5nm (1:1000000 ratio). This is because large particles scatter much more light than small particles (the intensity of scattering of a particle is proportional to the sixth power of its diameter). In conclusion, the basic distribution obtained from a DLS measurement is intensity all other distributions are generated from this and the intensity distribution provides a sensitive measure for the polydispersity and size of particles in a solution.

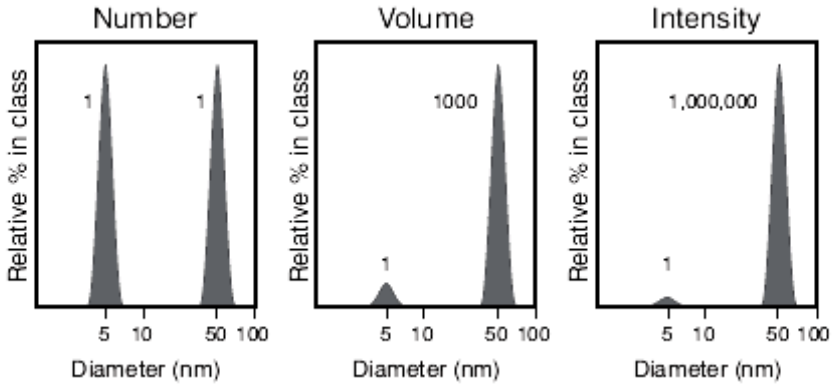

Figure 3.1: Difference between the intensity, volume and number size distribution differences of two sizes of particles; 5nm and 50nm.

Fractions of recombinant GST and GSTdMT proteins were analyzed for the presence of different oligomers by DLS using a Zeta-sizer Nano ZS (Malvern Instruments).

3.2.2.12 Small angle X-ray Scattering (SAXS)

Small angle X-ray scattering (SAXS) is an analytical X-ray application technique for the structural characterization of macromolecules. In SAXS experiments, the sample is irradiated by a well-defined, monochromatic X-ray beam. When a non-homogeneous medium, for example proteins in water, is irradiated, structural information of the scattering particles can be derived from the intensity distribution of the scattered beam at very low scattering angles.

The SAXS data were collected on the X33 camera of the European Molecular Biology Laboratory (EMBL) on the storage ring DORIS III of the Deutsches Elektronen Synchrotron (DESY) in Hamburg, using a mar345 Image Plate detector. Scattering patterns were recorded in the range of momentum transfer $0.15 < s < 3.5$ nm^{-1} where $s = 4\pi sin(\theta)/\lambda$, 2θ is the scattering angle and $\lambda = 0.15$ nm is the X-ray wavelength.

Solutions of GSTdMT fusion protein and GST protein in HEPES buffer were measured at several concentrations between 1 and 41 mg/ml. Because of aggregation at higher concentrations, only the scattering curves measured at concentrations about 3 mg/ml were used in analyses. Bovine serum albumin (BSA) was measured as a molecular mass standard at 5 mg/ml in a buffer with 50 mM Hepes, pH 8.0 and 150 mM NaCl. Data reduction, background subtraction and correction for detector response followed standard procedures using the program PRIMUS (Konarev et al., 2003).

The forward scattering *I(0)* and the radius of gyration R_g were evaluated using the Guinier approximation assuming that at very small angles ($s < 1.3/R_g$) the intensity is represented as $I(s) = I(0)\ exp(-(sR_g)^2/3)$. These parameters were also computed from the entire scattering pattern using the indirect transform package GNOM (Svergun, 1992), which also provides the distance distribution function *p(r)* of the particle. GNOM is an indirect transform program for small-angle scattering data processing. It reads one-dimensional scattering curves and evaluates a distance distribution function P(r) for monodisperse systems. The molecular mass (MM) of the solute was evaluated by comparison of the forward scattering with that from a reference solution of bovine serum albumin (66 kDa).

Low resolution models of the GSTdMT fusion protein were generated *ab initio* by the programs DAMMIN and GASBOR.

3.2.2.13 Extended X-ray Absorption Fine Structure (EXAFS)

Extended x-ray absorption fine structure (EXAFS) is a short-range technique that can provide structural information for a wide variety of materials and states of matter. For metalloproteins where transition metal atoms are in structurally or functionally important sites, EXAFS and x-ray absorption spectroscopy (XAS) can

provide detailed information on metal-ligand bond distances and geometry, respectively. This technique can be used independently or to supplement structural information derived from other techniques including X-ray crystallography or nuclear magnetic resonance spectroscopy.

The X-ray absorption spectra consist of two regions; the edge X-ray absorption near edge structure (XANES) and the EXAFS. The edge region spectrum reflects metal ion oxidation state, covalency, geometry, chemical shifts, etc. The role of metal site structure in enzymatic catalysis can be determined by comparing the XAS spectra of the active site with or without substrates or inhibitors. The EXAFS region provides direct structural information about the atomic neighbors of the metal atom such as number and identity of ligand atoms, and their precise bond distances.

EXAFS gives us information about the distances between central and neighboring atoms, the number and nature of neighboring atoms and changes in central-atom coordination with changes in experimental conditions. The main advantage of EXAFS analysis over X-ray Crystallography is that structures can be studied in non-crystalline forms (including liquid and frozen solutions). Among other applications, EXAFS has proven helpful in studying the behavior of non-crystalline materials, environmental samples, and metalloproteins in their naturally occurring states.

The EXAFS data were collected on recorded at beamline D2 of the European Molecular Biology Laboratory (EMBL) Outstation Hamburg at Deutsches Elektronen Synchrotron (DESY), Germany. The D2 DORIS storage ring operated at 4.5 GeV with Si (111) or Si (220) double-crystal monochromator.

3.2.2.14 Inductively Coupled Plasma Optical Emission Spectroscopy (ICP-OES)

ICP-OES is used for qualitative and quantitative determination of metals and certain non-metals in solution. The liquid sample is nebulised into plasma where the temperature is sufficiently high to break chemical bonds, release elements present and transform them into a gaseous atomic state. A number of the atoms pass into the excited state and emit radiation. The frequency of this radiation is characteristic of the element that emitted it and as such can be used for identification purposes.

The ICP uses very hot argon plasma to excite atoms into high energy states. As these atoms relax they emit light at characteristic wavelengths, or lines. The ICP can measure about 70 elements in aqueous solutions, including most metals. It cannot measure H, He, C, N, O, F, Ne, Cl, and some other elements. All sample solutions must be absolutely free of particulates, sediments, precipitates, suspended gels, or lipids. ICP was used for determination of Cd concentration in protein samples and for quantification of Cd from plant tissues.

3.2.3 Plant Methods

3.2.3.1 Plant Material

T. durum cv. Balcalı-85 cultivar is a Cd-tolerant genotype and was used in the experiments carried out under growth chamber conditions.

3.2.3.2 Plant Growth Conditions and Cadmium Treatments

Balcalı-85 seeds were surface sterilized with 1% (w/v) calcium hypochlorite for 10 minutes and then rinsed with distilled dH_2O. Seeds were germinated in perlite moistened with saturated $CaSO_4$ solution and germinated in the dark for 5 days at room temperature. Afterwards, seedlings were transferred to 2.5 L plastic pots containing continually aerated nutrient solutions composed of the following macro and micronutrients; 0.88 mM K_2SO_4, 2 mM $Ca(NO_3)_2$, 0.2 mM KH_2PO_4, 1.0 mM $MgSO_4$, 0.1 mM KCl, 100 µM Fe-EDTA, 1.0 µM H_3BO_3, 1.0 µM $ZnSO_4$, 1.0 µM $MnSO_4$, 0.2 µM $CuSO_4$, and 0.02 µM $(NH_4)6Mo_7O_{24}$.

Plants were grown for 7 days in a growth chamber under controlled conditions of light/dark regime 16/8 h, temperature 24/22^oC, relative humidity 60/70%, and photon flux density of 600-700 µmol m^{-2} s^{-1}. Nutrient solutions were renewed every 3 days.

After following 7 days, plants were treated with varying levels of Cd (0, 2, 5, 10 and 20 µM) in the form of $CdSO_4$. Nutrient solutions and Cd levels were renewed every 3 days. After 7 days following Cd application plants were harvested during which roots

and shoots were separated. Roots were rinsed with 2 mM $CaCl_2$ for about 15 minutes to remove surface absorbed Cd and then rinsed with distilled dH_2O. Then, roots and shoots used for determination of dry matter production and Cd concentration were dried at 70°C. Also 0.2 g roots and shoots were collected from each pot and immediately frozen in liquid nitrogen and stored at -80^{o}C.

3.2.3.3 Cadmium Concentration and Content

Dried root and shoot samples were ground and approximately 0.3 g ground sample was ashed at 500°C for 12 h followed by dissolving in 3.3 % HNO_3 (v/v) for determination of Cd concentration. The concentration of Cd was measured by inductively coupled argon plasma optical emission spectroscopy (ICP-OES, Varian, Australia) at 214.439 nm emission wavelength. The Cd content was calculated by multiplying the dry weight values of roots or shoots with their Cd concentration values.

Chapter 4

RESULTS

4.1 Purification of Homogeneous GSTdMT Protein

4.1.1 Calibration of the Column

HiLoad® 26/60 Superdex 75 size exclusion column (GE-Biosciences) was calibrated with low molecular weight calibration kit from GE-Biosciences and Vitamin B12 (Sigma) (Table 4.1). 20 mg of each low the molecular weight calibration proteins and 30 mg of Vitamin B12 were dissolved in 2 ml of 1x PBS buffer, pH 7.3 and eluted from column with the flow rate of 1.5 ml/min using the same buffer (Figure 4.1). The calibration curve was obtained from the elution profile and calculated according to the formula of Kav= (Ve-Vo)/(Vc-Vo) where Vc is the column volume, Vo is the column void volume and Ve is the elution volume. This curve was used for estimation of molecular weight of GST and GSTdMT (Figure 4.2) according to their elution volume from the size exclusion column.

Table 4.1: Protein samples used for column calibration and their molecular weights and elution volumes.

Protein	**loaded (mg)**	**MW (Da)**	**V_e (ml)**
Albumin	20	67000	147.44
Ovalbumin	20	49100	163.17
Chymotrypsinogen A	20	20400	187.97
Ribonuclease A	20	15200	213.56
Vitamin B12	30	1350	285.55

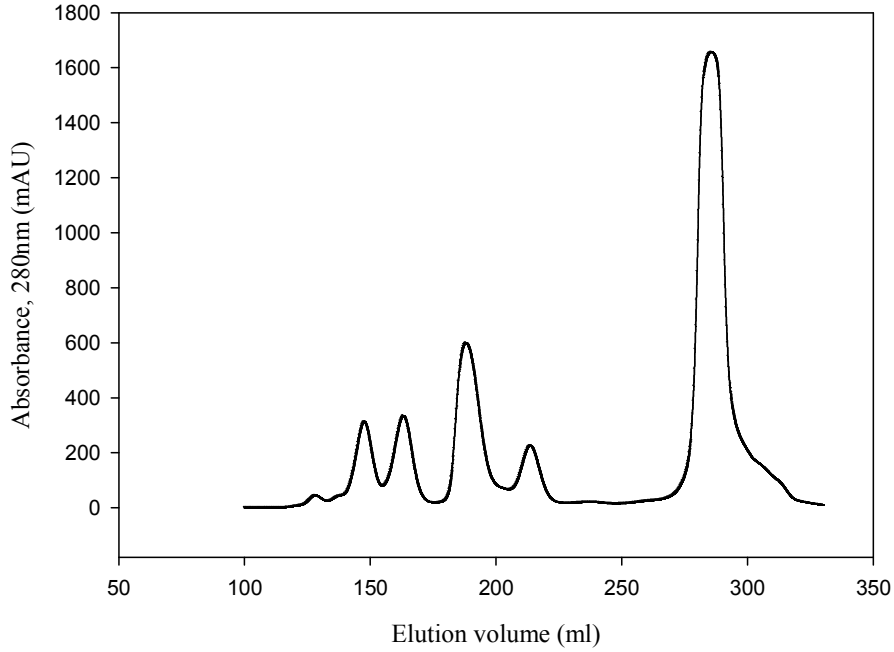

Figure 4.1: Elution profile of calibration proteins from the size exclusion column HiLoad® 26/60 Superdex 75.

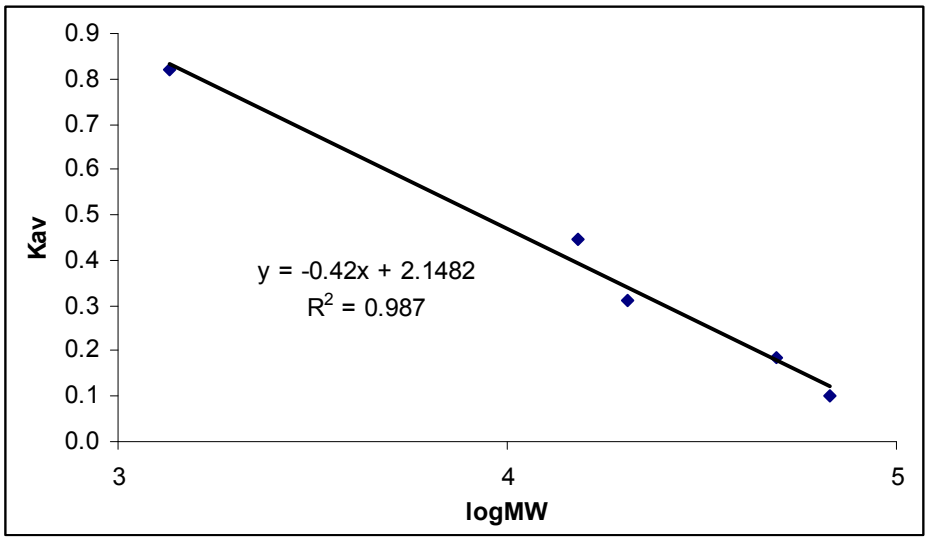

Figure 4.2: Calibration curve of HiLoad® 26/60 Superdex 75 size exclusion column.

4.1.2 Optimization of GSTdMT Purification

GSTdMT purification procedure was optimized with respect to the parameters listed below. During these studies protein was verified by western blotting, protein concentration was monitored by absorbance measurements at 280 nm, its integrity and homogeneity was monitored by SDS- and native-PAGE analysis, polydispersity of solutions were controlled by DLS, its metal content was determined by ICP-OES. During the optimization procedure the effect of new conditions were also monitored on GST samples to understand if the effects were due to GST or due to presence of dMT in the fusion protein.

In the beginning of this study phosphate-buffered saline (PBS) buffer system with 0.2 mM $CdCl_2$ was used in the purification procedure. PBS is a solution containing sodium chloride and sodium phosphate and potassium phosphate are used for maintaining a constant pH.

In the general scheme of the purification procedure (Figure 4.3), the GSTdMT was first fractionated by affinity chromatography. The elution profile from GSTrap FF column displayed two main peaks AI and AII (Figure 4.4). Fractions from AI and AII were pooled and were applied to HiLoad® 26/60 Superdex 75 column separately for further separation of GSTdMT from contaminants. As a result, for both pools, one main peak (GI) eluted at about 115 ml corresponding to molecular weight of 188 kDa which was about 5 times higher than expected for GSTdMT (Figure 4.5 and Figure 4.6).

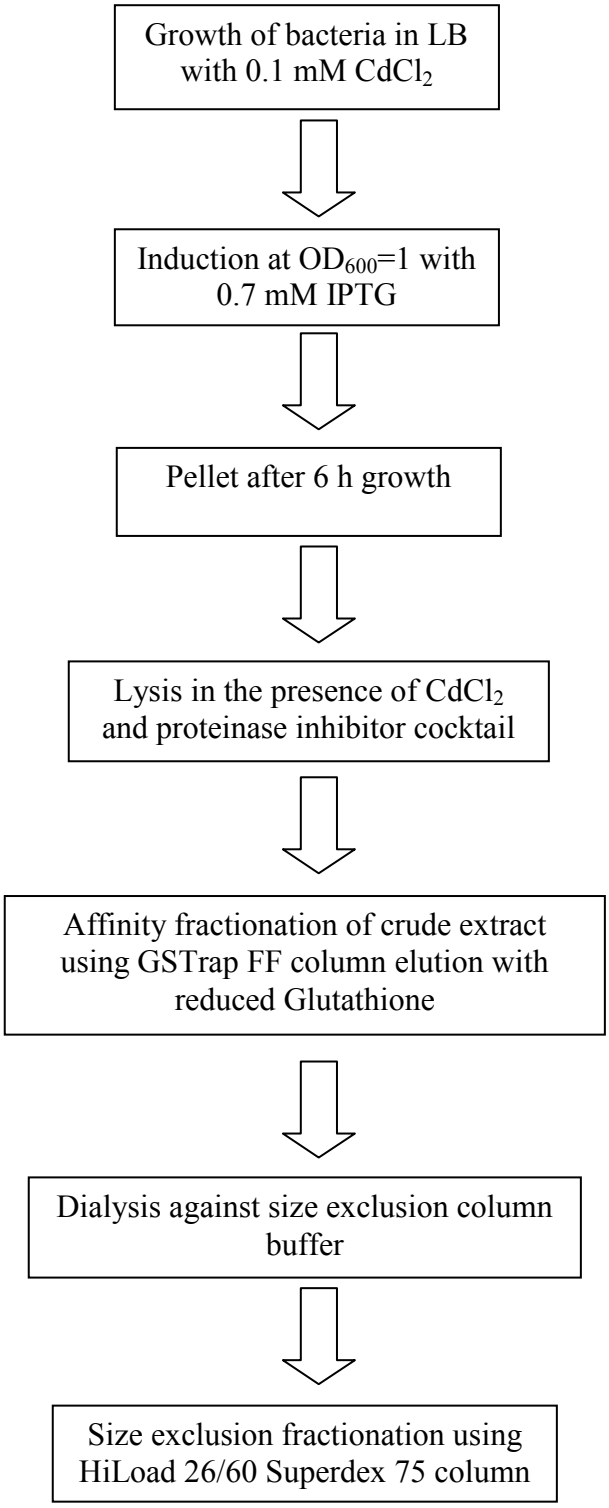

Figure 4.3: Experimental strategy of the purification of GSTdMT

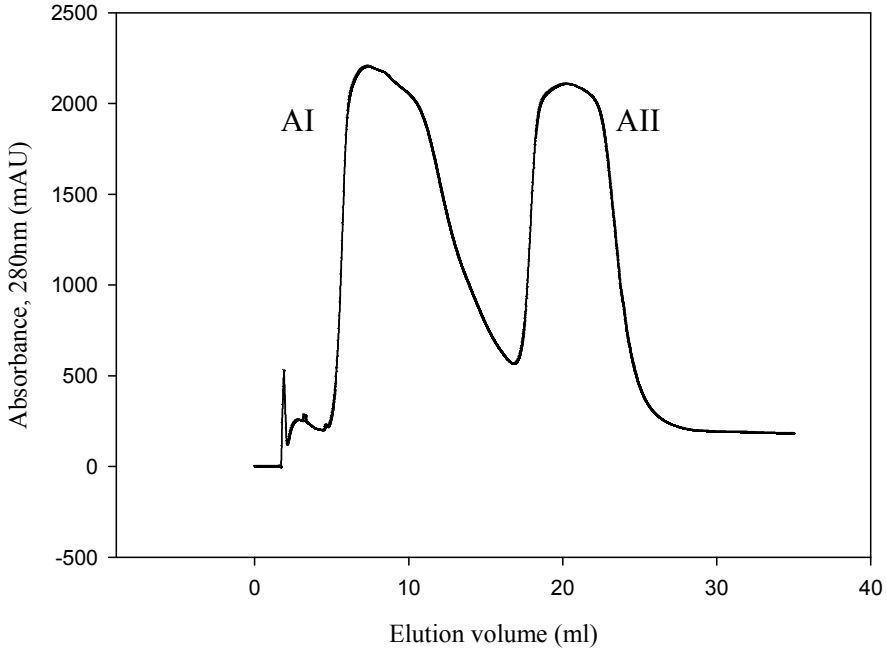

Figure 4.4: Elution profile of the GSTdMT from GST affinity chromatography using the PBS buffer system with 0.2 mM $CdCl_2$.

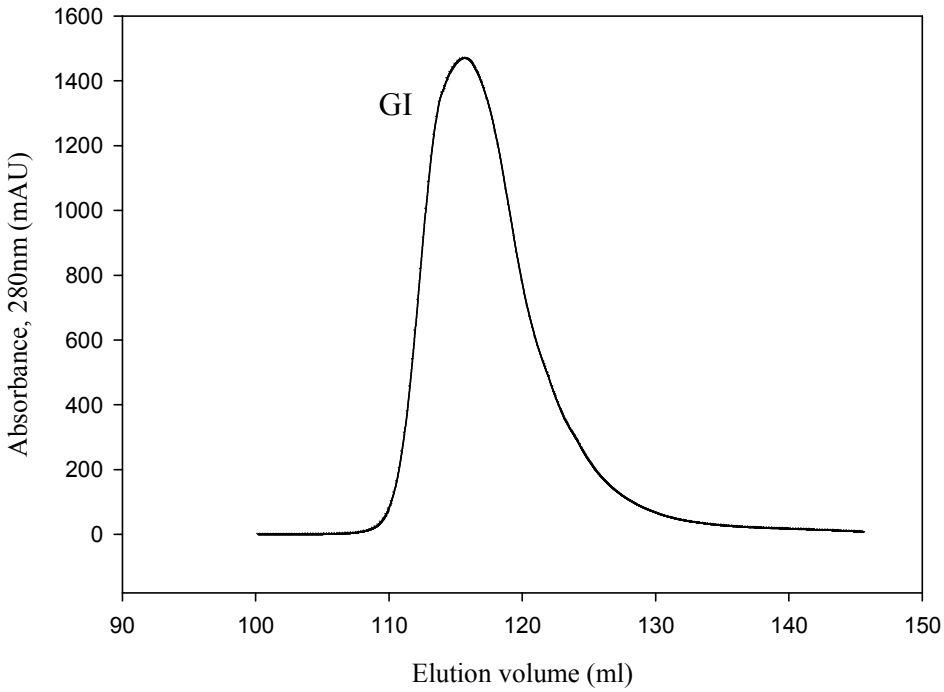

Figure 4.5: Size exclusion chromatography elution profile of AI using the PBS buffer system with 0.2 mM $CdCl_2$.

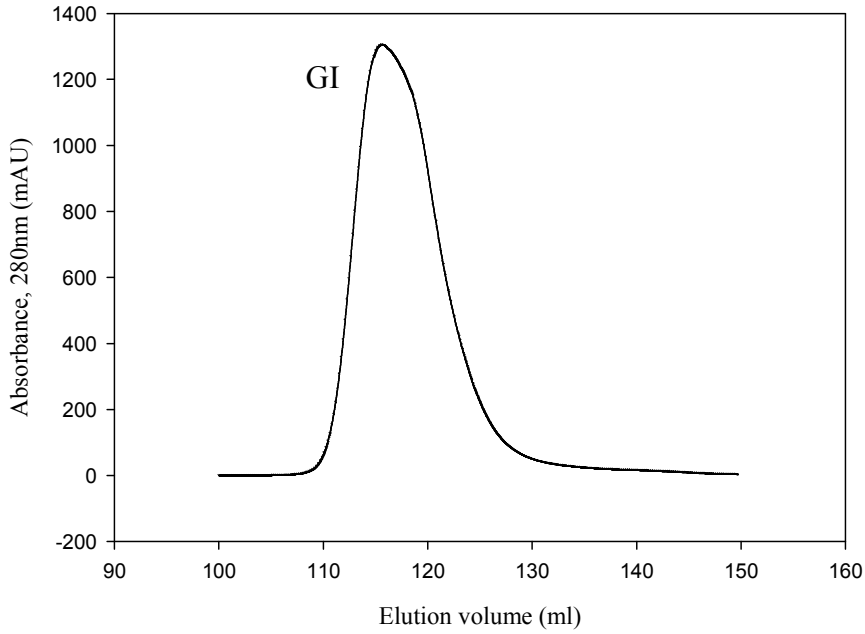

Figure 4.6: Size exclusion chromatography elution profile of AII using the PBS buffer system with 0.2 mM $CdCl_2$.

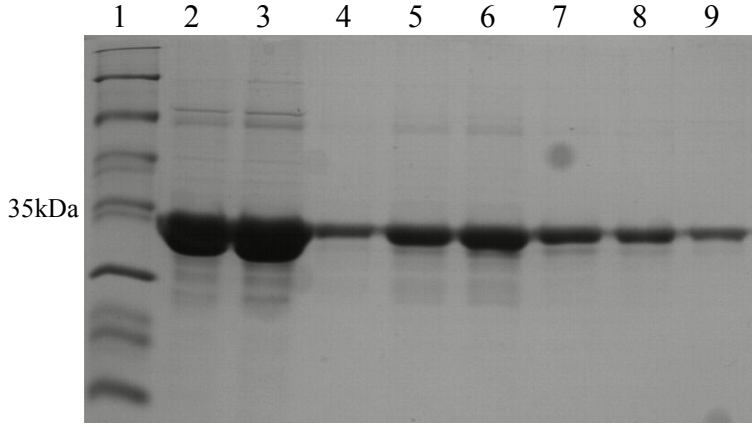

Figure 4.7: SDS-PAGE analysis of GSTdMT purification using the PBS buffer system with 0.2 mM $CdCl_2$. Lane 1, protein molecular weight marker; 2, eluate from GST affinity column before dialysis of peak AI; 3, eluate from GST affinity column after dialysis of peak AI; 4-9, eluted proteins of peak AI from size exclusion. Lane 6 is the top peak fraction.

Analysis of pools from affinity purification and fractions from the size exclusion column by 12% SDS-PAGE showed the expected major band at 34 kDa corresponding to GSTdMT (Figure 4.7). When the same material was analyzed by 10% Native-PAGE, however, more than one band was observed indicating the presence of aggregated

species (Figure 4.8). Presence of large molecular weight species was also demonstrated by DLS measurements where the intensity distribution of scattered light gives a major peak around 1000 nm indicating the dominance of aggregated species (Figure 4.9).

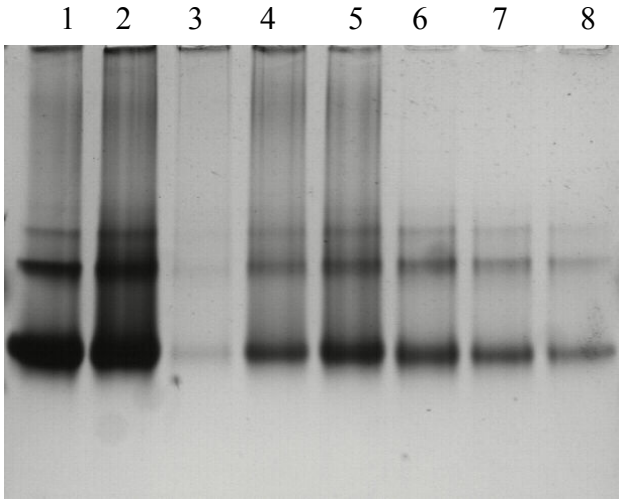

Figure 4.8: Native-PAGE analysis of fractions from GSTdMT purification using the PBS buffer system with 0.2 mM $CdCl_2$. Lane 1, eluate from GST affinity column before dialysis of peak AI; 2, eluate from GST affinity column after dialysis of peak AI; 3-8, eluted proteins of peak AI from size exclusion. Lane 5 is the top peak fraction.

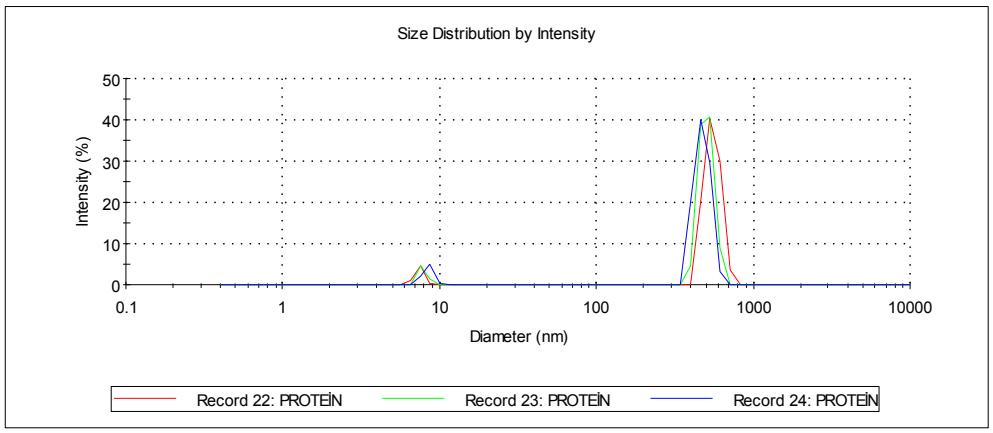

Figure 4.9: Intensity distribution of scattered light from top peak fraction of GSTdMT fusion protein purified using the PBS buffer system.

The effect of PBS buffer on the aggregation of the protein during purification was investigated first on the fusion partner GST alone. Elution profile from the GST affinity column displayed the same two peaks AI and AII (Figure 4.10) and native-

PAGE analysis showed again the aggregated species. However, it was also observed that AI and AII had different type of aggregates when analyzed by native-PAGE (Figure 4.11).

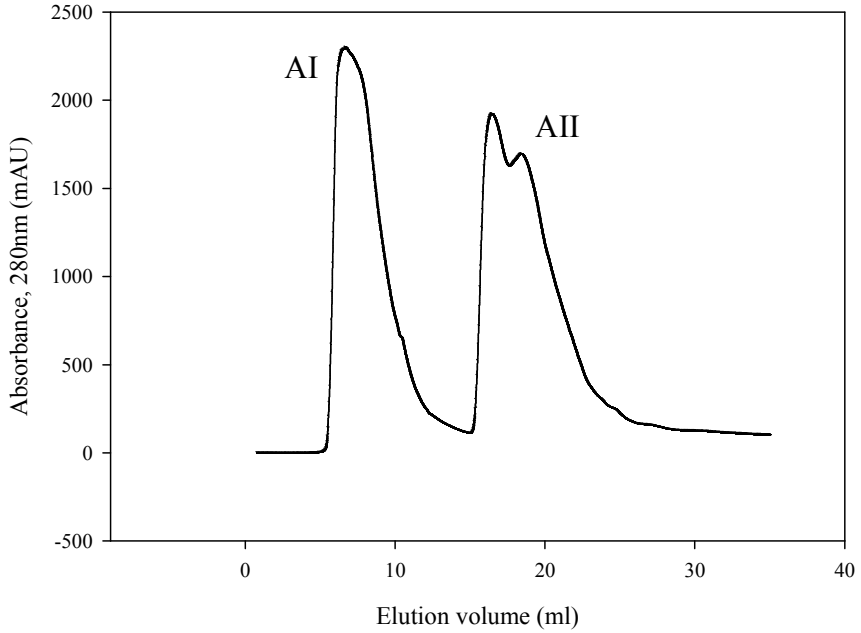

Figure 4.10: Elution profile of the GST from GST affinity column with the PBS buffer system.

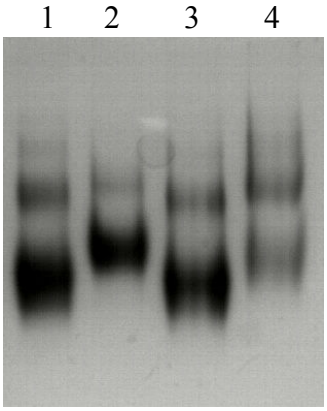

Figure 4.11: Native-PAGE analysis of GST purified from GST affinity column using the PBS buffer system. Lane 1, AI before dialysis; 2, AII before dialysis; 3, AI after dialysis; 4, AII after dialysis.

$CdCl_2$ was included in lysis buffer for preventing preteolytic degradation of GSTdMT, but it was also observed that $CdCl_2$ readily precipitated with PBS. In an attempt to solve this problem 0.1 mM $CdCl_2$ was tried for purification of GSTdMT. This again resulted in an elution profile with two peaks from the GST affinity column.

When AI and AII were further analyzed on the size exclusion column similar to previous results the main peak (GI) came at about 115 ml (Figure 4.12 and Figure 4.13). However, an additional, small peak (GII) was observed at about 137 ml corresponding to 79 kDa in the elution profile of AII (Figure 4.13). When the eluted proteins from GI and GII were analyzed by native-PAGE, contrary to main peak fractions no aggregated species was observed in the small peak fractions (Figure 4.15). SDS-PAGE analysis gave the same result as before (Figure 4.14).

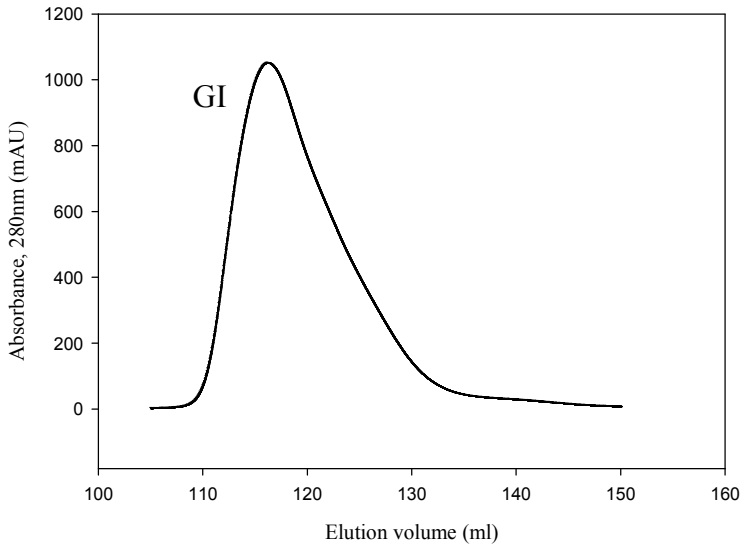

Figure 4.12: Size exclusion chromatography elution profile AI using the PBS buffer system with 0.1 mM $CdCl_2$.

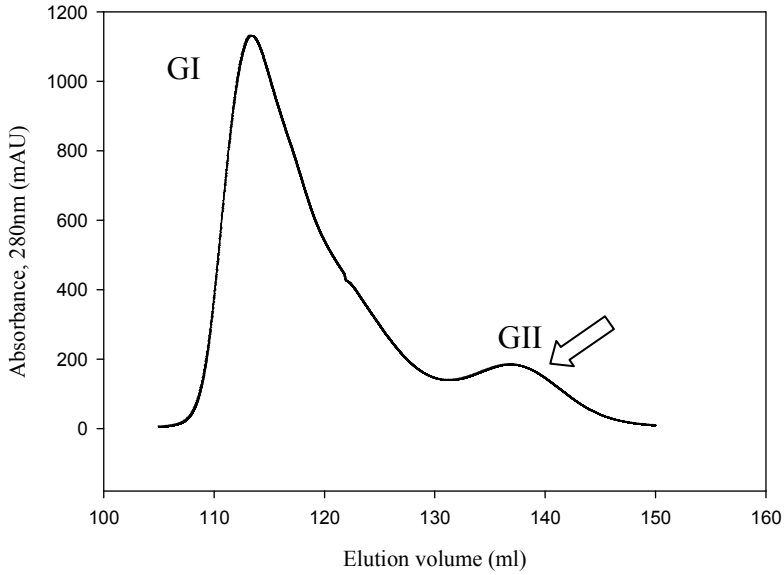

Figure 4.13: Size exclusion chromatography elution profile of AII using the PBS buffer system with 0.1 mM $CdCl_2$.

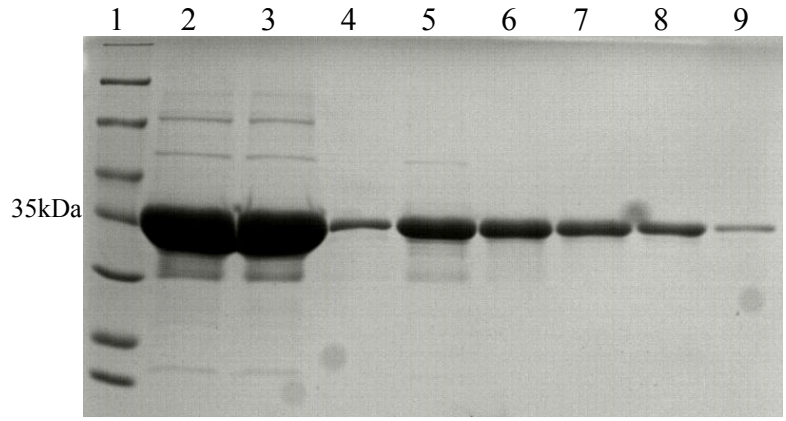

Figure 4.14: SDS-PAGE analysis of purified GSTdMT using the PBS buffer system with 0.1 mM $CdCl_2$. Lane 1, protein molecular weight marker; 2, AII before dialysis; 3, AII after dialysis; 4-8, fractions from GI; 9, fraction from GII.

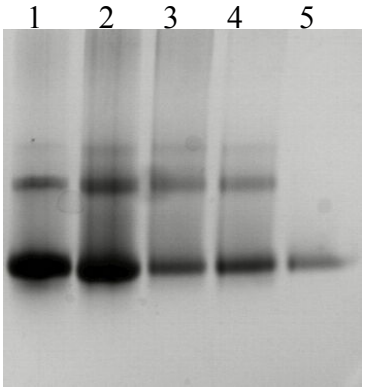

Figure 4.15: Native-PAGE analysis of purified GSTdMT using the PBS buffer system with 0.1 mM $CdCl_2$. Lane 1, Pool AII before dialysis; 2, Pool AII after dialysis; 3-4, fractions from pool GI size exclusion of AII; 5, fraction from GII.

The affect of using DTT ($C_4H_{10}O_2S_2$) as a reducing agent in GSTdMT purification buffers was investigated. 1 mM DTT was included in PBS buffer with 0.1 mM $CdCl_2$. Although the GST elution profile remained the same an increase in the amount of protein eluting in GII, corresponding to nonaggregated species, was observed (Figure 4.16, Figure 4.17).

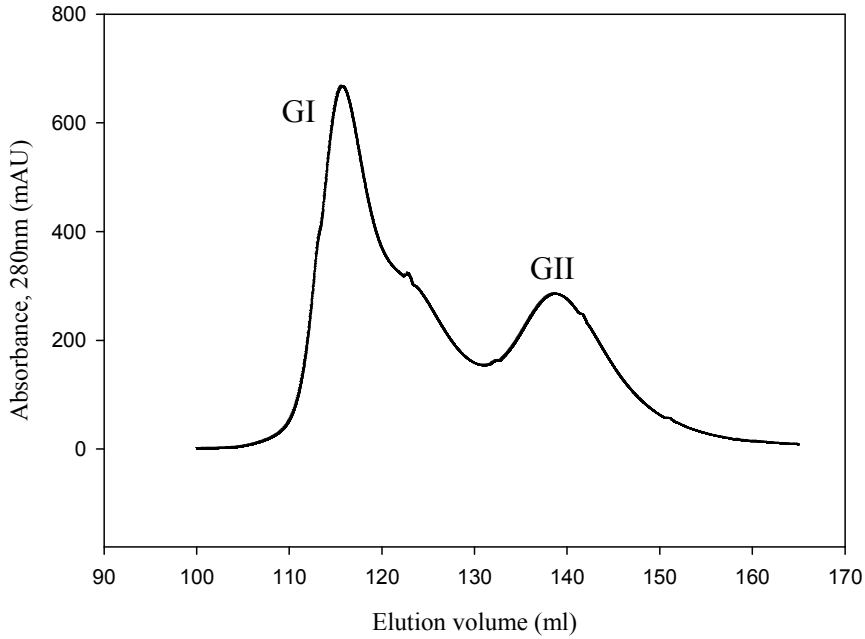

Figure 4.16: Size exclusion chromatography elution profile of AII using PBS as buffer system with 0.1 mM $CdCl_2$ and 1mM DTT.

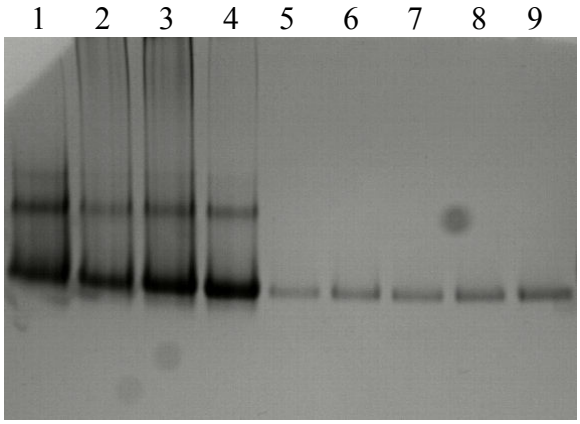

Figure 4.17: Native-PAGE analysis of purified GSTdMT using the PBS buffer system with 0.1 mM $CdCl_2$ and 1mM DTT. Lane 1-4, fractions from peak GI of AII; 5-9, fractions from GII.

Inclusion of 1 mM DTT as reducing agent improved the amount of GSTdMT dimer form but it did not solve fully the problem of aggregation. During purification procedures $CdCl_2$ could readily precipitate with PBS buffer as CdS_2. To avoid precipitation the buffer system was changed to Tris $[(HOCH_2)_3CNH_2]$ and 50 mM Tris-HCl, 2.5 mM $MgCl_2$ and 100 mM NaCl (Buffer A) was used during the purification procedure instead of the PBS buffer system.

The combined effect of changing the buffer to Tris and having DTT on protein aggregation was first examined during purification of GST. Only one peak was obtained in the elution profile of GST from GST affinity column under these conditions (Figure 4.18). Peak fractions were pooled and were applied to Hiload® 26/60 Superdex 75 size exclusion column for further separation. The elution profile displayed one main peak at about 157 ml (Figure 4.19). This elution volume corresponded to a molecular weight of 50 kDa and represented the dimeric GST species.

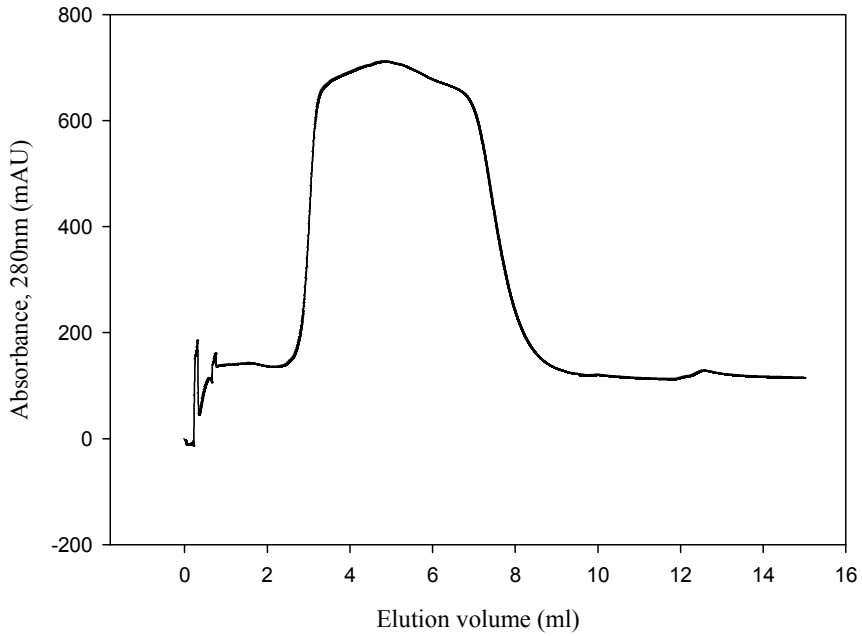

Figure 4.18: Elution profile of the GST from GST affinity column using Buffer A with 1mM DTT

Analysis of fractions from GST affinity column by SDS-PAGE showed a major band at about 25 kDa as expected (Figure 4.20). Native-PAGE analysis showed GST protein could be purified without aggregation (Figure 4.21).

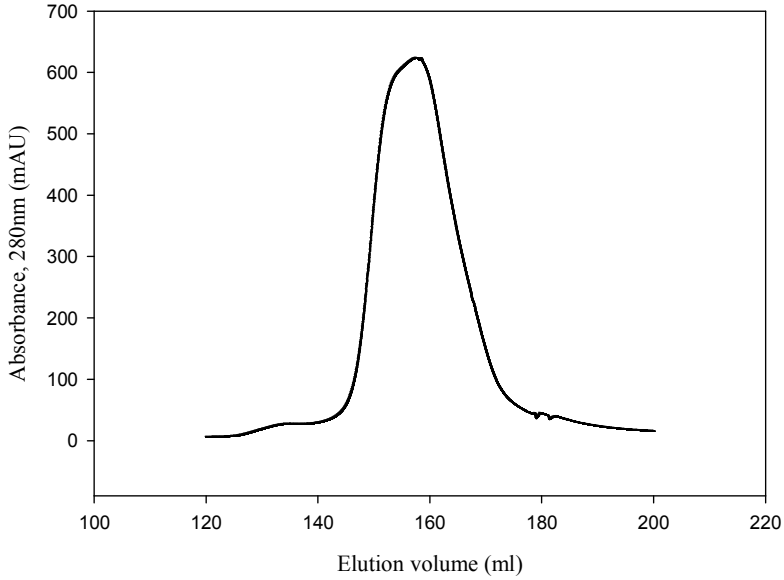

Figure 4.19: Size exclusion chromatography elution profile of GST affinity column using Buffer A with 1mM DTT.

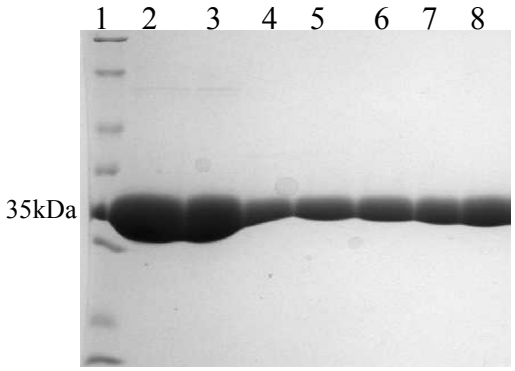

Figure 4.20: SDS-PAGE analysis of GST purified using Buffer A with 1mM DTT. Lane 1, protein molecular weight marker; 2, pool AI before dialysis; 3, pool AI after dialysis; 4-8, Pool GII fractions.

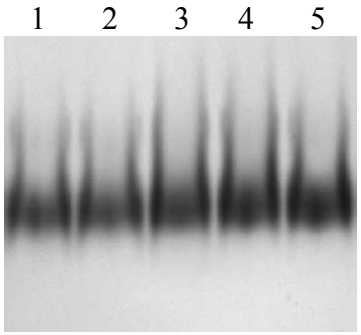

Figure 4.21: Native-PAGE analysis of GST purified using Buffer A with 1mM DTT. Lane 1-5, fractions from pool GII.

In order to eliminate the effect of excess Cd on protein aggregation GSTdMT purification was carried out without $CdCl_2$ using the Buffer A with 1mM DTT. As a result the same GST affinity elution profile with only one main peak was observed (Figure 4.22). The elution profile from size exclusion column, on the other hand, displayed changes; the main peak was eluted at 138 ml corresponding to about 79 kDa which is the expected size of the dimer of GSTdMT (Figure 4.23).

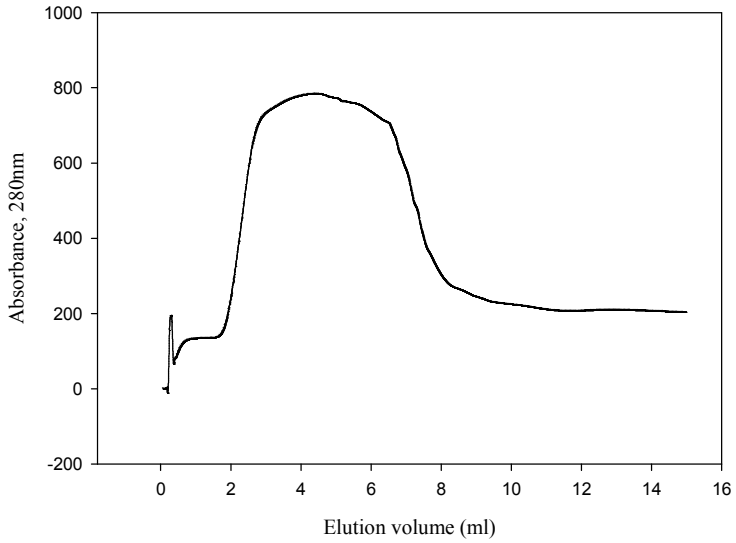

Figure 4.22: Elution profile of the GSTdMT from GST affinity column using Buffer A with 1mM DTT without $CdCl_2$.

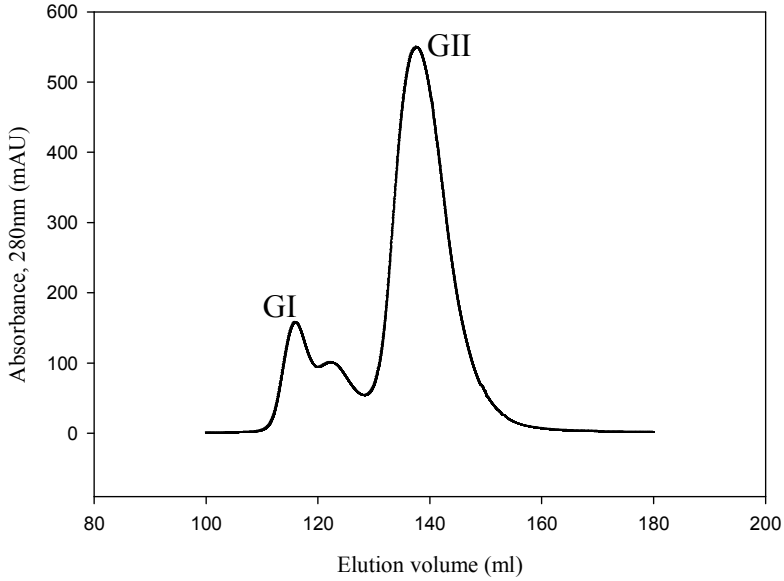

Figure 4.23: Size exclusion chromatography elution profile of pool AI from GST affinity column when using Buffer A with 1mM DTT without $CdCl_2$.

However, the effect of lack of Cd was observed in SDS-PAGE analysis of GSTdMT and proteolytic degradation was observed in fractions eluted from size exclusion column (Figure 4.24).

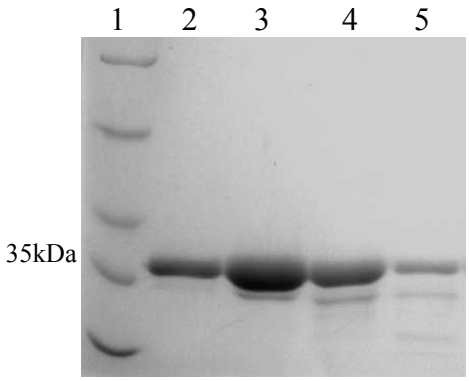

Figure 4.24: SDS-PAGE analysis of purified GSTdMT using Buffer A with 1mM DTT without $CdCl_2$. Lane 1, protein molecular weight marker; 2-5, fractions from GII. Lane 3 is the top peak fraction.

The usage DTT of as a reducing agent for the purification of GSTdMT had showed that DTT could prevent aggregate formation. However, the possibility of CdS_2 precipitation could not be avoided. A reducing agent lacking S groups called TCEP (Tris (2-carboxyethyl) phosphine hydrochloride, C9H15O6P.HCl) was also tried.

Purification of GSTdMT using Buffer A with 0.1 mM $CdCl_2$ and 0.1 mM TCEP was performed with the same conditions. As a result, again, only one peak was observed from the GST elution and the pooled fractions were applied to size exclusion column for further separation. As can be seen from the elution profile one main peak was observed at 115 ml (Figure 4.25). Native-PAGE analysis showed slightly aggregated fractions (Figure 4.26).

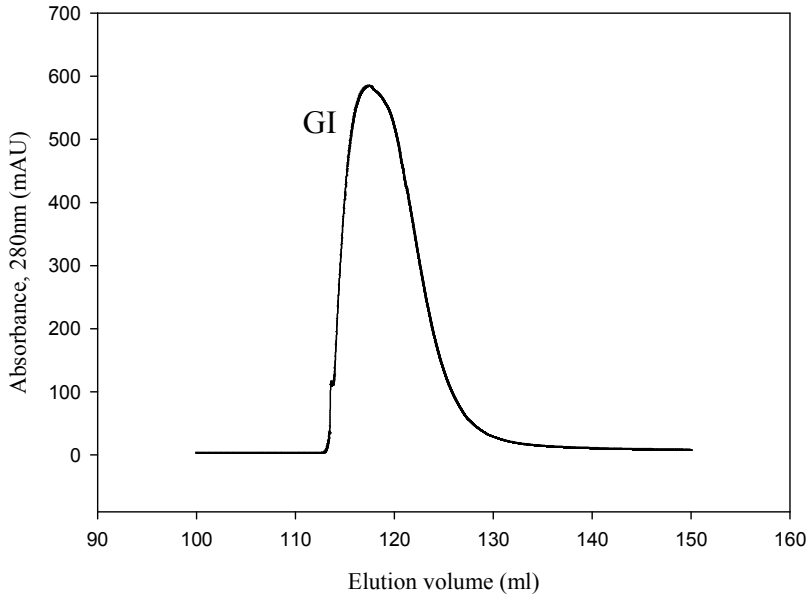

Figure 4.25: Size exclusion chromatography elution profile of GST affinity column using Buffer A with 0.1mM $CdCl_2$ and 0.1mM TCEP.

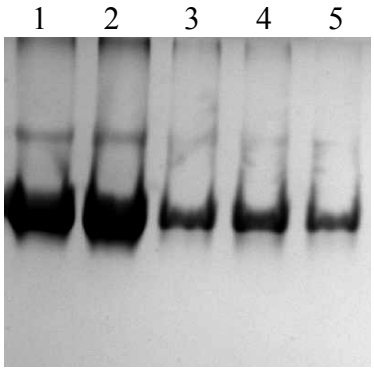

Figure 4.26: Native-PAGE analysis of purified GSTdMT using Buffer A with 0.1mM $CdCl_2$ and 0.1mM TCEP. Lane 1, Pool AI before dialysis; 2, Pool AI after dialysis; 3-5, fractions of GI. Lane 4 is the top fraction.

Results showed that TCEP partly prevented aggregation of purified GSTdMT, and the dimer form was not observed in the elution profile of the size exclusion column. In conclusion, either TCEP was not a good reducing agent for preventing aggregate formation or the concentration used was not sufficient.

The possibility of CdS_2 precipitation in the presence of DTT could be eliminated with the limited usage of $CdCl_2$. Therefore, the GSTdMT purification was performed

with Buffer A containing 1 mM DTT and 1 mM $CdCl_2$ which was added to the buffer only during lysis. This resulted in the same elution profiles for affinity and size exclusion chromatography as before (Figure 4.27). This limited usage was sufficient to protect against proteolytic cleavage of GSTdMT as observed by SDS-PAGE analysis (Figure 4.28). Native-PAGE analysis showed that the purified GSTdMT fractions from GII at about 140 ml were obtained without aggregated species whereas GI contained aggregated species (Figure 4.29).

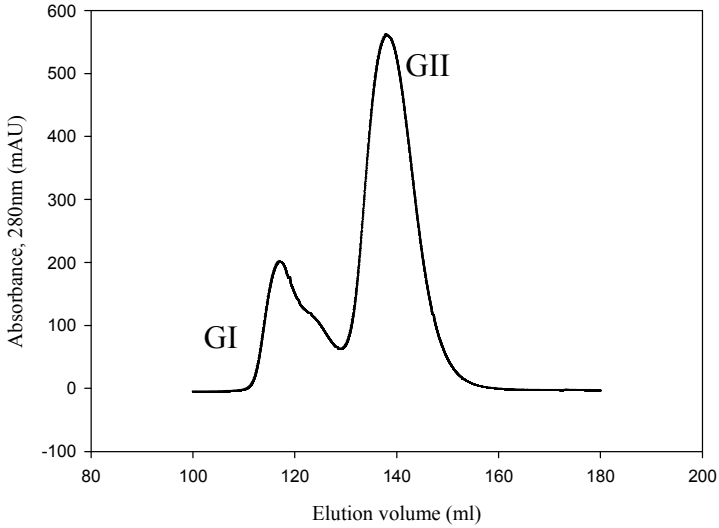

Figure 4.27: Size exclusion chromatography elution profile of Pool AI using Buffer A with 1 mM DTT and 0.1mM $CdCl_2$ only in lysis.

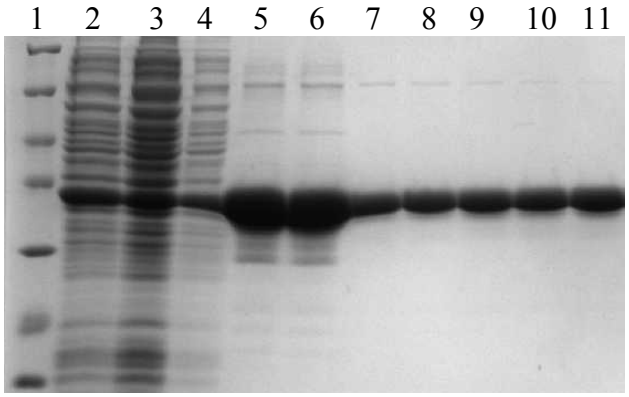

Figure 4.28: SDS-PAGE analysis of purified GSTdMT using Buffer A with 1 mM DTT and 0.1mM $CdCl_2$ only in lysis. Lane 1, protein molecular weight marker; 2, cell lysate; 3, flowthrough; 4, wash; 5, AI before dialysis; 6, AI after dialysis; 7-11, fractions from GII. Lane 10 is the top fraction.

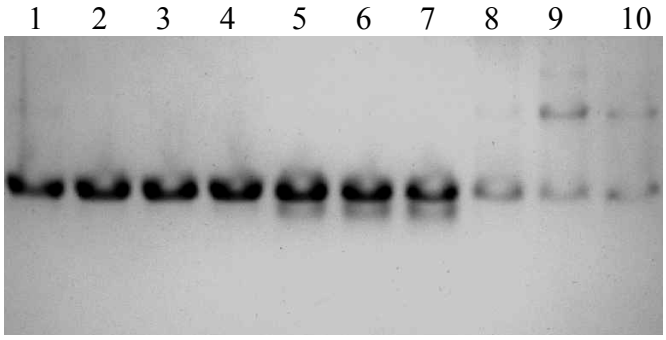

Figure 4.29: Native-PAGE analysis of purified GSTdMT using Buffer A with 1 mM DTT and 0.1mM $CdCl_2$ only in lysis. Lane 1-7 fractions from GII; 8-10, fractions from GI. Lane 4 is the top fraction of peak GII.

To further confirm that the isolated product was GSTdMT western blot analysis was carried out. Presence of GST was confirmed by using a GST-HRP conjugate. After electrophoresis of 0.2 mg/ml GSTdMT fusion protein on 12% SDS gel, the protein samples were incubated with 1:10000 diluted anti-GST HRP conjugate. The western blot result showed that there was no proteolytic cleavage and that the isolated GSTdMT was intact (Figure 4.30).

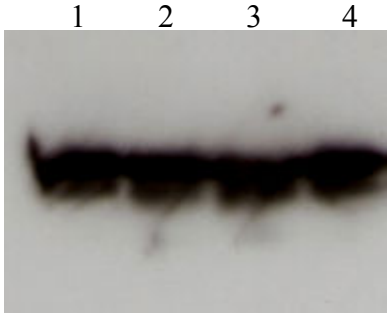

Figure 4.30: Western blot analysis of GSTdMT using Buffer A with 1 mM DTT and 0.1mM $CdCl_2$ only in lysis. Lane1-4, fractions of GII.

Having solved the precipitation problem with Buffer A and reduced concentration of $CdCl_2$, conditions for protein storage were investigated. It was observed that protein precipitation occurred due to the change in pH of Tris buffer at low temperatures. DLS measurement of fractions from peak GII stored at -80^{o}C showed that the intensity distribution of scattered light had a maximum around 1000 nm indicating the dominance of aggregated species (Figure 4.31). For comparison, a fraction from GI stored at -80^{o}C was also measured by DLS and showed more aggregated species (Figure 4.32).

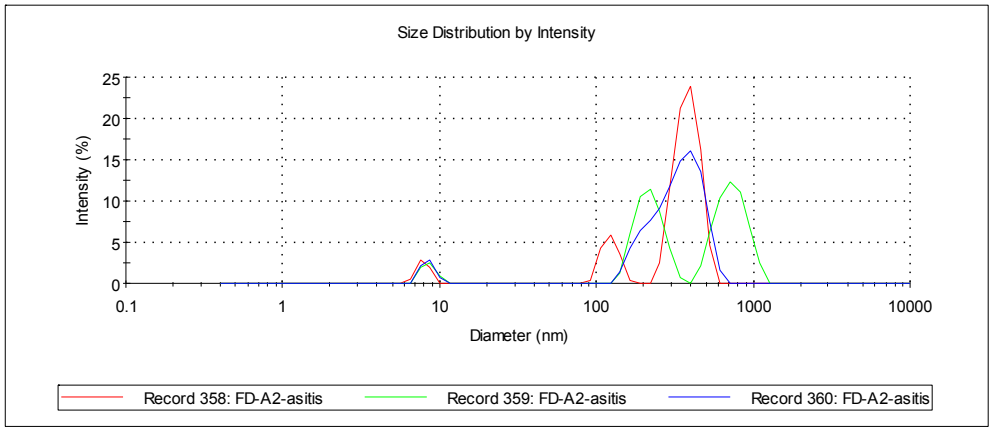

Figure 4.31: Intensity distribution of scattered light from a fraction of GSTdMT from peak GII after freezing and thawing. Buffer A system with 1 mM DTT and 0.1mM $CdCl_2$ only in lysis buffer.

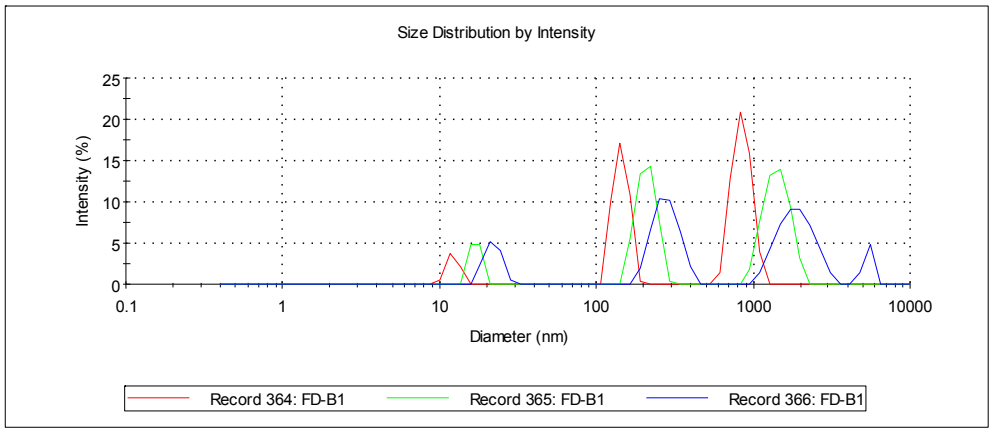

Figure 4.32: Intensity distribution of scattered light measurement from a fraction of GSTdMT from peak GI after freezing and thawing. Buffer A with 1 mM DTT and 0.1mM $CdCl_2$ only in lysis buffer.

The purification procedure was further improved using HEPES 4-(2-hydroxyethyl)-1-piperazineethanesulfonicacid ($C_8H_{18}N_2O_4S$) as the buffer. The final purification buffer at pH 8.0 included 20mM HEPES, 100mM NaCl and 2.5 mM $MgCl_2$ (Buffer B) to obtain pure intact GSTdMT.

Buffer B was first tried with the purification of GST and resulted in the same observations as that for the Buffer A. Only one main peak (AI) was eluted from GST affinity column (Figure 4.33) and a single peak at about 157 ml corresponding to the dimer form of GST protein was obtained from the size exclusion column (Figure 4.34).

SDS-PAGE analysis showed a major band at about 25 kDa (Figure 4.35) and no aggregation products were observed by native-PAGE analysis (Figure 4.36).

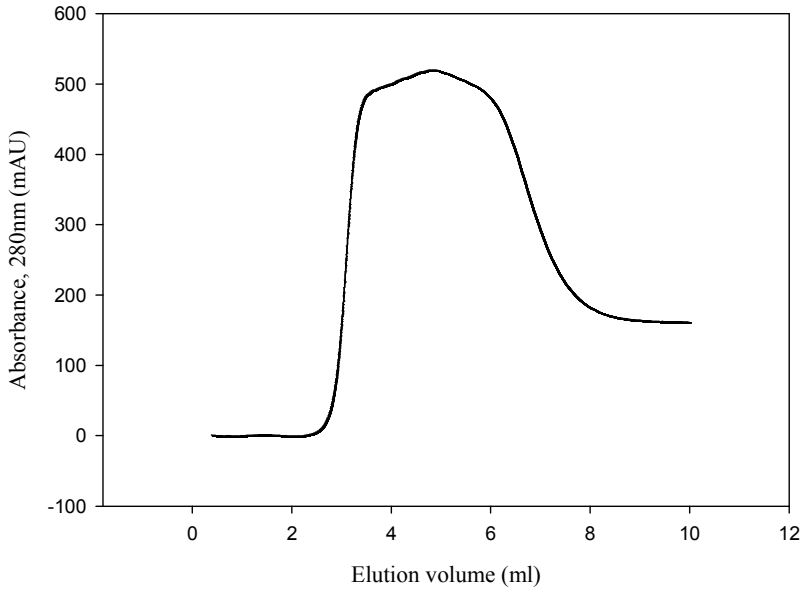

Figure 4.33: Elution profile of the GST from GST affinity chromatography using the Buffer B with 1 mM DTT.

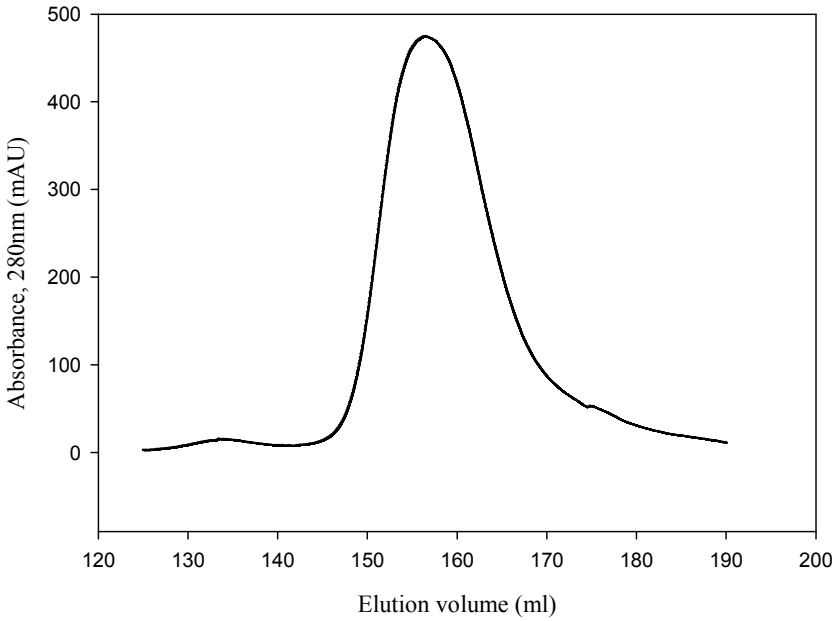

Figure 4.34: Size exclusion chromatography elution profile of GST from pool AI using Buffer B with 1 mM DTT.

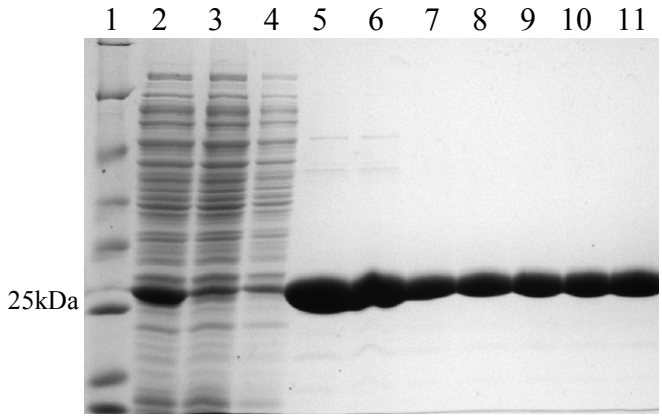

Figure 4.35: SDS-PAGE analysis of GST purification using Buffer B with 1 mM DTT. Lane 1, protein molecular weight marker; 2, cell lysate; 3, flowthrough; 4, wash; 5, Peak AI before dialysis; 6, Peak AI after dialysis; 7-11, fractions from peak GII. Lane 10 is the top fraction.

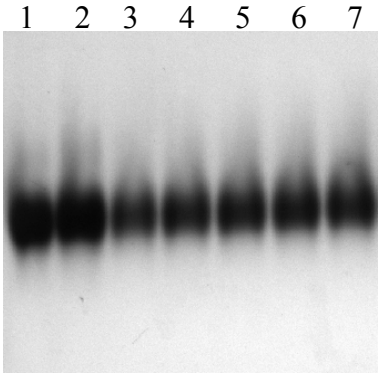

Figure 4.36: Native-PAGE analysis of GST purified using Buffer B with 1 mM DTT. Lane 1, Pool AI before dialysis; 2, Pool AI after dialysis; 3-7, fractions from peak GII. Lane 6 is the top fraction.

Purification of GSTdMT fusion protein with Buffer B also gave the same results obtained with Buffer B. Again only one peak was obtained in the elution profile from GST affinity column (Figure 4.37). Two peaks were obtained from the size exclusion column appearing at 116 and 140 ml. The main GII peak at 140 ml gave the dimer form of purified GSTdMT (Figure 4.38) whereas peak GI contained highly aggregated forms.

The SDS-PAGE analysis of the fractions showed the 34 kDa GSTdMT as the major component (Figure 4.39). In the analysis of native-PAGE only one band was observed. This indicated that there were no aggregated species (Figure 4.40).

DLS measurement on a fresh fraction from GII showed a single peak in the intensity distribution centered around on 10 nm indicating the dominance of the dimer form of GSTdMT (Figure 4.41).

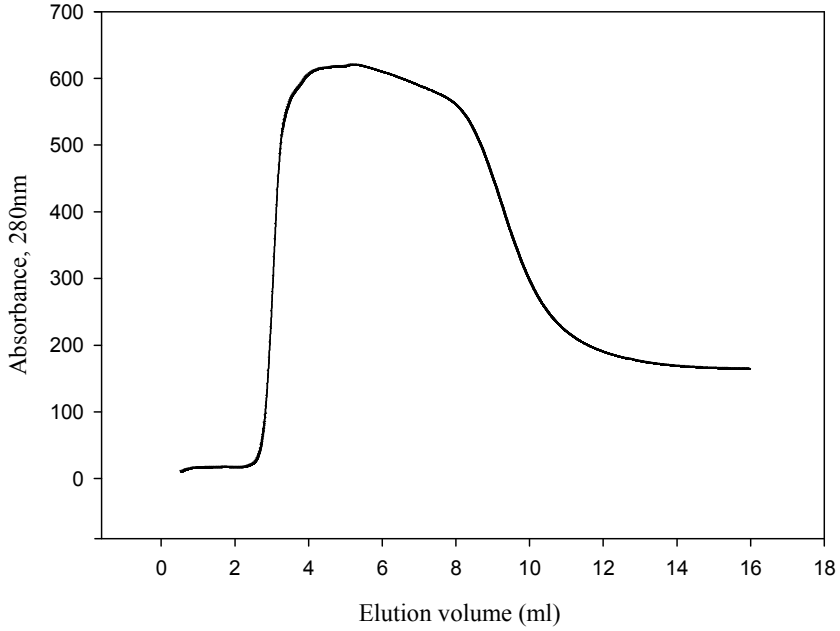

Figure 4.37: Elution profile of the GSTdMT from GST affinity chromatography using Buffer B with 1 mM DTT and 0.1 mM $CdCl_2$ only in lysis buffer.

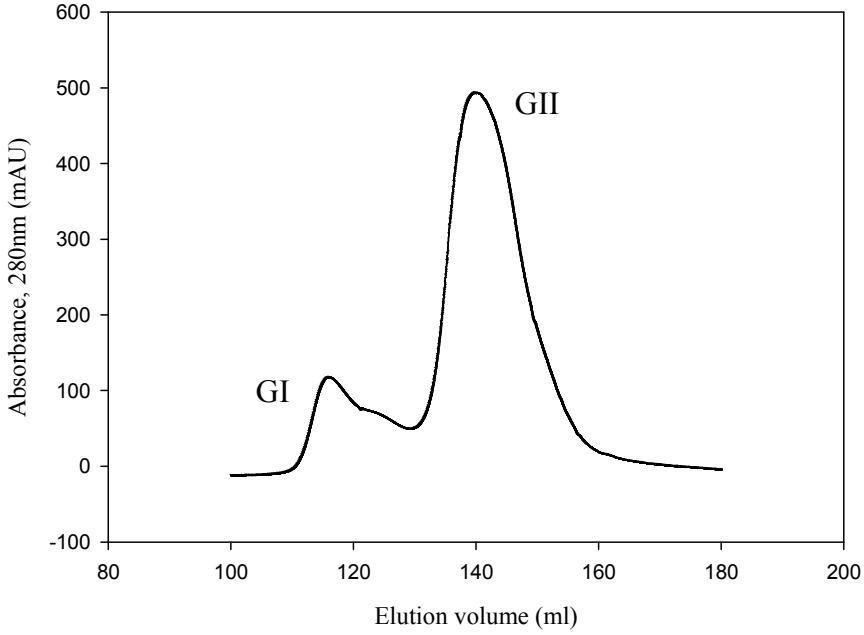

Figure 4.38: Size exclusion column elution profile of Pool AI using Buffer B with 1 mM DTT and 0.1mM $CdCl_2$ only in lysis buffer.

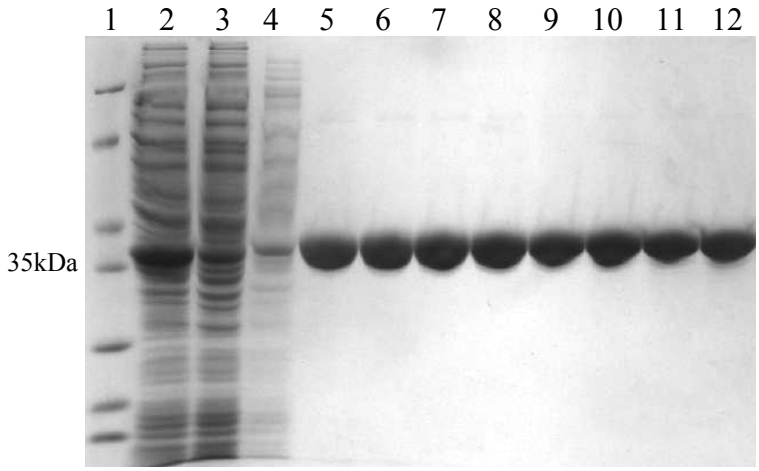

Figure 4.39: SDS-PAGE analysis of fractions from GSTdMT purification using Buffer B with 1 mM DTT and 0.1mM $CdCl_2$ only in lysis buffer. Lane 1, protein molecular weight marker; 2, cell lysate; 3, flowthrough; 4, wash; 5-12, fractions from pool GII. Lane 11 is the top fraction.

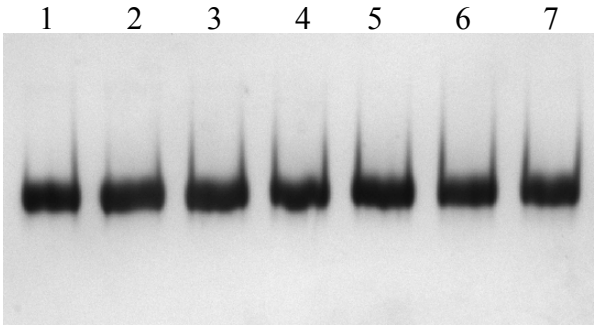

Figure 4.40: Native-PAGE analysis of purified GSTdMT using Buffer B with 1 mM DTT and 0.1mM $CdCl_2$ only in lysis buffer. Lane 1-7, fractions from pool GII. Lane 6 is the top fraction.

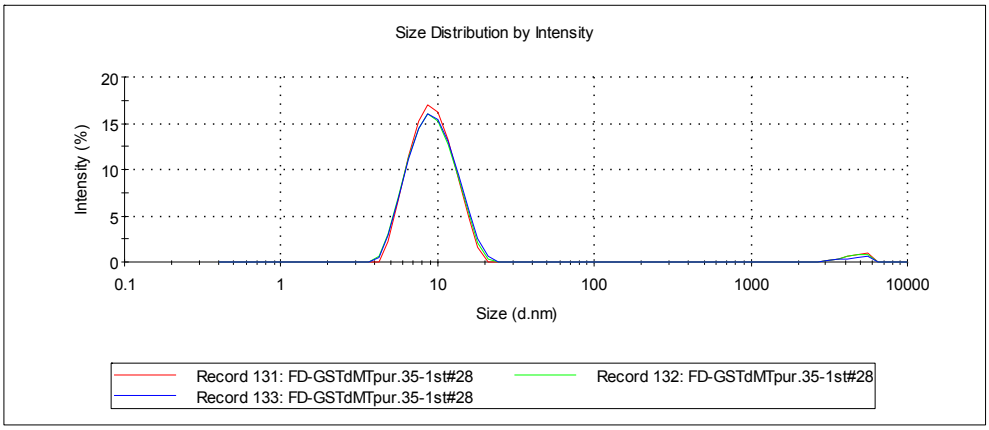

Figure 4.41: Intensity distribution of scattered light from GSTdMT purified using Buffer B with 1 mM DTT and 0.1mM $CdCl_2$ only in lysis buffer.

After the establishment of the purification procedure the yield of a GSTdMT prep was compared with that of GST. Yield of a typical GSTdMT purification from a 0.75 liter *E. coli* culture under optimized conditions was given together with that of GST prep (Table 4.2). Concentrations were calculated using $A_{280}^{1\%}$ = 1.232 for GSTdMT (Gill and von Hipple 1989). It was found that although the GSTdMT yield was less than that of GST the difference was not very significant.

Table 4.2: Comparison of yields of GSTdMT and GST purifications. SE; size exclusion column. Total protein content was estimated by taking into account the volume of fractions. *Concentration of the top fractions ** Estimated total protein from the sum of the protein content of individual fractions.

	GSTdMT		**GST**	
	C (mg/ml)	**Total Protein (mg)**	**C (mg/ml)**	**Total Protein (mg)**
Lysate	50	2000	50	2000
Pool A	10	75	12	72
Load SE	5	35	7.7	50
Pool GI	0.5**	4***	----	----
Pool G2	2.5**	25***	**3	***30

4.1.2.1 Determination of the Storage Conditions for GSTdMT

The effect of using Buffer B was first tested with GST. In order to find the best storage temperature, fractions from pool GII were grouped into three sets; group I: fractions to be stored at 4^{o}C, group II: fractions to be stored at -20^{o}C and group III: fractions flash frozen in liquid N_2 and stored at -80^{o}C. These fractions were analyzed by SDS- and native-PAGE and monitored by DLS three and six days after the purification. The SDS- and native-PAGE analysis gave the same results for the three and six days stored fractions (Figure 4.42 and Figure 4.43). Particularly the Native-PAGE analysis did not show any aggregated species for the three different conditions.

However, according to the DLS measurements the intensity distribution of scattered light from fractions stored at different temperatures gave different results. Although some aggregated species could be detected, a single peak centered around 10

nm indicated that mainly dimeric form was present in the fractions stored for three days at -20°C and 4°C (Figure 4.44 and Figure 4.45). For the six days storage in addition to the dimer larger oligomers were observed especially for the fraction stored at -20°C (Figure 4.46 and Figure 4.47). For the fraction stored for three and six days at -80°C one main peak centered around 1000 nm indicated the formation of aggregated species (Figure 4.48 and Figure 4.49). These results indicated clearly that the best storage temperature for the GST was 4°C.

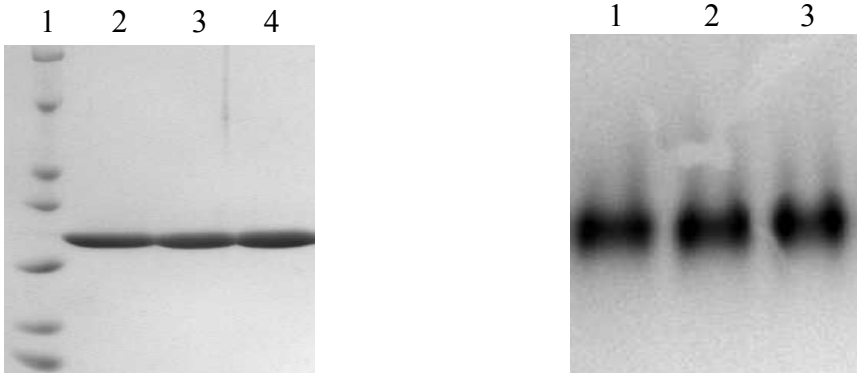

Figure 4.42: Electrophoretic analysis of GST fractions purified in Buffer B and stored for three days at different temperatures. SDS (L) - and Native (R) -PAGE analysis. Lane 1, protein molecular weight marker; 2, fraction stored at -80°C; 3; fraction stored at -20°C, 4; fraction stored at 4°C.

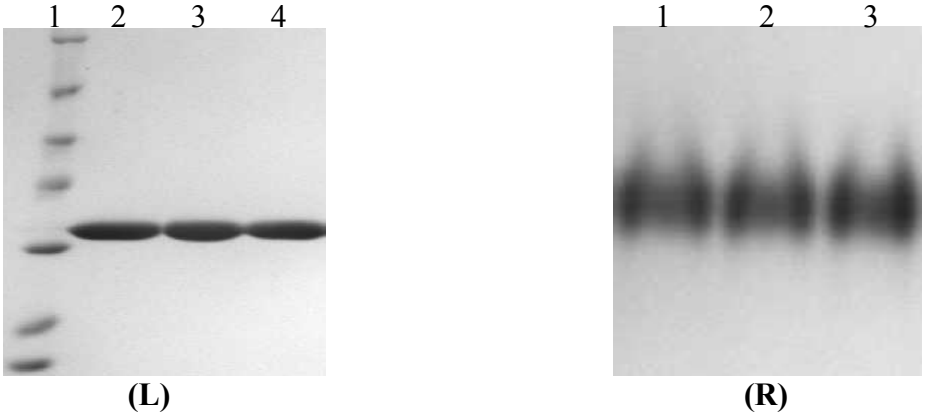

Figure 4.43: Electrophoretic analysis of GST fractions purified in Buffer B and stored for six days at different temperatures. SDS (L) - and Native (R) -PAGE analysis. Lane 1, protein molecular weight marker; 2, fraction stored at -80°C; 3; fraction stored at -20°C, 4; fraction stored at 4°C.

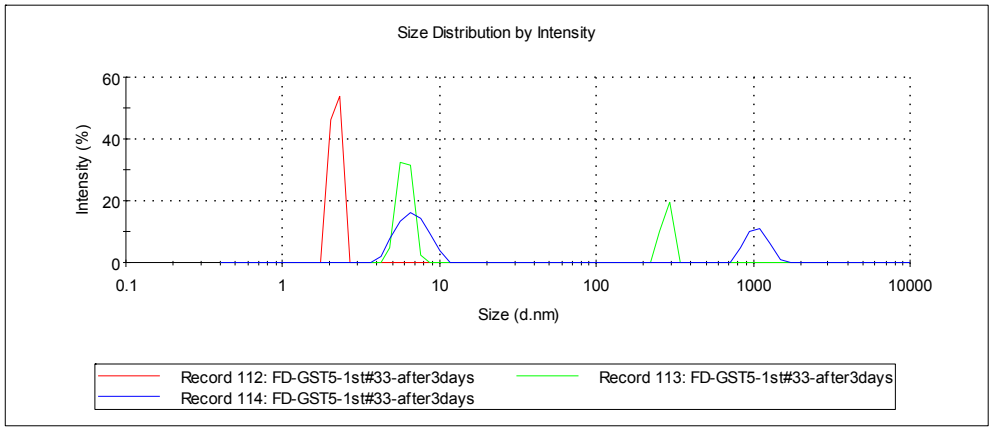

Figure 4.44: Dynamic light scattering measurement of the GST (lane 2 in Native-PAGE analysis) stored for three days at -20^{o}C.

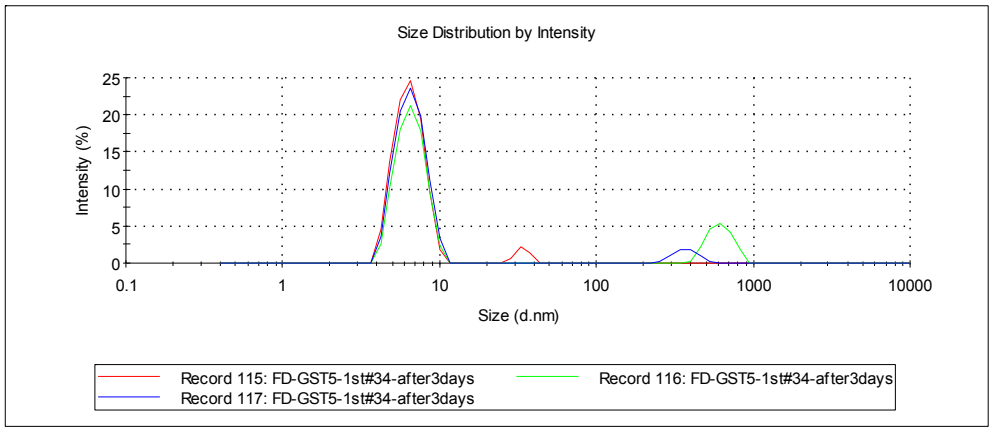

Figure 4.45: Dynamic light scattering measurement of the GST (lane 3 in Native-PAGE analysis) stored for three days at 4^{o}C.

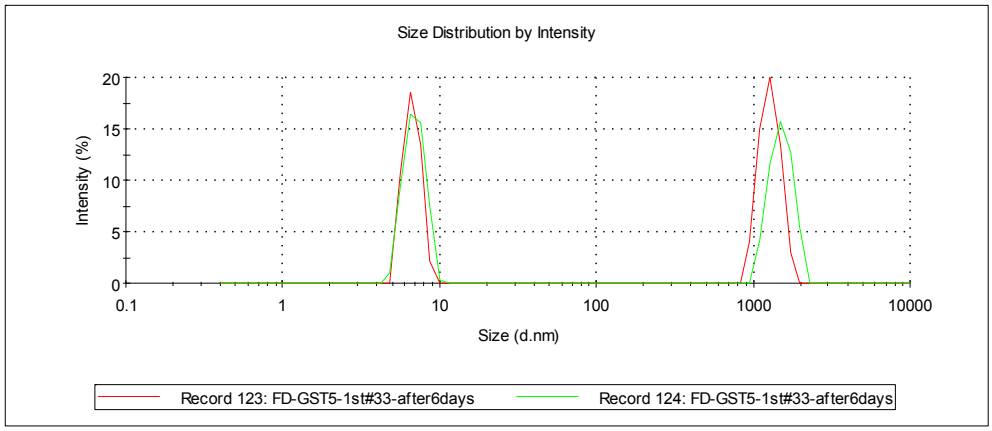

Figure 4.46: Dynamic light scattering measurement of the GST (lane 2 in Native-PAGE analysis) stored for six days at-20^{o}C.

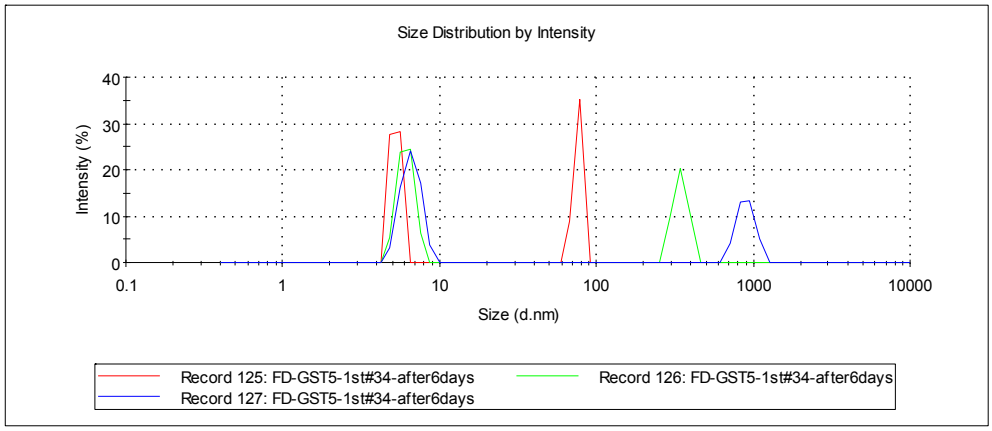

Figure 4.47: Dynamic light scattering measurement of the GST (lane 3 in Native-PAGE analysis) stored for six days at 4^{o}C.

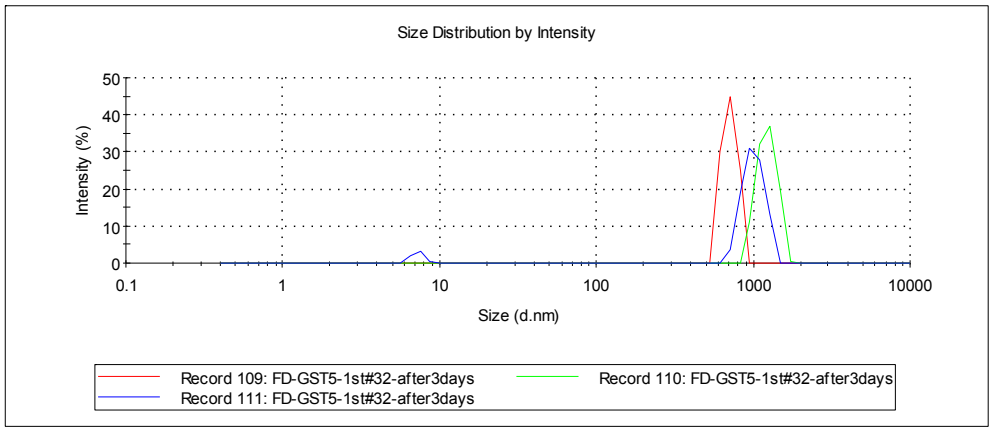

Figure 4.48: Dynamic light scattering measurement of the GST (lane 1 in Native-PAGE analysis) stored for three days at -80^{o}C.

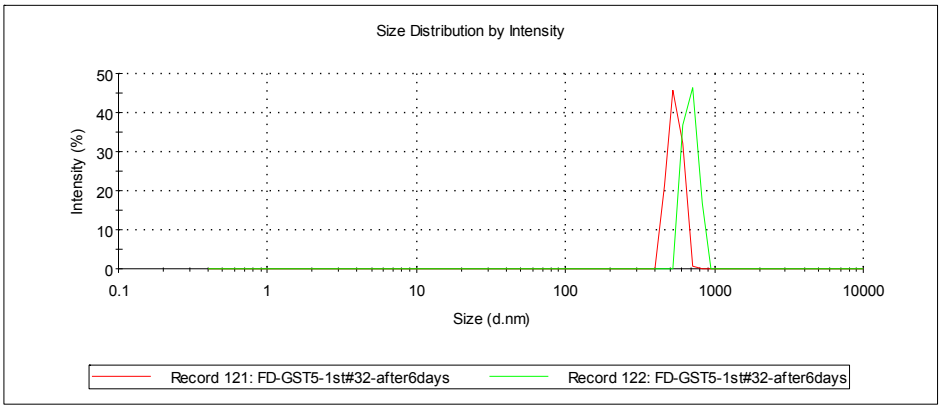

Figure 4.49: Dynamic light scattering measurement of the GST (lane 1 in Native-PAGE analysis) stored for six days at-80^{o}C.

Moving on from GST to GSTdMT the storage effect of Buffer B was also tested under the same experimental conditions and again the fractions were grouped into three sets; I stored at 4°C, II stored at -20°C and III flash freezen and stored at -80°C.

Similar results were obtained; native-PAGE analysis showed one band (Figure 4.50) for all groups. Aggregated forms were detected by DLS measurements in the fraction stored for six days at -80°C (Figure 4.51). For the fraction stored for six days at 4°C mainly dimeric form, centered around 10 nm, was observed (Figure 4.53). Aggregated forms were detected together with the dimeric species in the fraction stored for six days at -20°C (Figure 4.52).

These results showed that, similar to GST, the best storage temperature for the GSTdMT was 4°C.

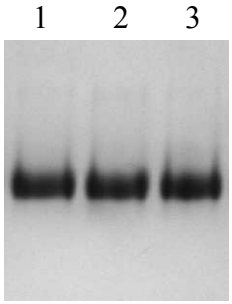

Figure 4.50: Native-PAGE analysis of purified GSTdMT fractions stored for six days in different conditions using Buffer B with 1 mM DTT and 0.1mM $CdCl_2$ only in lysis. Lane 1, fraction stored at -80°C; 2; fraction stored at -20°C, 3; fraction stored at 4°C.

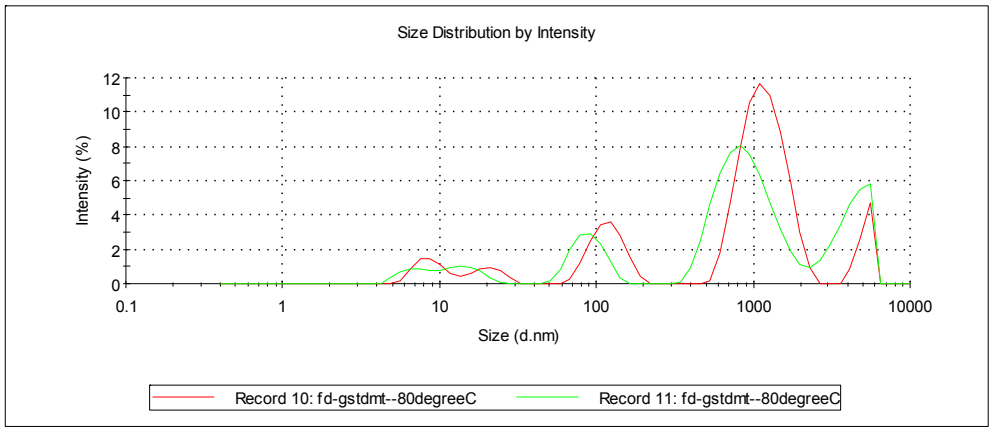

Figure 4.51: Dynamic light scattering measurement of the GSTdMT (lane 1 in Native-PAGE analysis) stored for six days at -80°C.

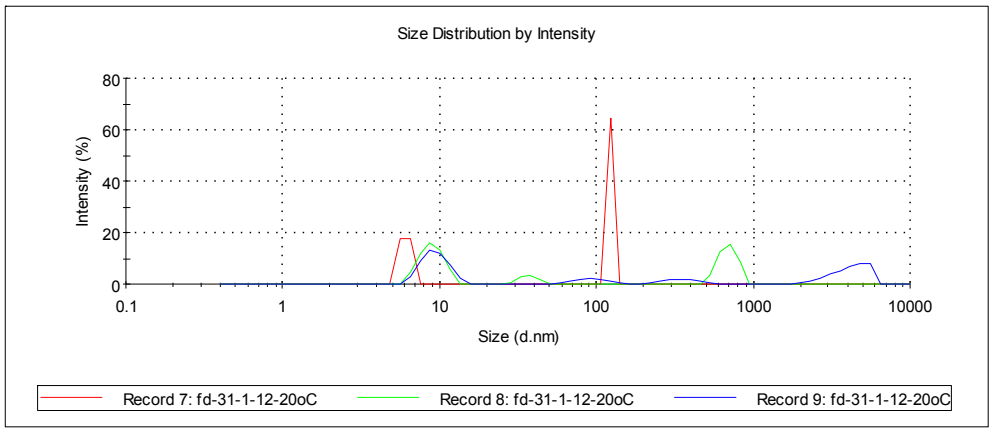

Figure 4.52: Dynamic light scattering measurement of the GSTdMT (lane 2 in Native-PAGE analysis) stored for six days at -20^{o}C.

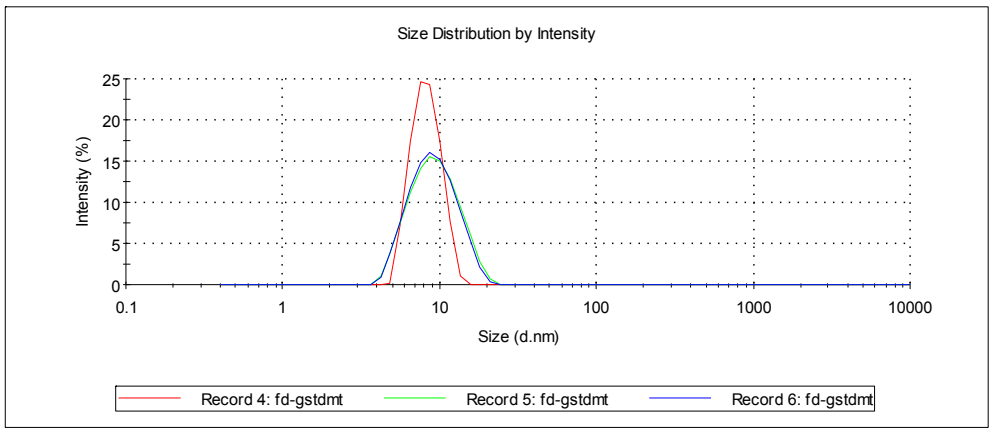

Figure 4.53: Dynamic light scattering measurement of the GSTdMT (lane 3 in Native-PAGE analysis) stored for six days at 4^{o}C.

4.1.2.2 Reversibility of Oligomerization of GSTdMT

Nature of GSTdMT oligomers were investigated by DLS measurements on pooled and concentrated GSTdMT. Table 4.3 shows the UV absorption measurements on concentrated fractions. Surprisingly DLS measurements on samples with a concentration of 13 mg/ml did not reveal aggregated species whereas when analyzed by native-PAGE the same samples appeared highly aggregated (Figure 4.54 and Figure 4.55). After six days the concentrated sample was measured by DLS again and the aggregation was detected (Figure 4.56). In order to see if the aggregation was reversible

the concentrated sample was 1/2 and ¼ diluted and analyzed by DLS. Results show that oligomerization was mostly abolished (Figure 4.57 and Figure 4.58). These results indicated that aggregate formation at high concentration was reversible.

Table 4.3: Absorption values for pooled, concentrated and diluted GSTdMT.

	A_{280}	mg/ml
Pooled GSTdMT	2.4	1.96
Concentrated GSTdMT	16	13
½ diluted GSTdMT	7.3	5.92
¼ diluted GSTdMT	3.5	2.84

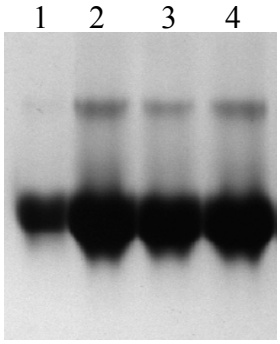

Figure 4.54: Native-PAGE analysis of concentrated GSTdMT fractions. Lane 1, pooled GSTdMT; 2-4, concentrated GSTdMT.

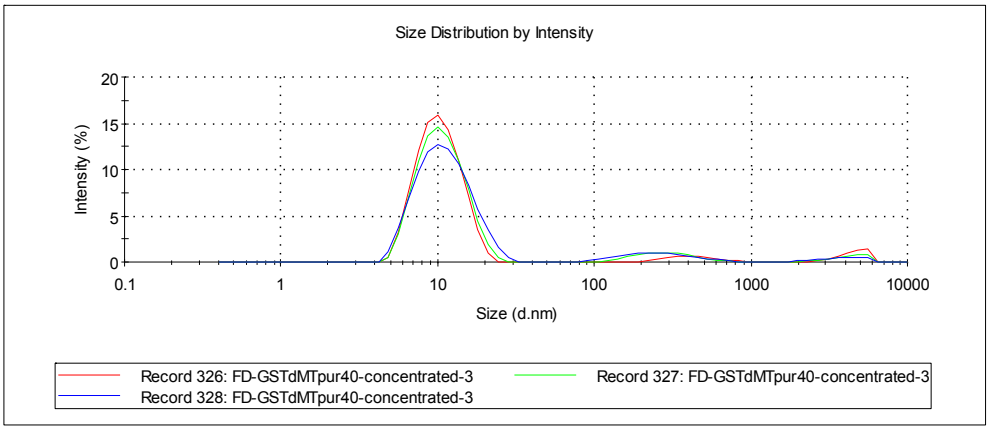

Figure 4.55: Dynamic light scattering measurement of concentrated GSTdMT.

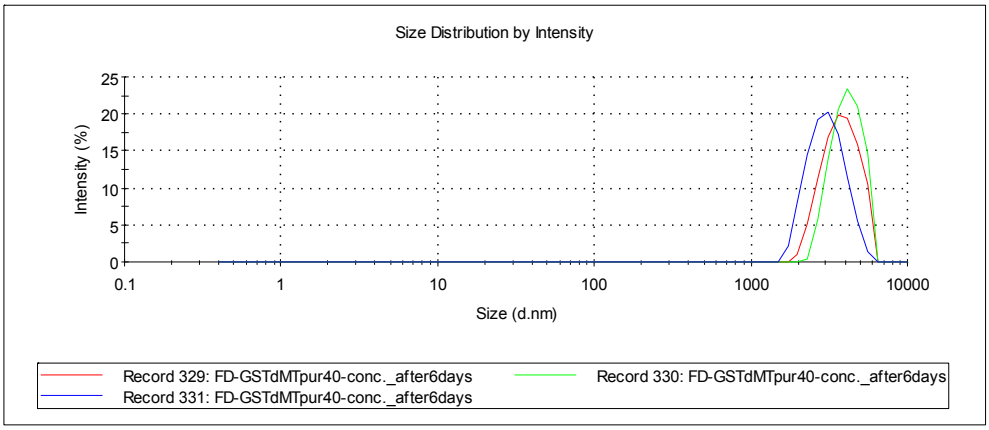

Figure 4.56: Dynamic light scattering measurement of concentrated GSTdMT stored for 6 days at 4^{o}C.

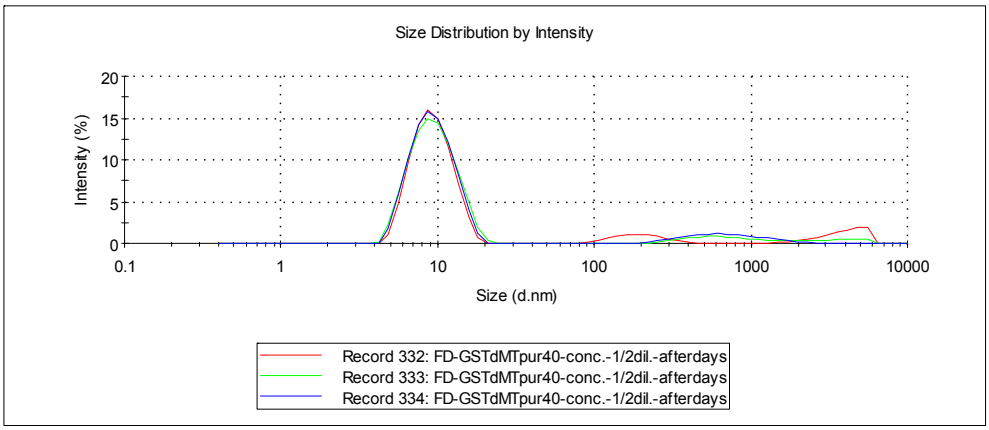

Figure 4.57: Dynamic light scattering measurement of ½ diluted GSTdMT.

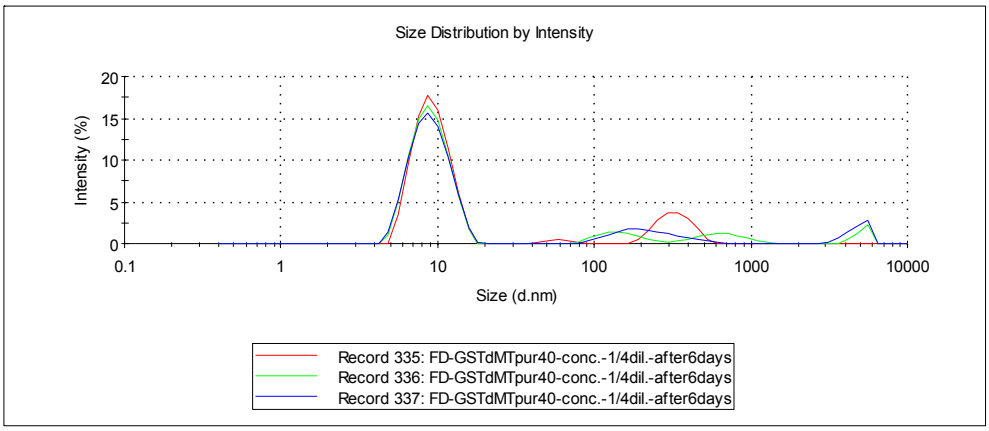

Figure 4.58: Dynamic light scattering measurement of ¼ diluted GSTdMT.

4.1.3 Determination of Cd Binding Ratio for GSTdMT

Binding ratio of Cd to dMT was investigated initially using the GSTdMT. Here it was assumed that since GST did not bind metals, any metal detected would be bound by dMT in the fusion protein. For this purpose, concentration of GSTdMT was calculated from absorbance at 280 nm and Cd was measured using ICP-OES. According to results of determinations from different preps the average Cd/protein ratio was found to be 3.4 ± 0.5 (Table 4.4).

Table 4.4: Cd/GSTdMT binding ratio for GSTdMT peak fractions from pool GII.

	Cd (µM)	**GSTdMT (µM)**	**Cd/protein**
Sample # 1	12.44	1.36	3.40
Sample # 2	15.4	1.9	3.05
Sample # 3	14.82	1.6	3.40
Sample # 4	22.2	2.8	2.97
Sample # 5	22.39	1.96	4.30
Average ± Stdev			**3.4 ± 0.5**

4.1.4 UV-Vis Spectrophotometric Characterization of GSTdMT

Unique features can be observed in the UV-Vis spectra of MTs due to the characteristic absorption bands originating from the bound metals. The position and intensity of these metal charge transfer bands are indicative for the bound metal ions. UV-vis spectroscopy was used for the initial characterization of GSTdMT.

The absorption spectrum of GSTdMT between 220 and 290 nm showed a shoulder at 280 nm due the aromatic residues in GST and the characteristic metal charge transfer band between 240 and 260 nm due to Cd-thiol interactions. The ratio of A_{250} to A_{280} can be used as an indicator of bound Cd (Figure 4.59). For fully metallated GSTdMT this ratio remained between 1.3 and 1.5 at different protein concentrations whereas for GST the ration was dependent on protein concentration (Table 4.5 and Figure 4.60).

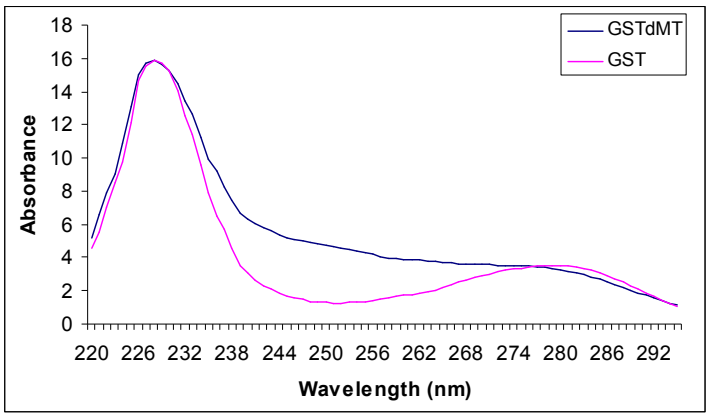

Figure 4.59: Absorbance spectrum of GSTdMT compared with that of GST at similar protein concentration.

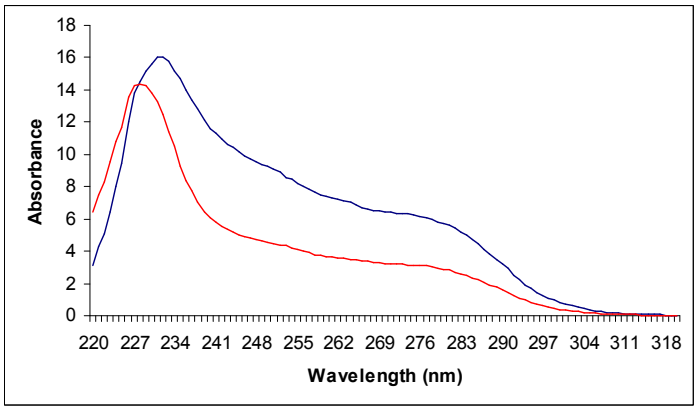

Figure 4.60: Concentration dependence of 250 nm band of GSTdMT at the concentrations of 4.62 mg/ml and 2.35 mg/ml.

Table 4.5: UV-vis absorbance values, concentrations and Cd^{2+}/GSTdMT determined by ICP-OES.

	mg/ml	**A_{250}**	**A_{280}**	**$A_{250/280}$**	**Cd^{+2}/GSTdMT**	**Average±Stdev**
GSTdMT	2.43	4.65	3.00	1.55	4.30	**3.5 ± 0.6**
	2.21	4.13	2.73	1.51	4.30	
	1.81	3.00	2.23	1.34	3.40	
	1.62	2.90	2.00	1.45	3.05	
	1.40	2.60	1.73	1.50	2.97	
	1.16	2.17	1.43	1.52	2.97	
GST	2.40	3.31	3.56	0.93	-	
	2.19	1.78	3.25	0.55	-	
	1.82	1.14	2.70	0.42	-	
	1.62	1.05	2.40	0.44	-	
	1.39	1.15	2.06	0.27	-	
	1.10	1.02	1.63	0.63	-	

Since the apo-dMT is expected to have negligible absorbance at 250 nm the difference of A_{250} values for GSTdMT and GST can be used to estimate the extinction coefficient (ε) at 250nm per Cd^{2+}. According to Beer-Lambert law

$$\varepsilon_{250/Cd2+} = \frac{A_{250}\,(\text{GSTdMT}) - A_{250}\,(\text{GST})}{\text{C x d x number of } Cd^{2+}}$$

Where C is the protein concentration and the d is the path length for incident light. Using the values for A_{250} and concentrations given in Table 4.4 $\varepsilon_{250/Cd2+}$ was estimated to be 9000 $M^{-1}cm^{-1}$.

4.1.5 Secondary Structure Analysis of GSTdMT

CD spectroscopy is a form of light absorption spectroscopy that measures the difference in absorbance of right- and left-circularly polarized light by a substance. It has been shown that CD spectra between 260 and approximately 180 nm can be analyzed for the different secondary structural types: alpha helix, parallel and antiparallel beta sheet, turn, and other.

Structural features of GSTdMT were investigated by recording its CD spectra in the range 200 to 290 nm and comparing with that from GST. The GST spectrum is typical of an α/β protein with a dominating α signal. Both spectra show the strong negative bands around 208 and 222 nm and the ratio of ellipticities at these wavelengths confirm the dominating α-helical secondary structure (Table 4.6). The GSTdMT spectrum has the 208 nm band is shifted to slightly lower wavelength and this band is sharper. The spectrum above 210 nm is less negative for GSTdMT and the 222 nm band is less pronounced. Both changes point towards a decrease in the α-helical content in the overall structure which could be achieved by incorporating more β structures or by having a less ordered structure superimposed on the main GST structure (Figure 4.61).

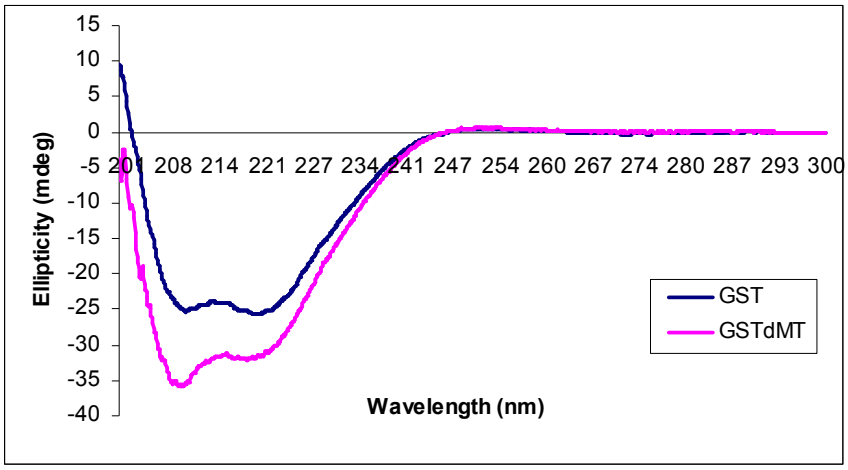

Figure 4.61: Comparison of GST and GSTdMT CD spectra. GST (blue solid line) GSTdMT (pink solid line).

Table 4.6: Comparison of the ellipticity values of GST and GSTdMT. θ represents the ellipticity.

	θ_{222}	θ_{208}	$\theta_{222/208}$
GST	-24.69	-24.18	1.02
GSTdMT	-30.19	-35.07	0.86

4.2 Purification of dMT

4.2.1 Calibration of Column

HiLoad® 16/60 Superdex 75 column (GE-Biosciences) was calibrated using 20 mg of Albumin, β-Lactoglobulin and Vitamin B12 in Buffer A with the flow rate of 1ml/min (Table 4.7). The calibration curve was obtained from the elution profile and calculated again according to the formula of Kav=(Ve-Vo)/(Vc-Vo) and used for molecular weight determination of dMT (Figure 4.62 and Figure 4.63).

Table 4.7: Protein samples used for column calibration and their molecular weights and elution volumes.

Protein	loaded (mg)	MW (Da)	V_e (ml)
Albumin	20	67000	54.86 ml
β-Lactoglobulin	20	36000 (trimer)	61.45 ml
Vitamin B12	20	1350	107.42 ml

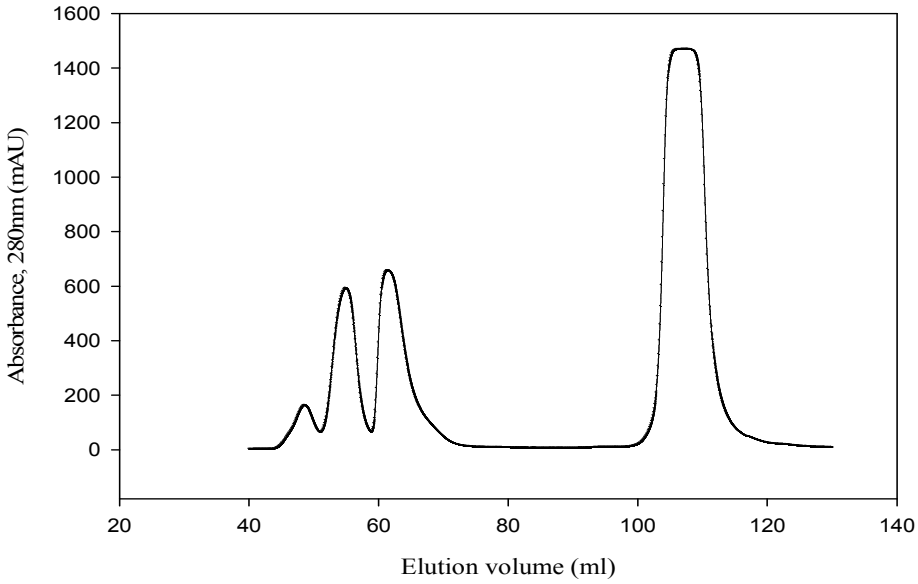

Figure 4.62: Size exclusion chromatography elution profile of calibration proteins.

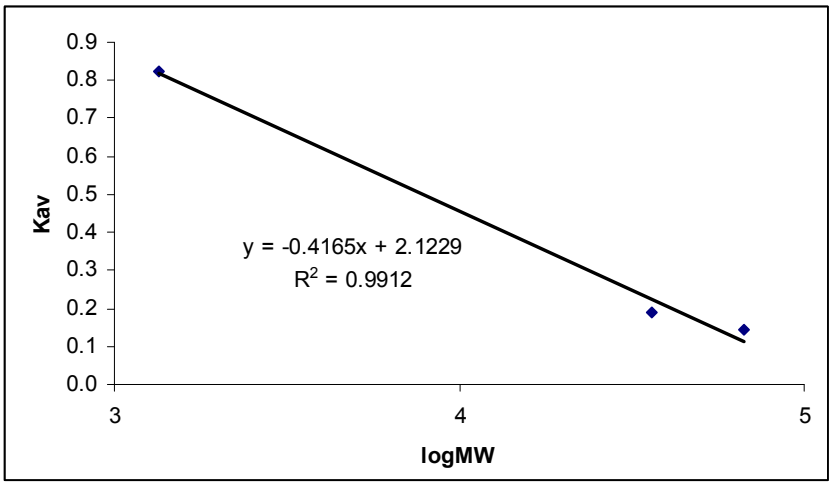

Figure 4.63: Calibration curve for HiLoad® 16/60 Superdex 75 size exclusion column, the calculated equation was used for molecular weight determination of dMT.

4.2.2 Size Exclusion Chromatography of dMT

The purification procedure of dMT was basically the same as that for GSTdMT up to the affinity purification step. This step was carried out in batch mode in the dMT procedure. Lysate was incubated with Gluthatione-Sepharose-4B beads for 4 hours. After washing the unbound protein cleavage was carried out overnight at 4^{o}C. The eluate from glutathione beads was concentrated and applied to HiLoad® 16/60 Superdex 75 column equilibrated and run with Buffer A for further separation of dMT from thrombin and residual GST in the cleavage solution. As can be seen from the elution profile proteins were separated in three peaks, two small ones coming at 42 and 60 ml and a major peak at 74 ml (Figure 4.64). The elution position of this last peak corresponded to a molecular weight of about 17 kDa which could represent dMT in dimeric or trimeric form.

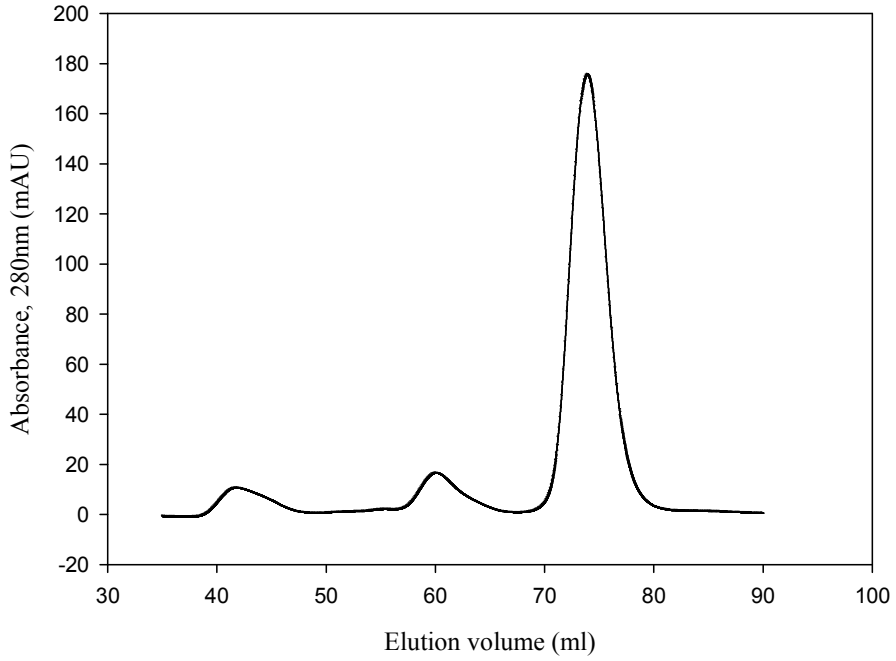

Figure 4.64: Size exclusion chromatography elution profile of dMT.

SDS-PAGE analysis of the fractions (Figure 4.65) showed that the first peak consisted mainly of GST, the second peak had oligomeric forms of dMT and the major peak displayed three bands. The band at about 25 kDa is GST that was carried over in trace amount in the dMT fractions and the lowest band represented the smallest oligomer of dMT that could be purified. The band in between the 25 kDa and the lowest

band were likely to be an insufficiently reduced form of dMT (see Chapter 5 for discussion). The fractions were also analyzed by Native-PAGE and after silver staining homogeneous dMT species were observed in all fractions (Figure 4.66).

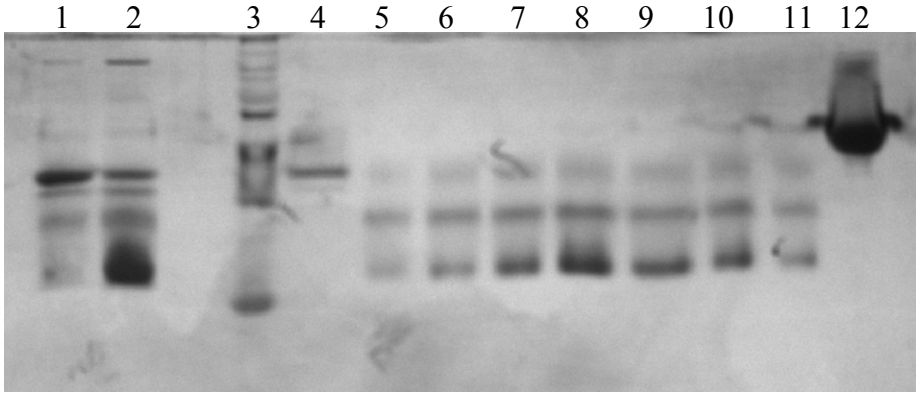

Figure 4.65: Silver stained 16% Tris-tricine analysis of purified dMT. Lane 1, eluate from the glutathione beads before concentration; 2, eluate after concentration; 3, Protein Ladder; 4, eluate from first peak from size exclusion column; 5-11, dMT fractions of the main peak from size exclusion column; 12, GSTdMT loaded as marker.

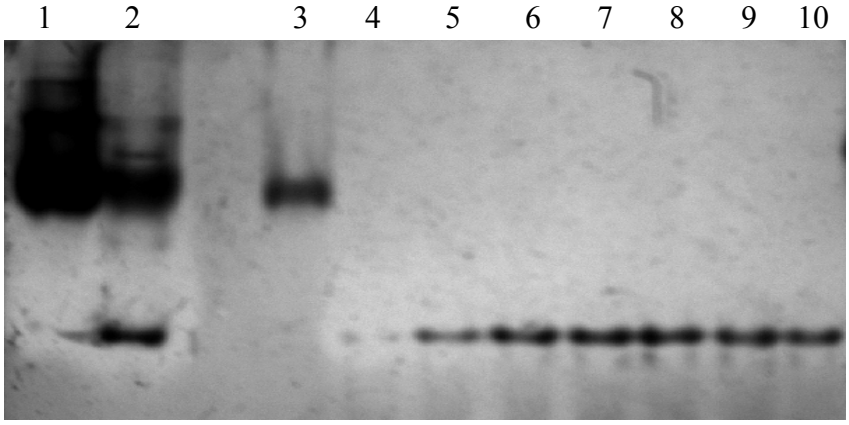

Figure 4.66: Silver stained 10% Native-PAGE analysis of purified dMT. Lane 1, eluate from the glutathione beads before concentration; 2, eluate after concentration; 3, eluate from first peak from size exclusion column; 4-10, dMT fractions of the main peak from size exclusion column.

Analysis of dMT fraction stored at 4^{o}C by DLS showed that although major portion of protein in solution was in the smallest oligomeric form. The presence of aggregated species could be detected in plots of the intensity distribution of scattered light (Figure 4.67).

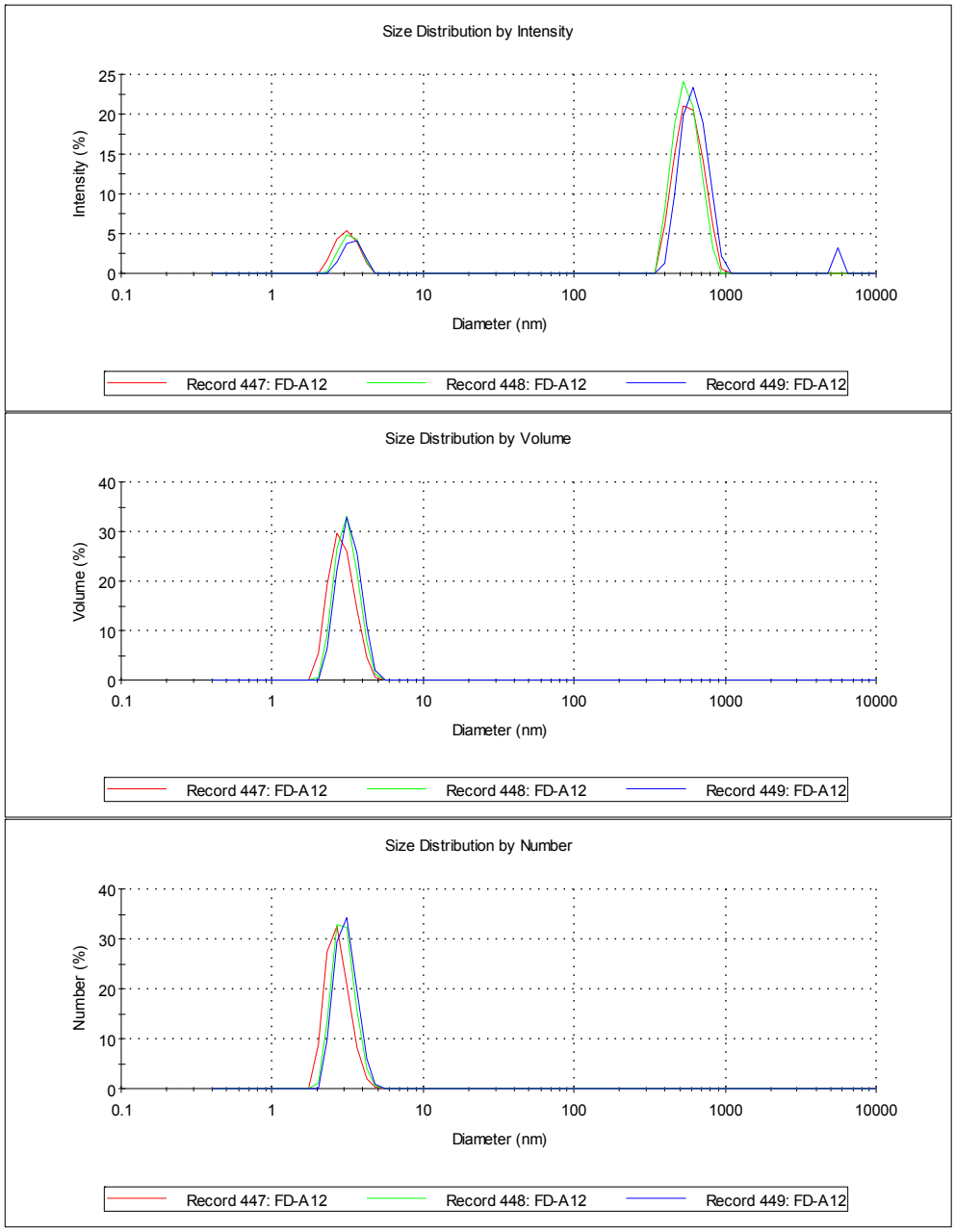

Figure 4.67: Dynamic light scattering measurements of dMT stored at 4°C.

DLS measurement of dMT fraction stored at -80°C showed the strong tendency of the protein to form aggregates when frozen (Figure 4.68) and confirmed that observations made on GSTdMT could be extrapolated to dMT. It appears that the best storage temperature for both proteins is 4°C.

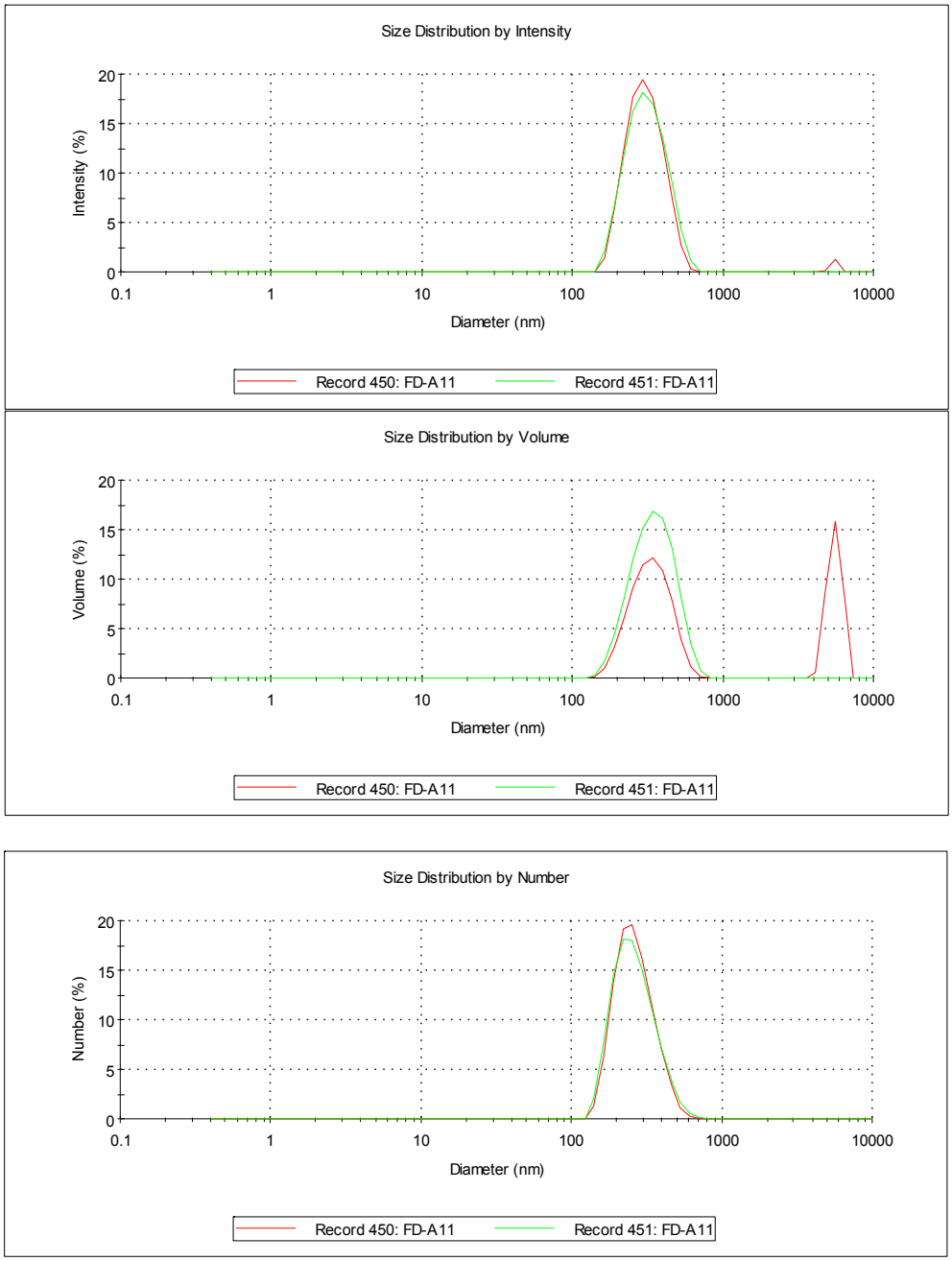

Figure 4.68: Dynamic light scattering measurement of dMT stored at 80°C.

Further characterization of purified dMT was carried out by measurement of UV-vis absorption spectra and CD spectra. The characteristic metal charge transfer band between 240 and 260 nm due to Cd-thiol interactions verified the presence of the bound Cd to dMT (Figure 4.69). The CD spectra (Figure 4.70) lacked any of the α-helical feature observed with GSTdMT (Figure 4.61) and the ratio of ellipticity at 222/208 was found to be 0.62 (Table 4.8). The fact that this value was <<1 indicated the lack of a major secondary structure.

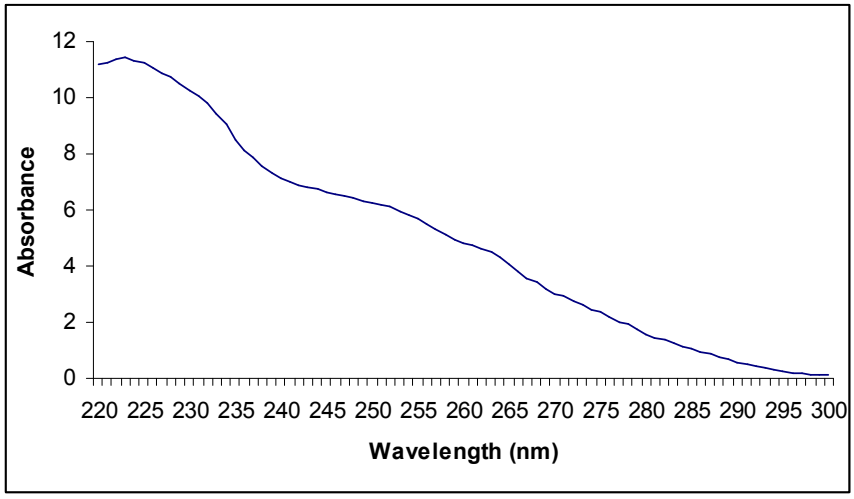

Figure 4.69: Absorption spectrum of purified dMT.

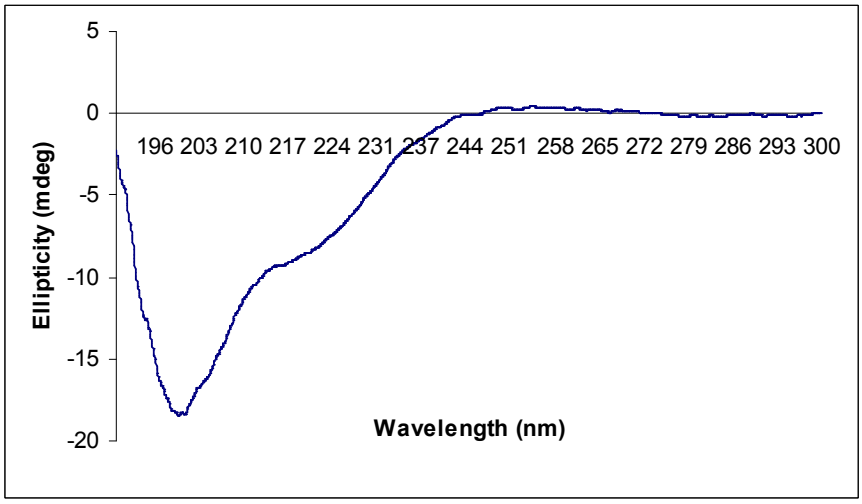

Figure 4.70: CD spectrum of purified dMT.

Table 4.8: Ellipticity values of purified dMT at 222 and 208 nm. θ represents the ellipticity.

	θ_{222}	θ_{208}	$\theta_{222/208}$
dMT	-7.97	-12.87	0.62

4.3 Structural Studies

4.3.1 Structural Analysis of GSTdMT Using SAXS

One of the major goals in the characterization of unstudied proteins is always the determination of the three-dimensional structure. For small proteins, this can be achieved in principle using single crystal X-ray crystallography and/or NMR spectroscopy. dMT and GSTdMT are proteins that do not readily crystallize and SAXS was used for establishing the shape models of GSTdMT.

SAXS data were collected from GSTdMT and GST solutions, and bovine serum albumin (BSA) was measured as a molecular mass standard. Scattering curves, after basic data reduction using PRIMUS software, for GSTdMT in Figure 4.71 and for BSA and GST in Figure 4.72. Differences in the shapes of the three proteins can be readily seen from the differences in the shapes of the curves. BSA and GST have more globular shapes and gave rise to scattering patterns with higher curvature whereas GSTdMT gave rise to an almost linear scattering curve indicating its asymmetric shape.

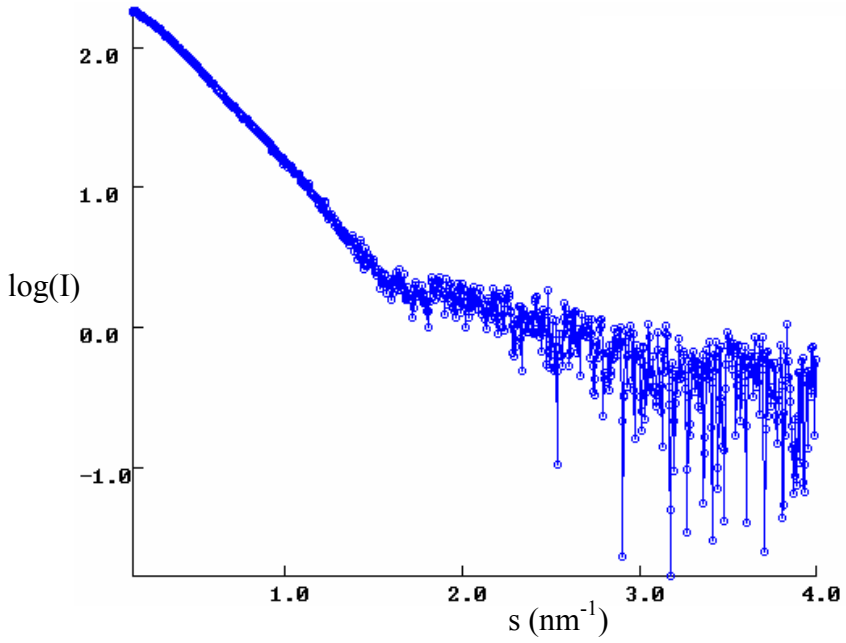

Figure 4.71: SAXS curve for GSTdMT. log(I) is the natural log of scattered intensity and $s = 4\pi \sin(\theta)/\lambda$ is the momentum transfer. GSTdMT was measured in Buffer B at 2.34 mg/ml.

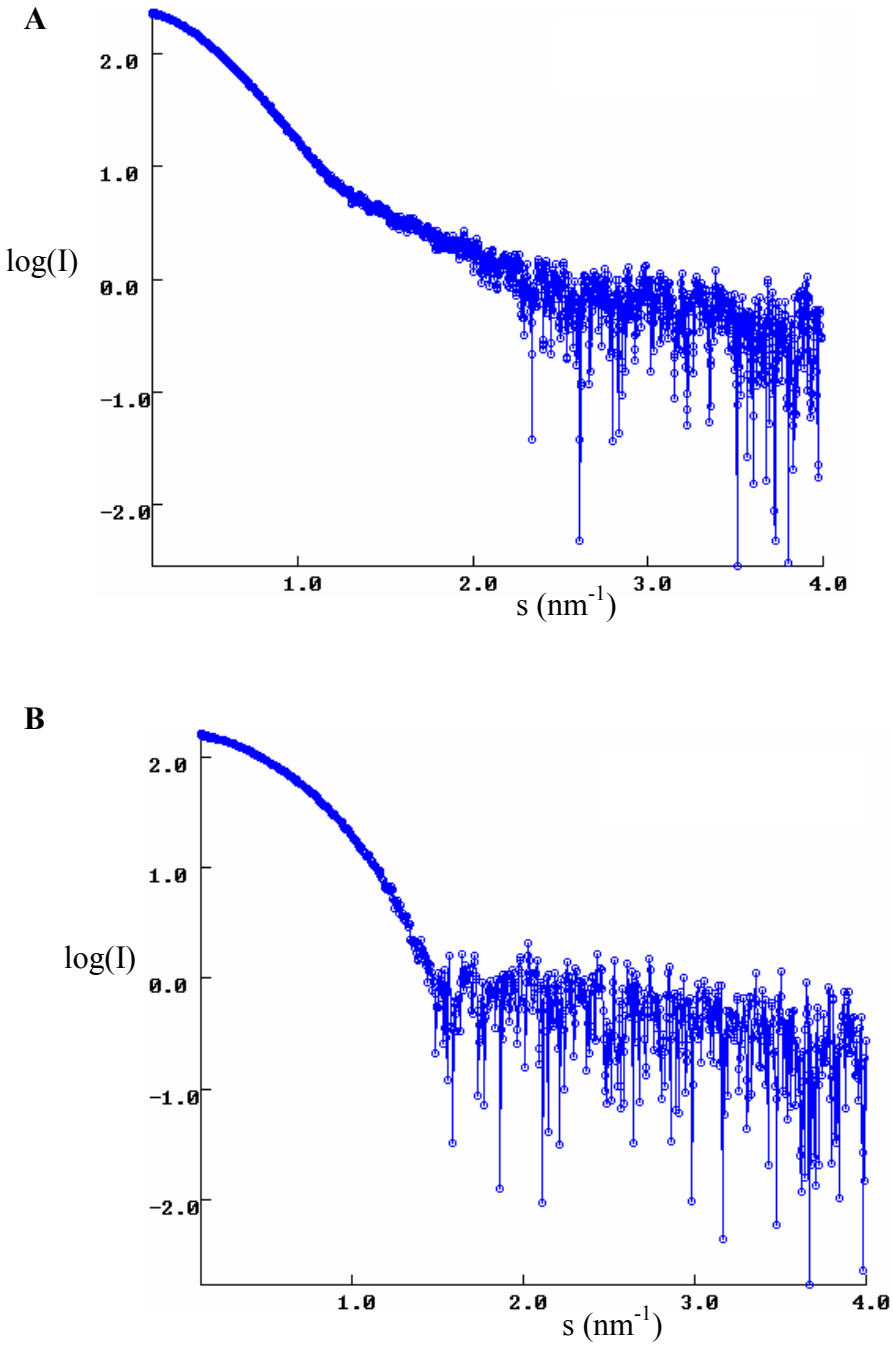

Figure 4.72: SAXS curves for BSA (A) and GST (B). BSA was measured at 4.17 mg/ml in HEPES; GST was measured in Buffer B at 2.15 mg/ml.

GSTdMT was measured at different concentrations to study the effect of aggregation on the scattering pattern and examples at 2.4 mg/ml and 4.6 mg/ml are shown in Figure 4.73. The shape of curve (2) is indicative of severe protein aggregation at this high protein concentration.

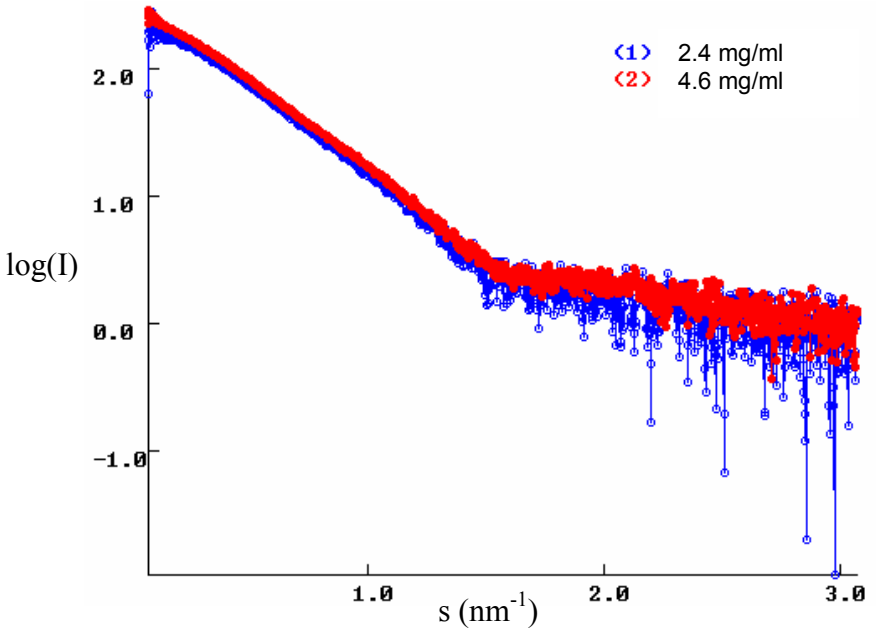

Figure 4.73: SAXS curves for GSTdMT samples at two different concentrations; (1) at 2.4 mg/ml, (2) at 4.6 mg/ml in Buffer B.

Provided that protein solutions are monodisperse, homogeneous and dilute the radii of gyration (Rg) of proteins can be calculated from the Guinier approximation (Guinier and Fournet, 1955) and the molecular mass can be estimated from I(0) relative to a standard protein with known molecular mass. Guinier curves for GSTdMT at 2.4 mg/ml and that for GST at 2.15 mg/ml in Buffer B, in the momentum transfer range 0.3<sRg<1.6, are shown in Figure 4.74 (A) and (B) respectively. The Rg and the molecular masses for GSTdMT, GST and BSA were calculated from analysis of several measurements and the average values are given in Table 4.9.

Table 4.9: Calculated molecular mass (MM) for GST and GSTdMT. MMexp is the molecular mass experimentally determined by taking BSA as reference and MMth is the molecular mass calculated from the primary sequence.

	Rg (nm)	**I(0)**	**MM_{exp}(kDa)**	**MM_{th}(kDa)**
GSTdMT	3.64 ± 0.14	199.67±10.0	50.8	34,04
GST	2.50 ± 0.07	155.92 ± 3.45	39.7	26.67
BSA	3.0 ± 0,02	259.22 ± 8.99	66.0	66.46

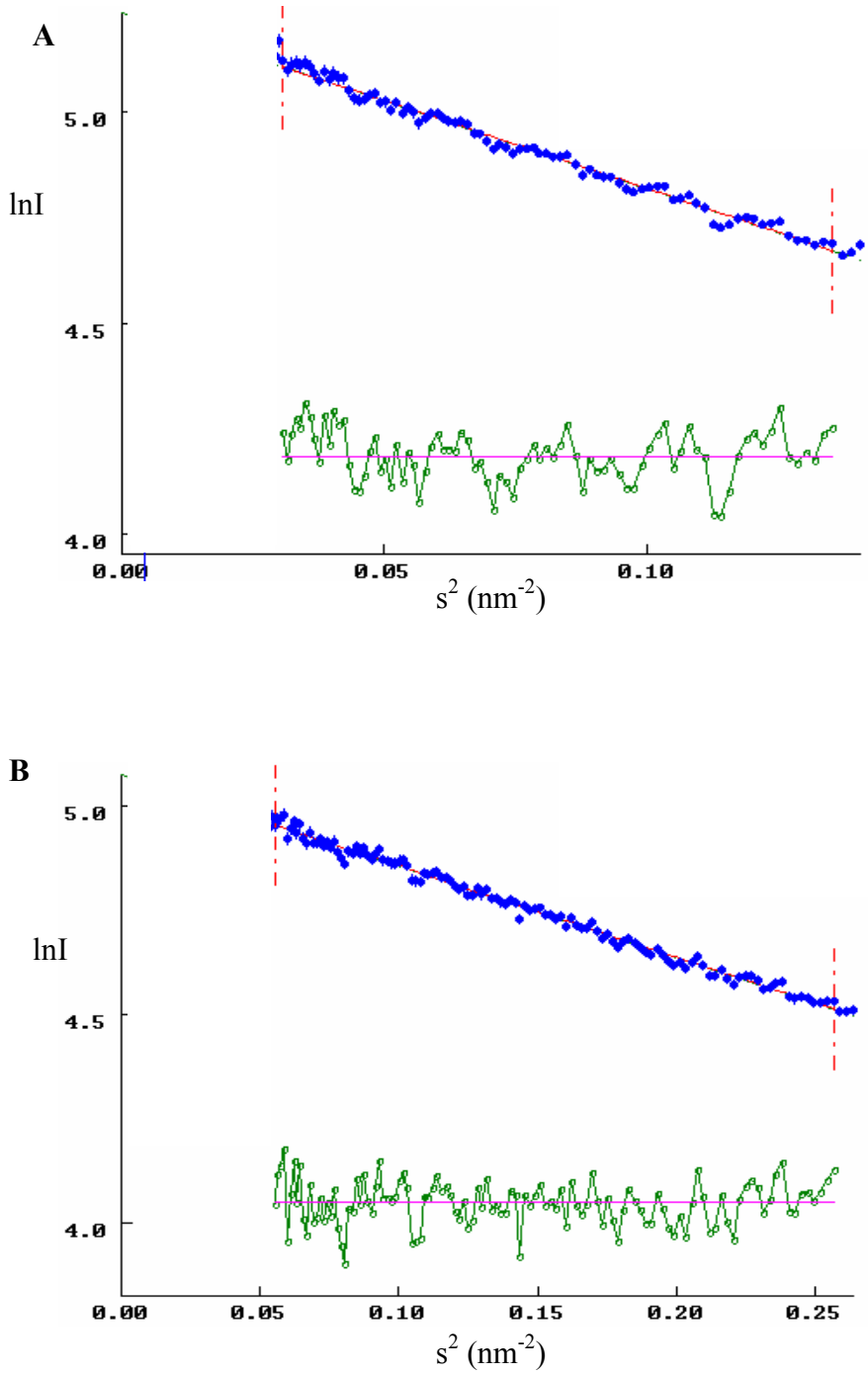

Figure 4.74: Guinier plots for GSTdMT (at 2.4 mg/ml) (A) and that for GST (at 2.15 mg/ml) (B) in Buffer B.

Any effect of aggregation on the scattering curves for GSTdMT was ruled out by checking the correlation between Rg and protein concentration as shown in Figure 4.75. Rg was found to be 3.64 ± 0.14 nm and was independent of concentration. As expected the value of Rg does not change with protein concentration. The Rg value for GST was

2.50 ± 0.07 which was smaller than that for GSTdMT again pointing to a significant difference in the shape of the two molecules. The average molecular mass was found to be 50.8 kDa for GSTdMT and 39.7 kDa for GST indicating the dimeric state of these proteins in solution. Experimental values for the molecular mass of GSTdMT and for GST were lower than those calculated. The difference in the observed and calculated values for the molecular masses will be discussed in Chapter 5.

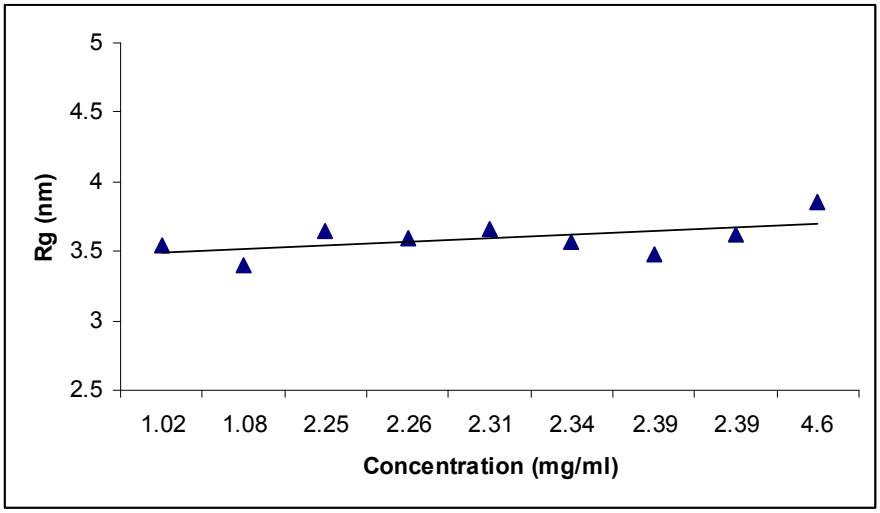

Figure 4.75: Correlation between Rg and GSTdMT concentration. Rg was determined using AutoRg software (▲) in the range of 0.3 < sRg< 1.6.

Preliminary shape information from the SAXS curves was obtained using the indirect transform algorithm GNOM. The software calculates the distribution function (electron density, distance..) that would give rise to a particular scattering pattern using indirect transforms. The scattering pattern is recalculated from the distribution function and this back and forth process is repeated until the best fit to the experimental data is found (Svergun, 1992). Results of this analysis for the scattering patterns from GST and GSTdMT are shown in Figures 4.76 and 4.77 respectively.

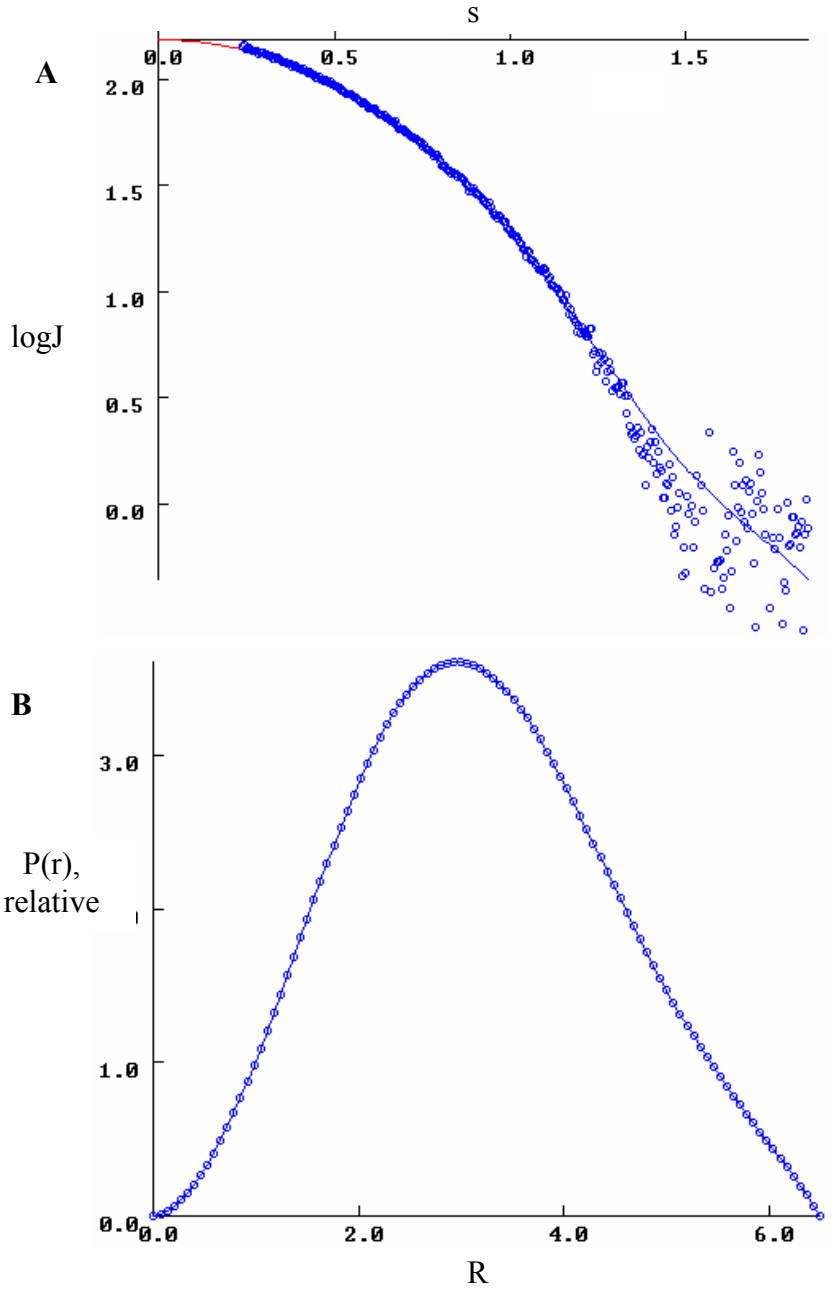

Figure 4.76: Analysis of SAXS data for GST using GNOM algorithm. (A) The fit to the experimental data (B) the pair distribution function. In this calculation D_{max}, maximum macromolecular dimension, was taken as 6.5 nm.

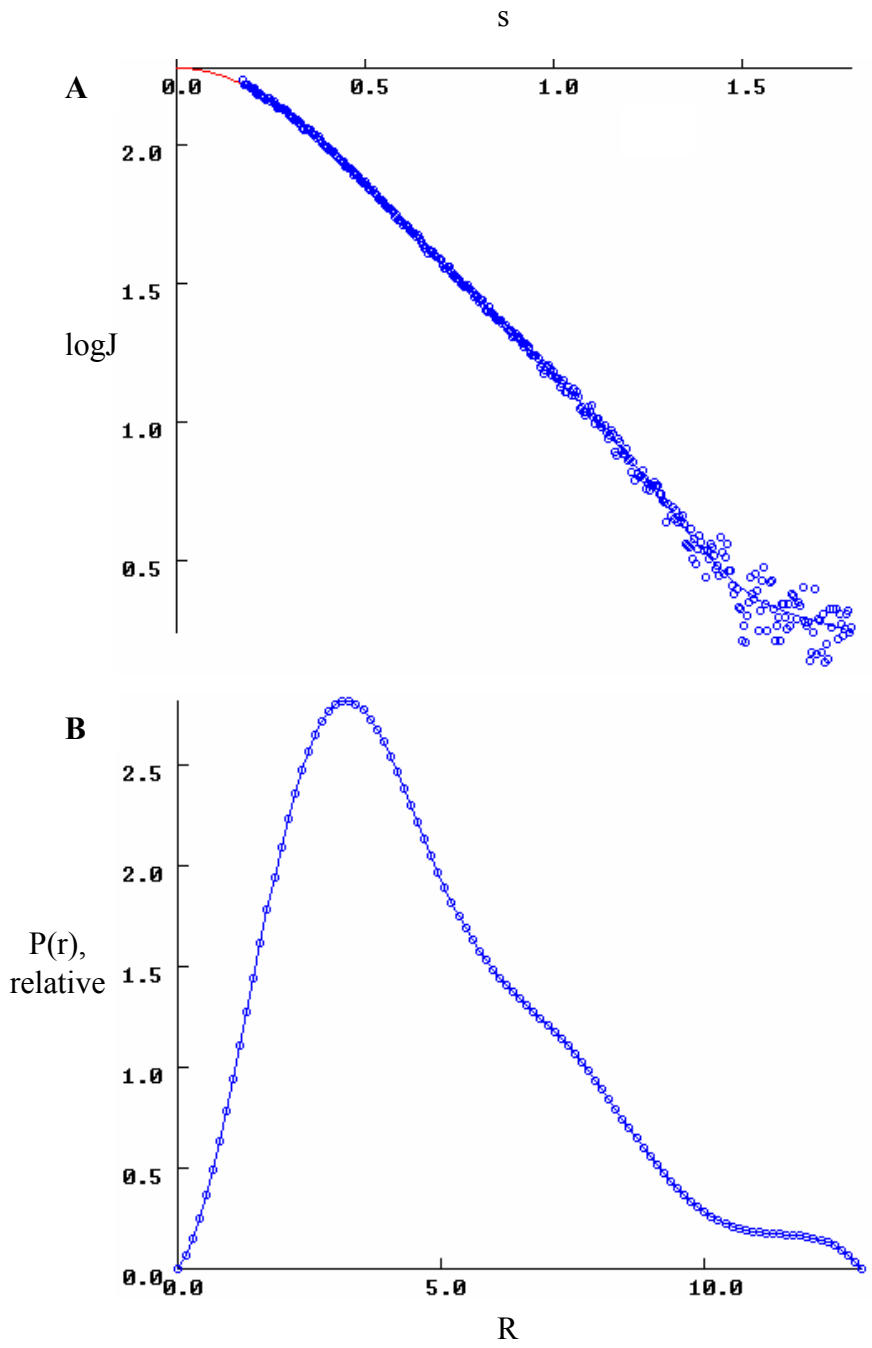

Figure 4.77: Analysis of SAXS data for GSTdMT using GNOM algorithm. (A) The fit to the experimental data (B) the pair distribution function. In this calculation D_{max} was taken as 13.5 nm.

The results shown in Figure 4.76 and 4.77 emphasize the shape difference between GST and GSTdMT. D_{max} for GSTdMT was found to be 13.5 nm as compared to 6.5nm for GST. The deviation of the p(R) function from a Gaussian was indicative of the asymmetric, elongated shape of GSTdMT.

Modeling of the GSTdMT shape was carried out using DAMMIN and GASBOR algorithms. Both are *ab initio* shape modeling programs and both utilized output files that are produced by GNOM analysis. In DAMMIN the particle that has been investigated is represented by a collection of a large number of densly packaged beads inside a search volume (Svergun, 1999). In GASBOR, on the other hand, simulated annealing is used to find a chain-compatible spatial distribution of dummy residues which fits the experimental scattering pattern (Svergun et al., 2001). No symmetry conditions were imposed on the structure although it was known that the proteins are in dimeric form in solution.

GASBOR calculations converged to the model shown in Figure 4.78 and an example of those calculated by DAMMIN is shown in Figure 4.79. In both models, as expected, the structure of the dimer was found to be highly asymmetric. There was an electron dense region at one end where the GST molecules were likely to be located and the two dMT molecules extended from this region.

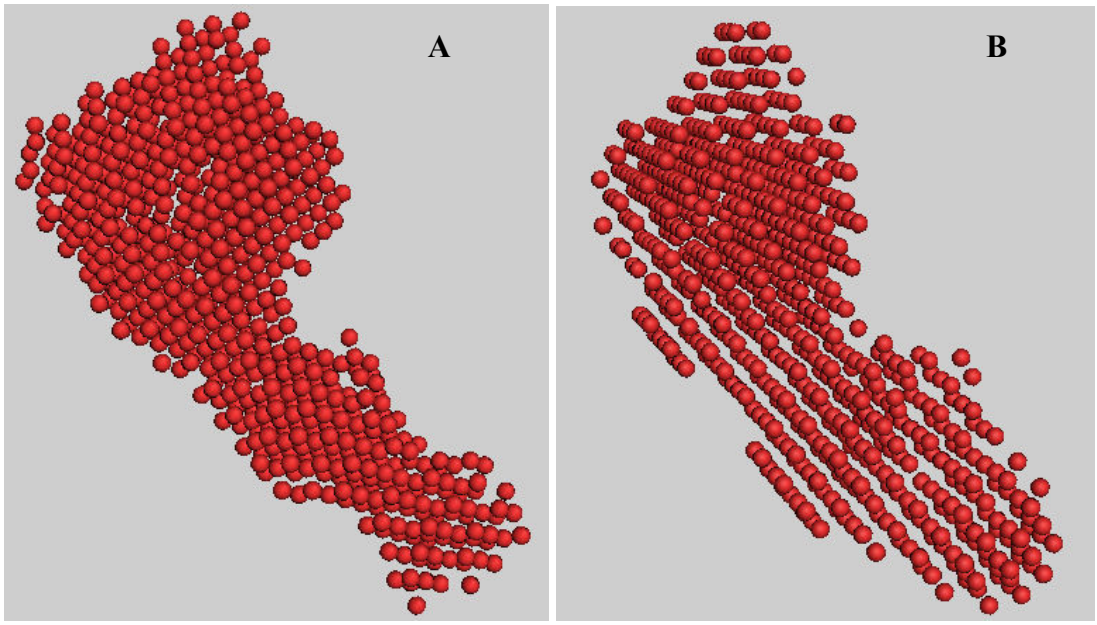

Figure 4.78: Shape model for GSTdMT developed using GASBOR (A). Its rotation by 90^0 (B).

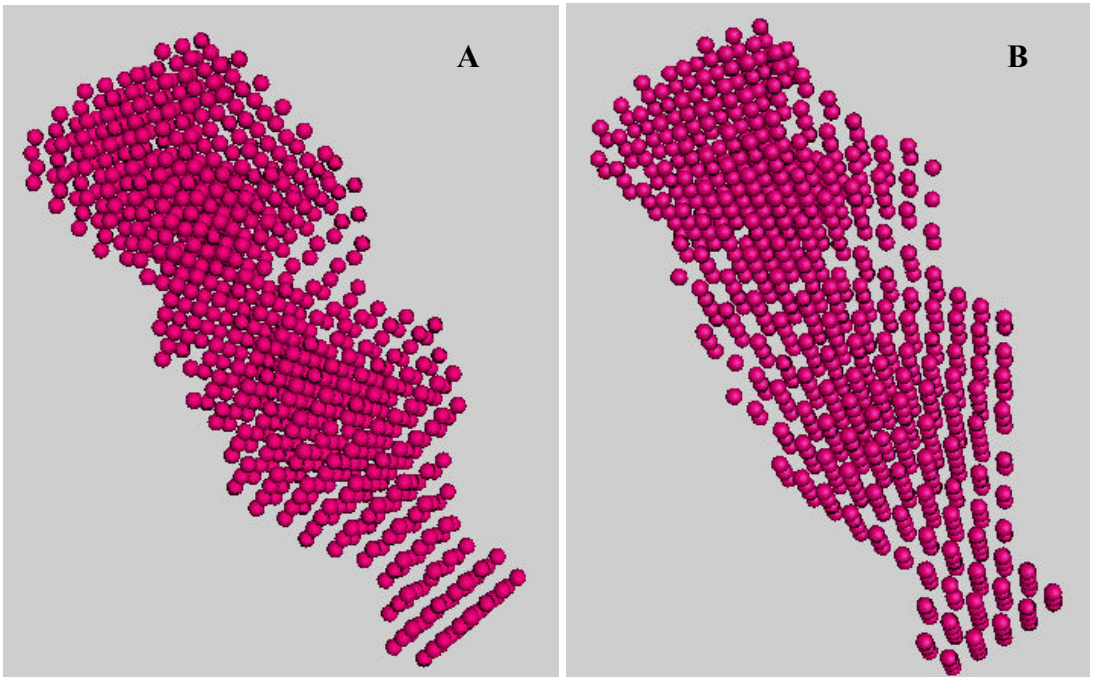

Figure 4.79: Shape model for GSTdMT developed using DAMMIN (A). Its rotation by 90^0 (B).

4.3.2 EXAFS Analysis on GSTdMT

EXAFS is the oscillating part of the X-ray Absorption Spectrum (XAS) that extends to about 1000 eV above an absorption edge of a particular element of a sample. EXAFS spectra are extremely specific to the nature of the metal coordination site. The periodicity of each spectrum provides information about the distance between the scattering atom and its neighbors, and the edge profiles of each spectrum can be used to determine coordination numbers. X-ray absorption spectroscopy (XAS) allows for element specific characterization of metal sites in biological systems and yields information about the types and distances of coordinating ligands as well as the oxidation state of metal centers. For multi-nuclear, metal containing proteins, the metal-metal distance can also be determined (Penner-Hahn 1999).

The geometry of the metal binding site and the metal coordinating ligands in GSTdMT were investigated by X-ray absorption fine structure (XAFS) measurements. The energy range for measurements included both the X-ray Absorption Near Edge Structure (XANES) and the Extended X-ray Absorption Fine Structure (EXAFS)

regions. Features in the XANES region are sensitive to the geometric and electronic structure of the metal site and serve as indicators for coordination number and/or ligand sphere homogeneity. The fine structure, on the other hand, is sensitive to the type of ligand and their distances. Since metals in the GSTdMT fusion protein are coordinated only by the thiolate groups of the Cys residues in dMT it is expected that these results obtained on GSTdMT would be relevant for dMT.

The smooth increase of intensity in the pre-edge region indicates homogeneity of the metal environment in GSTdMT (Figure 4.80). This is further supported by the Fourier transform of k3-weighted EXAFS spectrum (Figure 4.81). Results indicated that that there are 4 sulfurs in the first coordination shell of Cd^{2+} ions and the Cd-S distances were of 2.535 A.

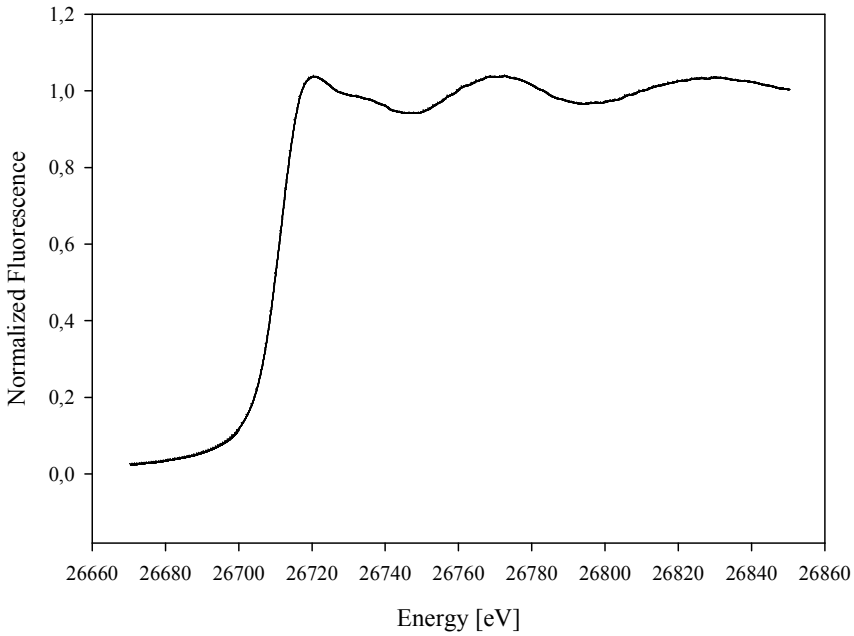

Figure 4.80: The normalized K-edge X-ray absorption spectrum of Cd4-GSTdMT.

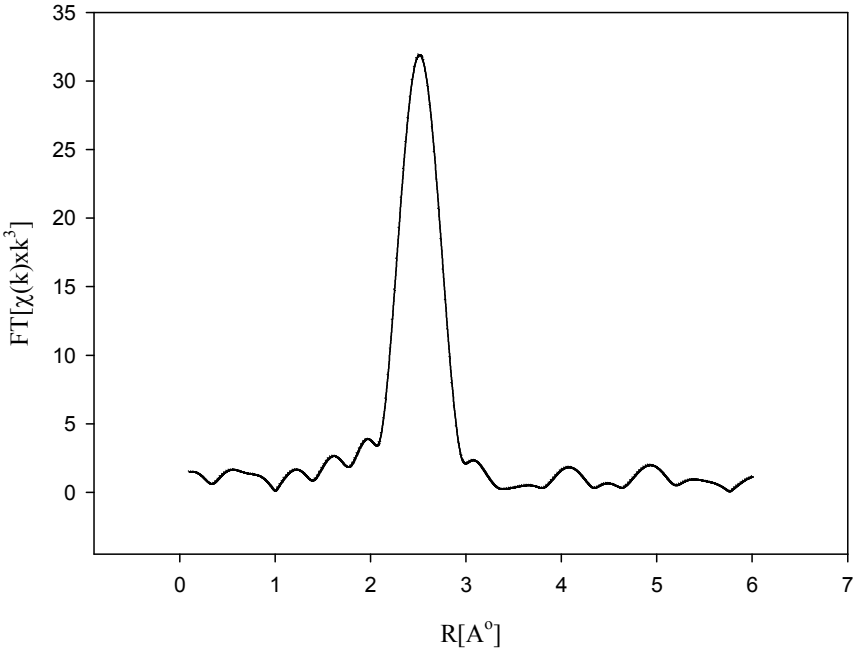

Figure 4.81: Fourier transform spectra of GSTdMT. χ; EXAFS signal, k; photoelectron wavenumber, R; interatomic distance, FT; Fourier transform.

4.4 Functional Studies

4.4.1 cDNA Synthesis

cDNA of *mt-d* gene was synthesized from isolated total RNA from Balcalı-85 plant by Omniscript reverse transcription kit with primers Oligo 1 and Oligo 2 (Table 4.10) with annealing temperature of 53.5°C. Agarose gel analysis of RT-PCR products of cDNA of *mt-d* showed bands as expected at a position between 200 and 300 bp (Figure 4.82).

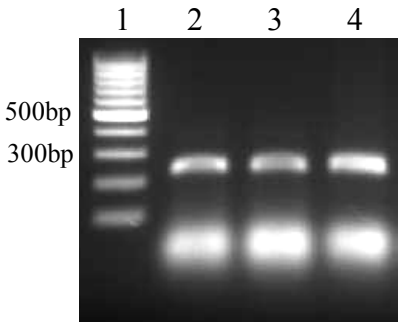

Figure 4.82: Agarose gel analysis of RT-PCR showing cDNA for *d-mt*. Lane 1, 100bp DNA Ladder; 2-4; *d-mt* cDNA bands.

Table 4.10: Primers designed for *mt* gene identification on *T. durum* genomic DNA.

Oligo 1	5'-ATGTCTTGCAACTGTGGA-3'	forward primer
Oligo 2	5'-TTAACAGTTGCAGGGGTT-3'	reverse primer with stop codon

4.4.2 Southern Blotting of *mt-d* gene

To investigate the copy number of *mt-d*, genomic DNA of *T. durum* cv. Balcalı-85 was digested with *Eco*RI, *Bam*HI and a double digestion with *Eco*RI and *Bam*HI, which do not cut the *mt-d* cDNA was also carried out. The digested genomic DNA samples were then hybridized with radioactively labeled *mt-d* cDNA. *T. durum* has a tetraploid genome (2n=28, AABB), and in order to find the localization of *mt-d* gene on *T. durum* genome different Triticum species; *A. tauchii* (DD), *T. monococcum* (AA), Bezostoya (AABBDD), *T. dicoccoides* (AABB) were digested with same restriction enzymes and hybridized with radioactively labeled *mt-d* cDNA. Digested samples were analyzed by 1% Agarose gel electrophoresis and a smear bands were observed (Figure 4.83). Southern blot analysis resulted in a single band detected with both restriction enzymes for all *Triticum* species (Figure 4.84).

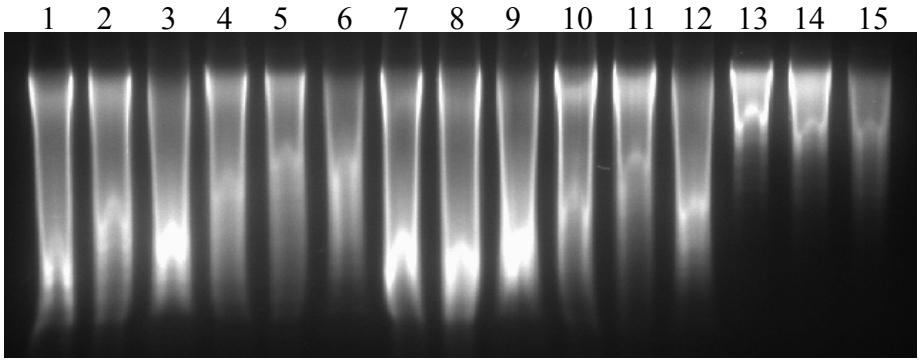

Figure 4.83: Agarose gel analysis of Triticum species digested with *Eco*RI, *Bam*HI and double digestion with *Eco*RI and *Bam*HI, respectively. Lane 1-3, Balcalı-85; 4-6, *A. tauchii*; 7-9, *T. monococcum*; 10-12, Bezostoya; 13-15, *T. dicoccoides.*

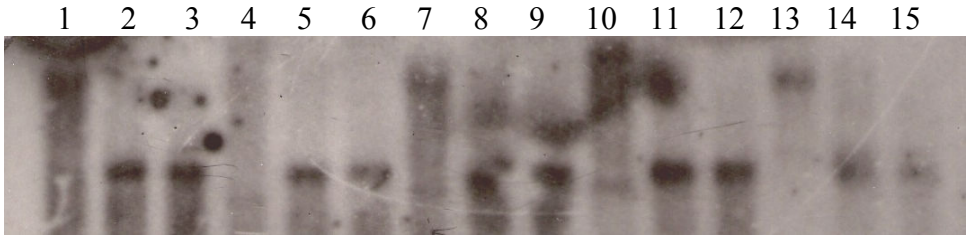

Figure 4.84: Southern blot analysis of Triticum species digested with *Eco*RI, *Bam*HI and double digestion with *Eco*RI and *Bam*HI, respectively. Lane 1-3, Balcalı-85; 4-6, *A. tauchii*; 7-9, *T. monococcum*; 10-12, Bezostoya; 13-15, *T. dicoccoides.*

The above restriction digestion experiment was repeated omitting the double digestion with *Eco*RI and *Bam*HI. Agarose gel analysis of digested genomic DNA samples resulted in same smear bands (Figure 4.85) and Southern blot analysis again resulted in a single band for both restriction enzymes for all *Triticum* species (Figure 4.86). These results suggest that *mt-d* gene exists at a single locus in the genome of all *Triticum* species.

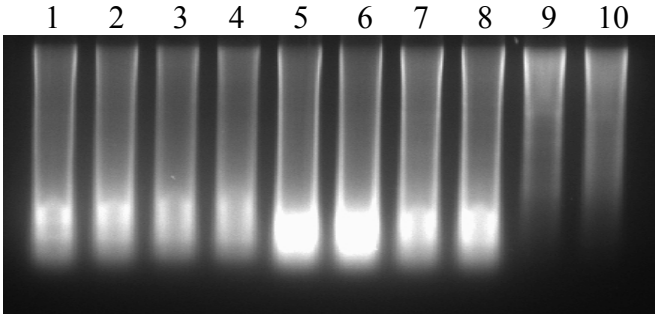

Figure 4.85: Agarose gel analysis of the *Triticum* species digested with *Eco*RI, *Bam*HI, respectively. Lane 1-3, *T. durum* cv. Balcalı-85; 4-6, *A. tauchii*; 7-9, *T. monococcum*; 10-12, Bezostoya; 13-15, *T. dicoccoides.*

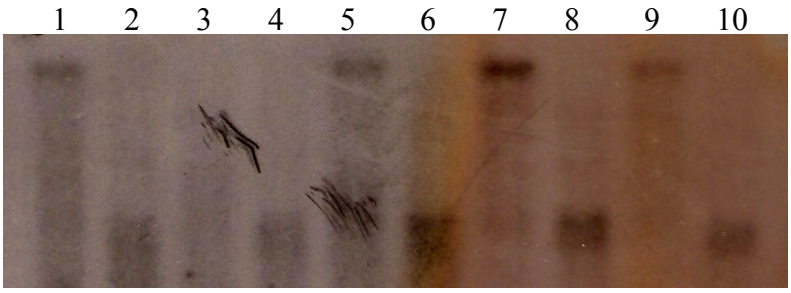

Figure 4.86: Southern blot analysis of the Triticum species digested with *Eco*RI, *Bam*HI, respectively. Lane 1-3, *T. durum* cv. Balcalı-85; 4-6, *A. tauchii*; 7-9, *T. monococcum*; 10-12, Bezostoya; 13-15, *T. dicoccoides.*

However these results did not give information about the localization of *mt-d* gene on the *T. durum* genome.

4.4.3 Plant Growth and Cadmium Treatments of Balcalı-85

1 week old seedlings of Balcalı-85 were exposed to 2, 5, 10 and 20 µM of Cd and the level of response depended on the degree of Cd application. A significant decrease was observed in both shoot and root growth (Figure 4.87). In addition continuous decrease was found in the dry weights of shoots and roots by increasing Cd application (Figure 4.88). With increasing Cd supply from 0 to 20 µM the shoot dry weight of Balcalı-85 was decreased by 28 % whereas the decrease in root dry weight was 60 %.

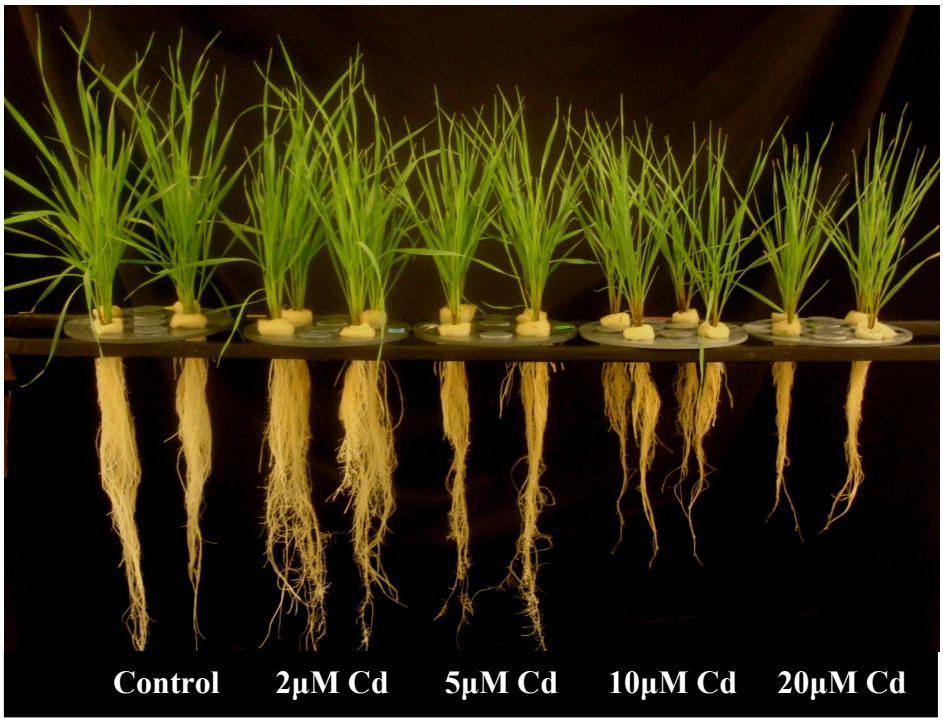

Figure 4.87: Shoot and root growth of the durum wheat cultivar Balcalı-85 with increasing Cd application. After 7 days of growth without Cd application in nutrient solution, plants were treated for 7 days by increasing Cd concentrations.

Increasing Cd concentration in the growth media resulted in higher amount of Cd uptake both in shoots and roots. The difference in Cd concentration between roots and shoots showed that Cd was accumulated in the roots in much higher amounts than in the shoots in Balcalı-85 plants (Figure 4.89 and Figure 4.90).

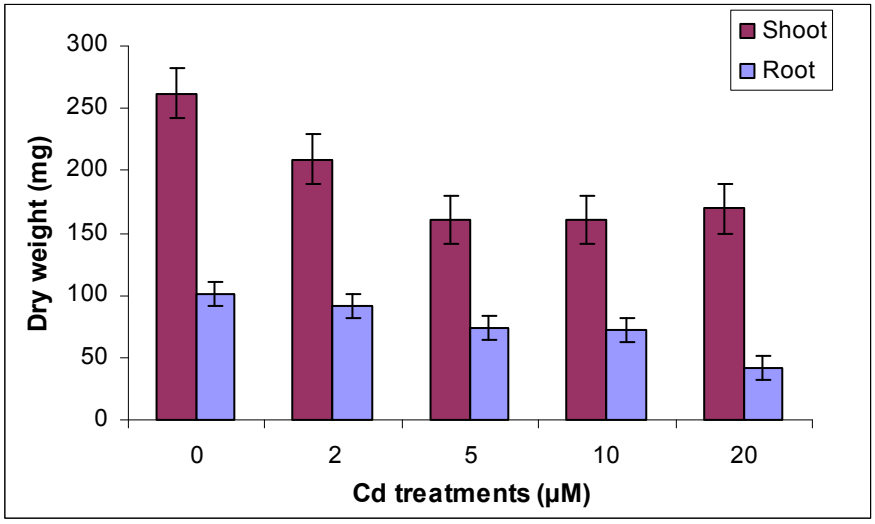

Figure 4.88: Effect of increasing Cd application on shoot and root dry weight.

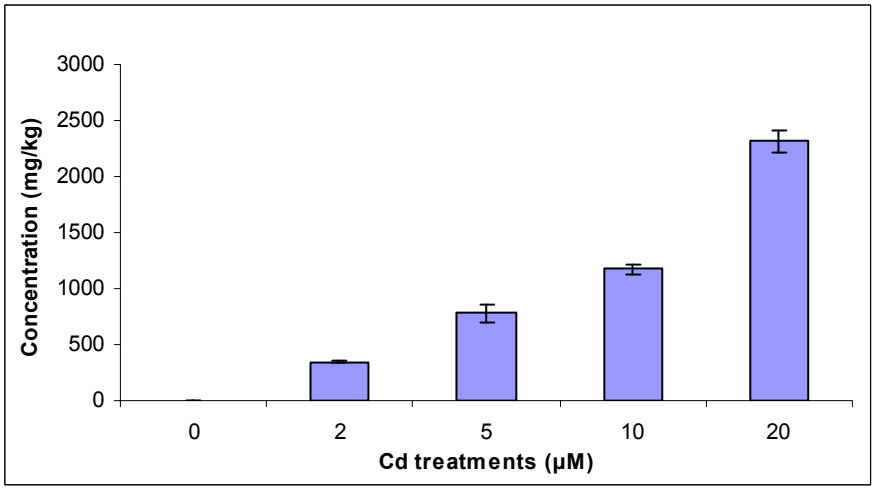

Figure 4.89: Effect of increasing Cd application on root Cd uptake.

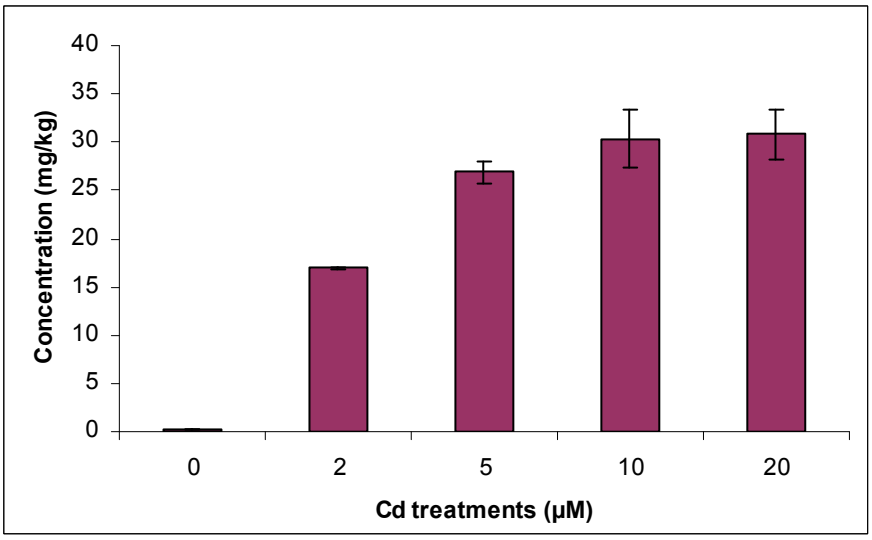

Figure 4.90: Effect of increasing Cd application on shoot Cd uptake.

4.4.4 Investigation of DNA Binding of GSTdMT

In order to investigate possible DNA binding activity of dMT, a whole genome PCR (WGPCR)-based screening method, based on Kinzler and Vogelstein (1989), was used with some modifications. In this method, recombinant GSTdMT is incubated with the pool of linker-ligated DNA fragments to allow binding. The small amount of bound DNA fragments can be amplified using PCR, and selection followed by amplification can be repeated to achieve the desired purity and quantity of bound DNA fragments which could be sequenced subsequently.

In the WGPCR method, the strategy involves converting total genomic DNA to a form which can be amplified by PCR. A diagram of the modified WGPCR strategy we have utilized is shown in Figure 4.91 and is described in detail in the Methods section. In the first step, total Balcalı-85 genomic DNA is digested with a 4-cutter *Taq*I enzyme (T^CGA) and sonicated for 25 minutes to obtain a pool of DNA fragments that has an average size of 300 bp (Figure 4.92). The *Taq*I digested DNA fragments are then ligated to linkers which contain half of recognition site of the same enzyme at their termini and serve as an efficient template for the PCR.

Each linker was designed such that it had one half of *Taq*I restriction endonuclease recognition site at its termini. This was needed for preventing self ligation of linkers. Single stranded forms of linkers were used as primers for PCR amplification (Table 4.11).

The ligation mixture was digested with *Taq*I enzyme to eliminate self ligated linkers. As controls, digested and sonicated DNA and linker samples were also self-ligated and digested with *Taq*I enzyme. Bands were obtained only from undigested samples of self-ligated DNA, linker-ligated DNA and self-ligated linkers when analyzed by 1.5 % agarose gel electrophoresis (Figure 4.93).

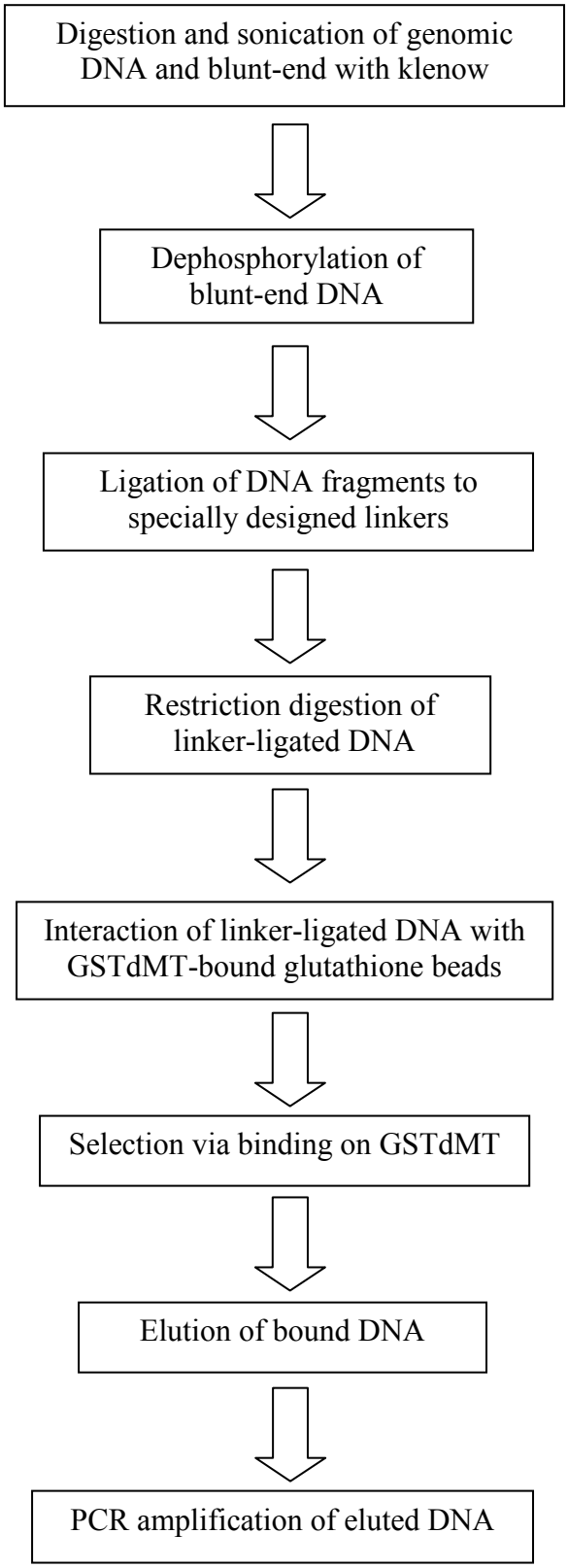

Figure 4.91: Experimental strategy of Whole Genome PCR.

Table 4.11: Linkers and primers designed for Whole Genome PCR. The red arrows represent sites of primers and bold shaded nucleotides shows the half of *Taq*I recognition sites.

Linker F1 (20 bp)	**Primer f1** 5'-**GA**TCCAGAATTCTTATAG**TC**-3' 3'-**CT**AGGTCTTAAGAATATC**AG**-5' **Primer f2**
Linker F2 (20 bp)	**Primer f2** 5'-**GA**CTATAAGAATTCTGGA**TC**-3' 3'-**CT**GATATTCTTAAGACCT**AG**-5' **Primer f1**
Primer f1 (20 bp)	5'-**GA**TCCAGAATTCTTATAG**TC**-3'
Primer f2 (20 bp)	5'-**GA**CTATAAGAATTCTGGA**TC**-3'

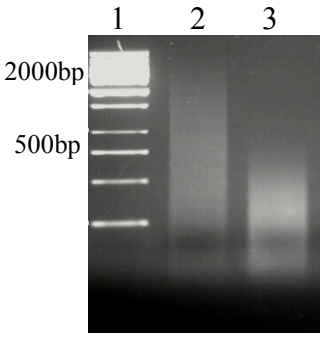

Figure 4.92: 1.5% Agarose gel analysis of digested and sonicated Balcalı-85 genomic DNA. Lane 1, 1kb DNA Ladder; 2, *Taq*I digested Balcalı-85; 3, 25 min sonicated Balcalı-85.

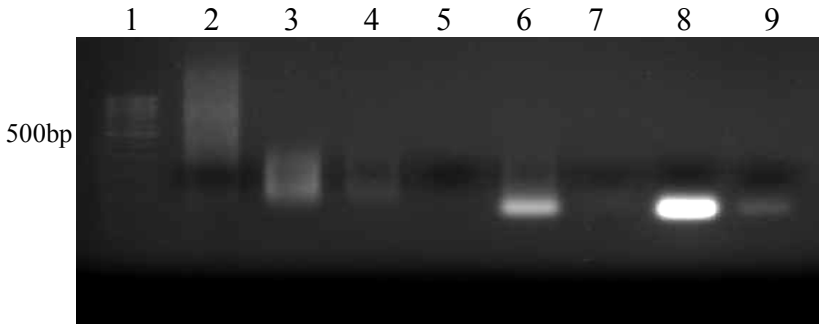

Figure 4.93: 1.5% Agarose gel analysis of ligation and *Taq*I digestion products from Balcalı-85 genomic DNA. Lane 1, Low range DNA ladder; 2, *Taq*I digested DNA; 3, 25 min sonicated DNA; 4, self-ligated DNA; 5, digested ligated DNA; 6, linker-ligated DNA; 7, digested linker-ligated DNA; 8, self-ligated linkers; 9, digested self-ligated linkers.

Ligation products were amplified with PCR using linkers as primers with the annealing temperature of 50°C in order to check efficiency of ligation. As can be seen in Figure 4.94, only linker-ligated DNA samples were amplified, which indicated that ligation process had been accomplished.

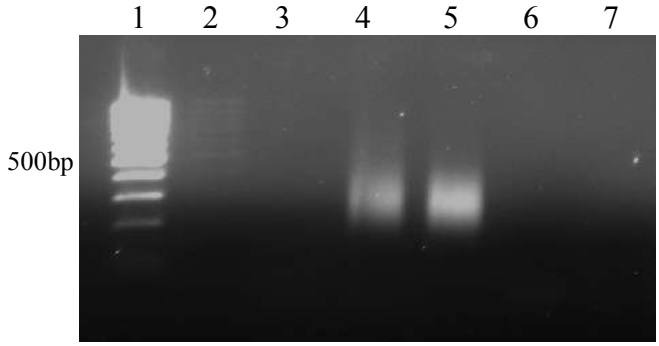

Figure 4.94: 1.5% Agarose gel analysis of PCR products in control experiments for WGPCR. Lane 1, Low range DNA ladder; 2, self-ligated DNA; 3, digested ligated DNA; 4, linker-ligated DNA; 5, digested linker-ligated DNA; 6, self-ligated linkers; 7, digested self-ligated linkers.

To test DNA binding initially 89 µg GSTdMT and as negative control 145 µg GST were incubated with 200 ng linker-ligated DNA. DNA samples from GSTdMT and GST reactions were amplified with PCR, and varying amounts (1 µl, 2.5 µl and 5 µl) were tested as template. As a result, only primer dimers were obtained from the 1st round PCR and both eluates from GSTdMT and GST gave smear bands for the 2nd round PCR (Figure 4.95). It was unexpected to have results with GST since it was used as negative control. This result is likely to be due to nonspecific binding of protein to DNA.

In order to overcome nonspecific binding of protein to DNA, poly-dIdC was used as competitor. The above binding conditions were tried with 2 µg poly-dIdC. 1 µl and 2.5 µl eluted DNA samples from GSTdMT and GST reactions were used as templates for the 1st round of PCR. Similar results were detected despite the presence of nonspecific competitor poly-dIdC (Figure 4.96). Agarose gel electrophoresis of samples from wash steps of protein DNA binding experiments for GSTdMT and GST showed that these samples also contained eluted DNA (Figure 4.97).

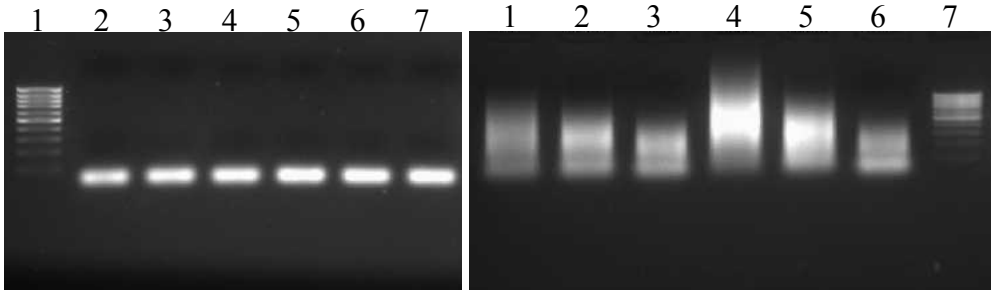

Figure 4.95: 1.5% Agarose gel analysis of PCR products of the 1st round (on the left) and 2nd round (on the right) of WGPCR experiments. Left: Lane 1, Low range DNA ladder; 2-4, 1st round PCR amplification of 1, 2.5 and 5 µl eluates from GSTdMT reaction; 5-7; 1st round PCR amplification of 1, 2.5 and 5 µl eluates from GST reaction. Right: 1-3, 2nd round PCR amplification of templates from the 1st round PCR of GSTdMT reaction; 4-6; 2nd round PCR amplification of templates from the 1st round PCR of GST reaction; 7, Low range DNA ladder.

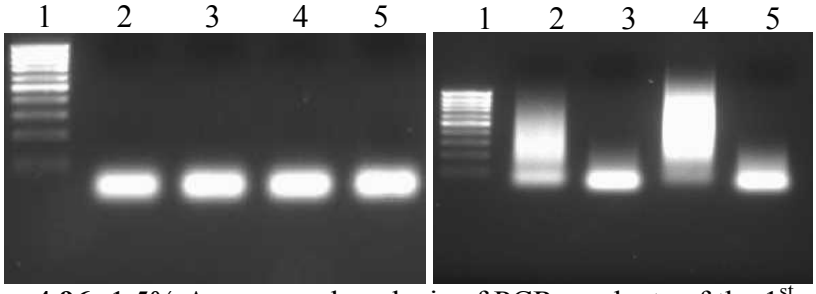

Figure 4.96: 1.5% Agarose gel analysis of PCR products of the 1st round (on the left) and 2nd round (on the right) amplifications of WGPCR experiments in the presence of poly-dIdC. Left: Lane 1, Low range DNA ladder; 2-3, 1st round PCR amplification of 1 and 2.5 µl eluates from GSTdMT reaction; 4-5; 1st round PCR amplification of 1 and 2.5 µl elutes from GST. Right: 1, Low range DNA ladder; 2-3, 2nd round PCR amplification of templates from the 1st round PCR of GSTdMT; 4-5; 2nd round PCR amplification of templates from the 1st round PCR of GST.

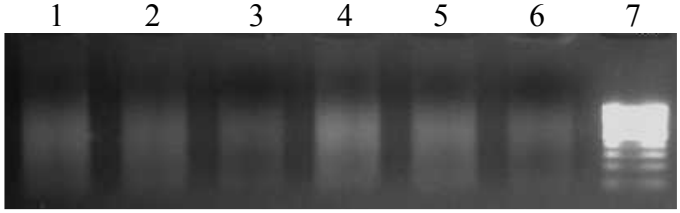

Figure 4.97: 1% Agarose gel analysis of samples from washing steps of WGPCR experiments. Lane 1-3, wash samples of GSTdMT reaction; 4-6, wash samples of GST reaction; 7, Low range DNA ladder.

To investigate the effect of the amplification of poly-dIdC and primer dimers, poly-dIdC and usage of primers were tested with 1st and 2nd round PCR and amplified and non amplified forms of poly-dIdC and the primers were loaded on agarose gel and also on 7% nondenaturing polyacrylamide (PAGE) gels to detect the exact molecular weight. Also, linker-ligated DNA was amplified with both primers and only primer f1 to test the usage of primers.

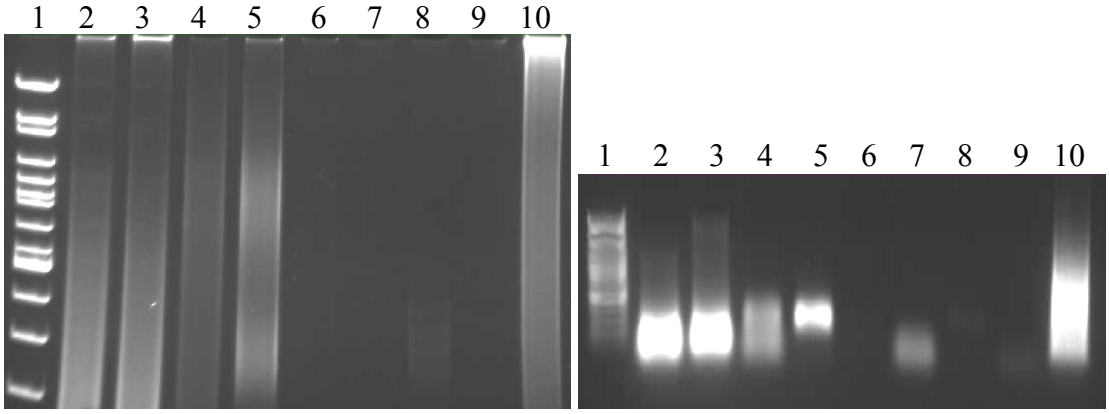

Figure 4.98: 7% Nondenaturing PAGE (on the left) and 1% Agarose gel analysis (on the right) of PCR products of the 1st round. Lane 1, 100 bp Ladder plus marker; 2, 0.8 µg poly-dIdC with primers f1+f2; 3, 0.8 µg poly-dIdC without primers; 4, linker-ligated DNA with primers f1+f2; 5, linker-ligated DNA with primer f1; 6, linker-ligated DNA without primers; 7, only primers f1+f2; 8, only primer f1; 9, nonamplified only primer f1; 10, nonamplified 0.8 µg poly-dIdC.

Results obtained from nondenaturing PAGE and agarose gel also showed that poly-dIdC could be amplified by PCR with and without primers (Figure 4.98). This amplification was also observed from spectroscopic measurements at 260 nm, amplified poly-dIdC with and without primers had much higher A_{260} value than non amplified form (Table 4.12). These results showed more clearly that poly-dIdC was amplified with PCR and the usage of poly-dIdC as nonspecific competitor was not suitable.

Table 4.12: Absorption values for amplified and nonamplified forms of poly-dIdC.

	A_{260}	**ng/µl**
Amplified Poly-dIdC with primers	10.6	530.6
Amplified Poly-dIdC without primers	9.6	480.2
Poly-dIdC with primers	1.1	52.4

The usage of primers was also tested. Linker-ligated DNA amplification with primers f1+f2 and only with primer f1 gave the same results for the 1st round. However amplification with primers f1+f2 was increased for the 2nd round in addition to amplification of primers f1+f2 whereas amplification of only primer f1 for the 1st round and then amplification of primer f2 for the 2nd round resulted in a weak smear band (Figure 4.99). These results showed that the exact amplification of linker-ligated DNA could be obtained only with the usage of primers separately.

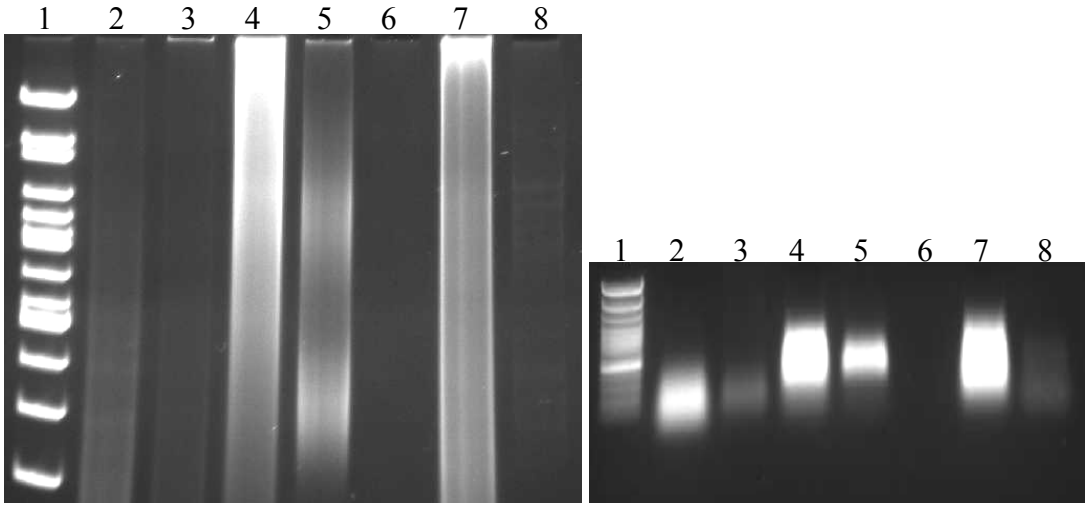

Figure 4.99: 7% Nondenaturing PAGE (on the left) and 1% Agarose gel analysis (on the right) of PCR products of the 2nd round amplification. Lane 1, 100 bp Ladder plus marker; 2, 0.8 µg poly-dIdC with primers f1+f2; 3, 0.8 µg poly-dIdC without primers; 4, linker-ligated DNA with primers f1+f2; 5, linker-ligated DNA with primer f2; 6, linker-ligated DNA without primers; 7, only primers f1+f2; 8, only primer f2.

In order to prevent primer dimer formation three different annealing temperatures 55°C, 60°C and 65°C were tested. Linker-ligated DNA was amplified with only one of the primers in each round and amplification of primers alone or together was also tested. Linker-ligated DNA amplification with primer f1 for the 1st round and with primer f2 for the 2nd round was observed at 55°C and 60°C. But using primers separately and together also gave smear bands at same temperatures for the 2nd round and this amplification was much more observed when primers used together (Figure 4.100).

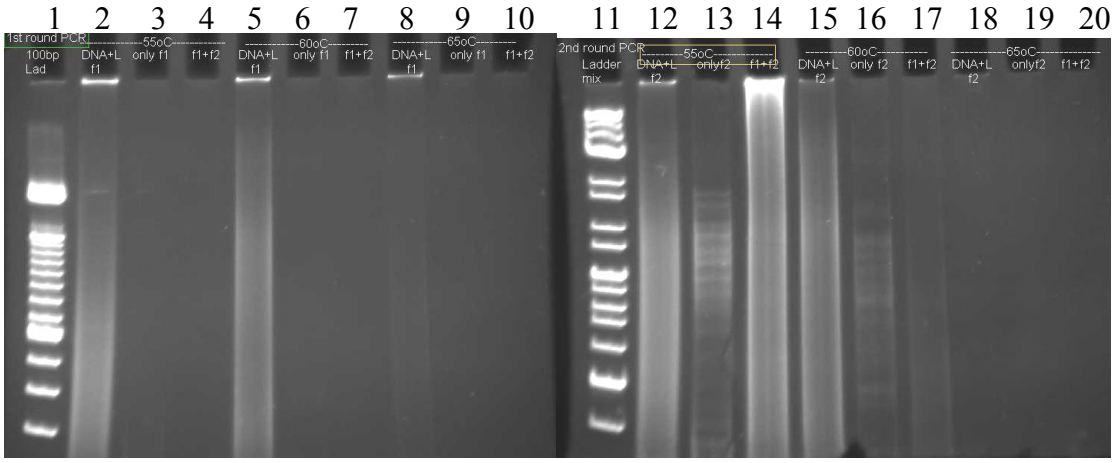

Figure 4.100: 7% Nondenaturing PAGE analysis of PCR products of the 1st and 2nd round PCR. Lane 1, 100 bp DNA Ladder; 2-10, 1st round PCR with 55°C, 60°C and 65°C respectively: 2,5,8, linker-ligated DNA with primer f1; 3,6,9, only primer f1; 4,7,10, primer f1+f2; 11, DNA Ladder mix; 12-20, 2nd rounds round PCR with 55°C, 60°C and 65°C respectively: 12,15,18, linker-ligated DNA with primer f2; 13,16,19, only primer f1; 14,17,20, primer f1+f2.

Primers f1 and f2 designed for whole genome PCR based on the linker sequences was reverse complementary for each other and it was thought that this reverse complementation led to amplification of primers f1 and f2 especially when used together.

In order to overcome this problem new linkers and primers were designed according to Watson et al., (2000) (Table 4.13). This allowed DNA precipitation and PCR to be repeated three times with Primer I and the selected fragments are subjected to a final round of amplification using Primer II.

To find the best annealing temperature for the new primers three different temperatures were tested; 55°C, 60°C, 65°C for the 1st and 2nd round PCR. Also, linker-ligated DNA amplification with primer fd1 for the 1st round and with primer fd1 and fd2 for the 2nd round were tested. Analysis with nondenaturing PAGE showed that linker-ligated DNA was amplified with fd1 for the 1st round also 2nd round but as negative controls primers were also amplified when used separately and together. For the 2nd round amplification with primer fd2 was tried and gave the same results (Figure 4.101).

Table 4.13: Linkers and primers designed for Whole Genome PCR. The red arrows represent sites of primers and bold shaded nucleotides show the half of *Taq*I recognition sites.

LinkerI (45bp)	Primer I → Primer II → 5'-**GA**GGAGCTGAGACGCGAG**TC**CCATG**GA**CGCTACACGTGACCGG**TC**-3' 3'- **CT**CCTCGACTCTGCGCTC**AG**GGTAC**CT**GCGATGTGCACTGGCC**AG**-5'
LinkerII (45bp)	5'-**GA**CCGGTCACGTGTAGCG**TC**CATGG**GA**CTCGCGTCTCAGCTCC**TC**-3' 3'-**CT**GGCCAGTGCACATCGC**AG**GTACC**CT**GAGCGCAGAGTCGAGG**AG**-5' ← Primer II ← Primer I
Primer fd1 (20 bp)	5'-**GA**GGAGCTGAGACGCGAG**TC**-3'
Primer fd2 (20 bp)	5'-**GA**CGCTACACGTGACCGG**TC**-3'

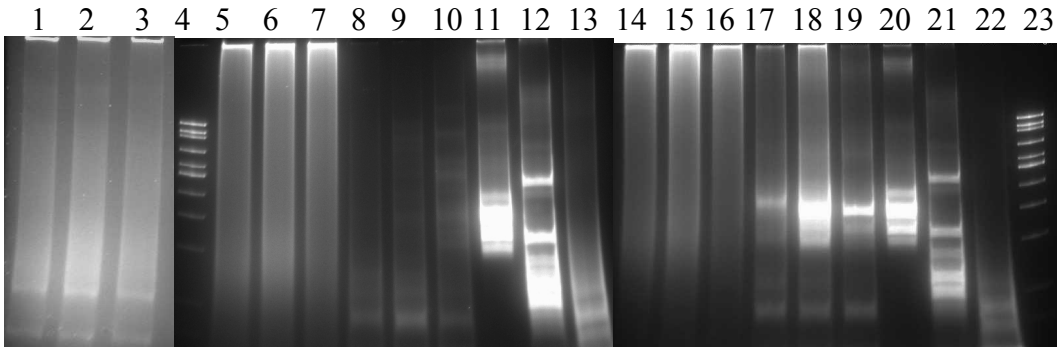

Figure 4.101: 7% Nondenaturing PAGE analysis of PCR products of the 1st, 2nd and 3rd rounds. Lane 1-3, 1st round PCR of linker-ligated DNA with primer fd1 at 55°C, 60°C and 65°C respectively, 4, Low range DNA ladder; 5-13, 2nd round PCR with primer fd1; 14-22, 3rd round PCR with primer fd2; 5-7, 14-16, linker-ligated DNA at 55°C, 60°C and 65°C; 8-10, 17-19, only linker at 55°C, 60°C and 65°C; 11, only primer fd1 at 55°C; 12, only primer fd2 at 55°C; 13, primer fd1+fd2 at 55°C; 20, only primer fd1 at 65°C; 21, only primer fd2 at 65°C; 22, primer fd1+fd2 at 65°C; 23, Low range DNA ladder.

The effect of primer concentration was investigated by decreasing the primer concentration from 1 µM to 0.5 µM. Again linker-ligated DNA with primer fd1 and as a negative control primer fd1 was amplified by PCR with the annealing temperatures of 55 and 60°C. This resulted in only amplification of linker-ligated DNA at both temperatures (Figure 4.102).

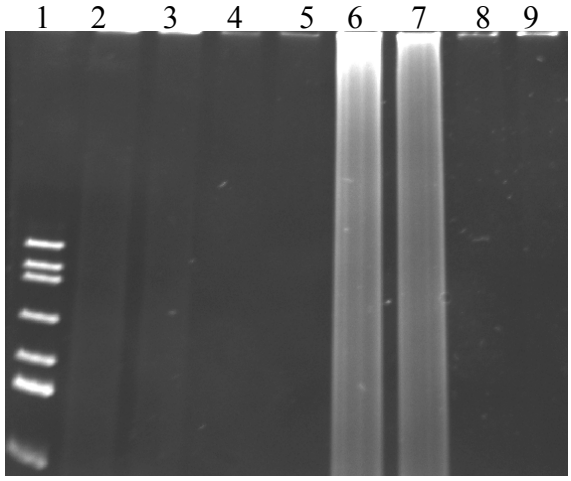

Figure 4.102: 7% Nondenaturing PAGE analysis of PCR products of the 1st and 2nd rounds with primer fd1 at 55°C and 60°C. Lane 1, Low range DNA ladder; 2-5, 1st round PCR, 6-9, 2nd round PCR: 2-3, 6-7, linker-ligated DNA; 4-5, 8-9, only primer fd1.

After solving primer amplification problem, DNA-protein binding was examined with 1:1 protein/DNA ratio. 100 ng of eluted DNA fragments from GST and GSTdMT reactions were amplified with 0.5 μM primer fd1 for the 1st and 2nd round PCR with the annealing temperature of 55°C. However, the same problem was encountered; primer fd1 used as a negative control was also amplified (Figure 4.103).

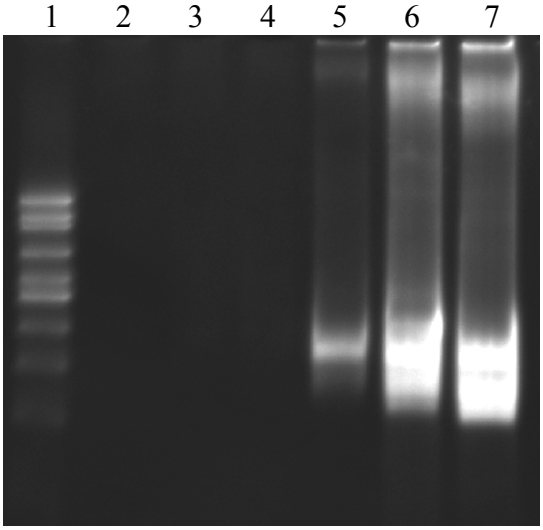

Figure 4.103: 7% Nondenaturing PAGE analysis of PCR products of the 1st and 2nd rounds with 0.5 μM primer fd1 at 55°C. Lane 1, Low range DNA ladder; 2-4, 1st round PCR, 5-7, 2nd round PCR: 2, 5, eluted DNA from GSTdMT; 3, 6, eluted DNA from GST; 4, 7 only primer fd1.

With the purpose of eliminating the problem of amplification of primers especially formed in the 2nd round, amplification of linker-ligated DNA without primers were examined. For the 1st round linker-ligated DNA was amplified with 1 μM primer fd1 at 55°C and for the 2nd and 3rd rounds amplified with and without primer. However as observed in nondenaturing PAGE analysis in Figure 4.104, amplification of linker-ligated DNA was detected in both cases in addition to amplification of primer fd1 used as negative control for the 2nd round PCR. The amplification linker-ligated DNA and primer fd1 on its own had decreased but was still observable for the 3rd round. This was more pronounced the primer was included. Therefore, for the 3rd and 4th rounds amplification of linker-ligated DNA and negative control primers with primer fd2 and without primers were tried (Figure 4.105). But, same results were detected. Consequently, amplification without primers did not solve the problem of amplification of primers themselves.

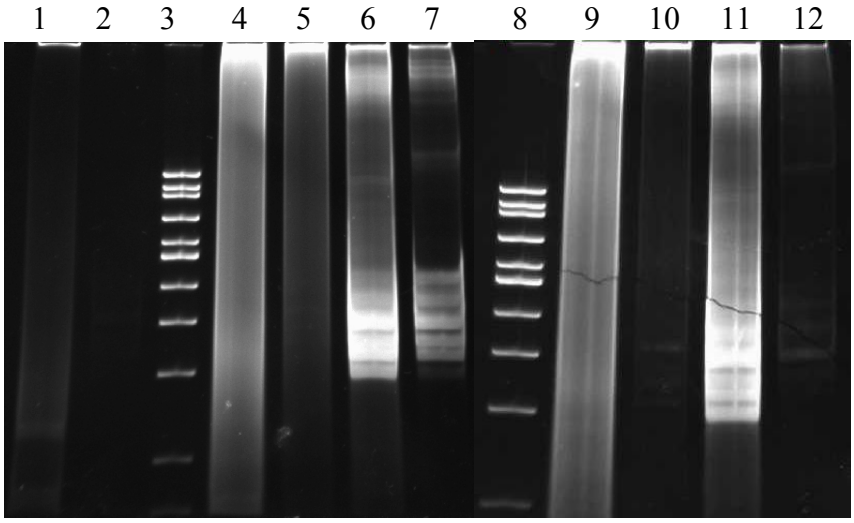

Figure 4.104: 7% Nondenaturing PAGE analysis of PCR products of the 1st, 2nd and 3rd rounds. Lane 1-2, 1st round PCR, 4-7, 2nd round PCR, 9-12, 3rd round PCR; 1,4,9, linker-ligated DNA with 1 μM primer fd1; 2,6,11, only primer fd1; 5,10, linker-ligated DNA without primer; 7,12, only primer fd1 (for the 1st round) without primer; 3, 8, Low range DNA ladder.

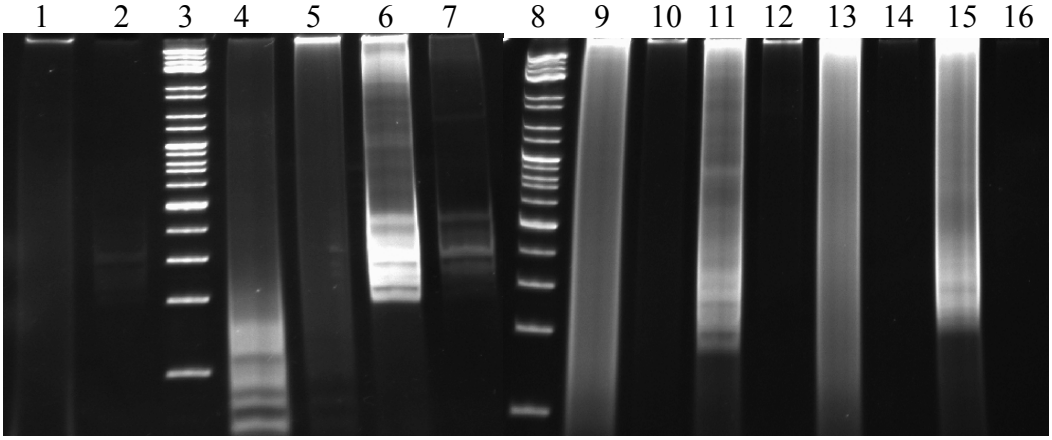

Figure 4.105: 7% Nondenaturing PAGE analysis of PCR products of the 1st, 2nd, 3rd and 4th rounds. Lane 1-2, 1st round PCR, 4-7, 2nd round PCR, 9-12, 3rd round PCR; 1,4,9,13, linker-ligated DNA with 1 μM primer fd1; 2,6,11,15 only primer fd1; 5,10, 14, linker-ligated DNA without primer; 7,12,16, only primer fd1 (for the 1st round) without primer; 3, 8, Low range DNA ladder.

Another strategy for testing DNA-protein binding was selection and amplification of linker-ligated DNA fragments separately for each round of PCR. For this purpose 1:1 protein/DNA ratio was examined. Eluted DNA fragments of the first protein-DNA interaction from GST and GSTdMT reactions were amplified with 1 μM primer fd1 for the 1st round PCR and used for second protein-DNA interaction and this process was repeated for three times. According to nondenaturing PAGE analysis the negative control primer fd1 was also amplified and gave the same banding position with eluted DNA samples from GST and GSTdMT reactions (Figure 4.106).

In addition, nondenaturing PAGE analysis of samples from wash steps of protein-DNA interaction experiments showed that linker-ligated DNA fragments were mostly eluted from these washing steps for both GSTdMT and GST (Figure 4.107).

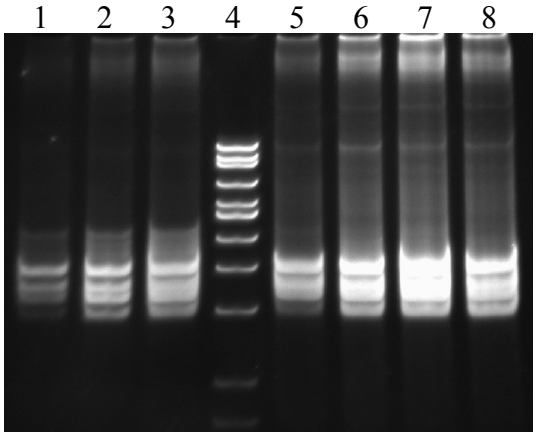

Figure 4.106: 7% Nondenaturing PAGE analysis of PCR products of the 1st, 2nd and 3rd rounds of amplifications with products of WGPCR experiments using 1 μM primer fd1. Lane 1-3, 1st round PCR, 5-7, 2nd round PCR, 7-8, 3rd round PCR, 4, Low range DNA ladder; 1,5,7, eluted DNA from GSTdMT reaction; 2,6,8, eluted DNA from GST reaction; 3, only primer fd1.

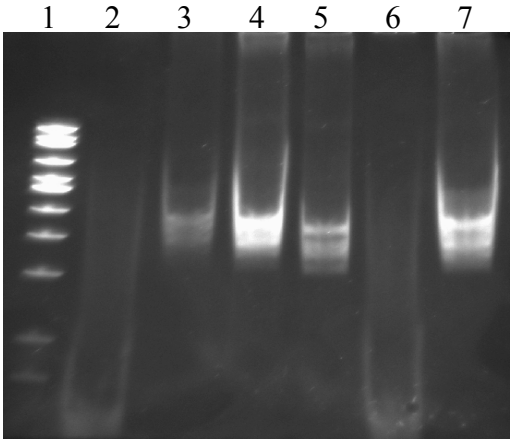

Figure 4.107: 7% Nondenaturing PAGE analysis samples from wash steps. Lane 1, Low range DNA ladder; 2-4, washing samples of GSTdMT; 5-7, washing samples of GST.

The same protein-DNA interaction strategy and same conditions were repeated with 0.5 μM primer fd1. However identical amplification results were detected (Figure 4.108). Additionally similar results were obtained from wash steps (Figure 4.109).

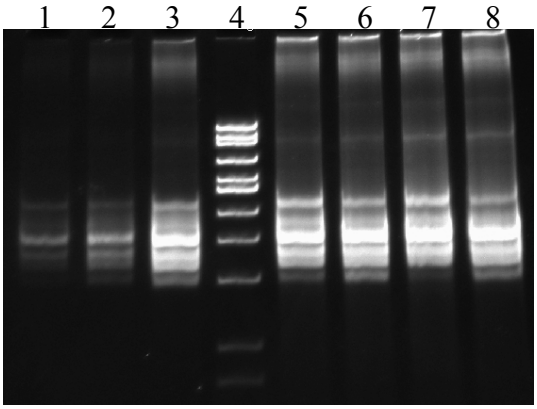

Figure 4.108: 7% Nondenaturing PAGE analysis of PCR products of the 1st, 2nd and 3rd rounds. Lane 1-3, 1st round PCR, 5-7, 2nd round PCR, 7-8, 3rd round PCR, 4, Low range DNA ladder; 1,5,7, eluted DNA from GSTdMT; 2,6,8, eluted DNA from GST; 3, only primer fd1.

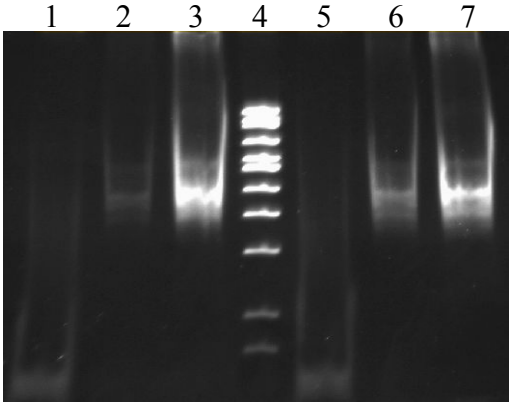

Figure 4.109: 7% Nondenaturing PAGE analysis samples from washing steps. Lane 1-3, washing samples of GSTdMT; 4, Low range DNA ladder; 5-7, washing samples of GST.

These results showed clearly that, the WGPCR method was not suitable for investigation of DNA binding of GSTdMT protein.

Chapter 5

DISCUSSION

5.1 Purification of Homogeneous GSTdMT and dMT

As can be seen from the amino acid sequence of dMT given in Figure 5.1 dMT contains 12 Cys residues, has a molecular weight of about 7 kDa and it contains only two aromatic amino acids phenylalanine (F51) and tyrosine (Y21). Unlike most mammalian MTs, dMT contains a long hinge region which separates the Cys-motif containing terminal regions. These features combined with instability of the holo-protein in the presence of oxygen and its susceptibility to proteolytic degradation especially within the long hinge region contribute to difficulties in obtaining pure, monodisperse and biophysically well characterized protein solutions. One more factor which hinders direct studies on purified protein is its propensity for aggregation. It appears that two main reasons contribute to nonspecific aggregation one is the fact that intra- and inter-molecular disulphide bonds are formed when metal ions are lost. The second reason is not well understood but appears to be related to the presence of excess metals.

Some of these difficulties can be circumvented if the protein is expressed with a larger fusion partner such as GST in a recombinant expression system. The fusion partner would facilitate purification and quantification of the protein and with an efficient system high levels of expression can yield large quantities of recombinant protein. It was also shown that in fusion proteins GST structure appeared to be unchanged compared to native protein and that it did not interfere with the structure of the fusion partner (Zhan et al., 2001).

Plant MTs have often been purified in fusion with GST for biochemical and biophysical characterization and some examples include work by Foley et al., 1997 on fava bean Type 1 and Type 2 MTs, by Murphy et al., 1997 on Arabidopsis MT1, MT2 and MT3 proteins, by Abdullah et al., 2002 on Type 3 MT3-A from the oil palm, by Mir et al. 2004 and Domenech et al., 2005 on Type 2 MT, QsMT from *Quercus suber*. In all these studies a protease deficient *E. coli* strain such as BL21 (DE3) was selected as the host for expression to minimize protein degradation. In addition since stabilization of the protein structure and protection of the spacer region from proteolytic degradation through metal-binding had been established (Kille et al., 1991) MTs were expressed in the presence of divalent metals usually Zn^{2+} or Cd^{2+}.

In the study reported in this thesis basically dMT was expressed in fusion with GST using the pGEX-4T2 expression system (GE-Biosciences) in BL21 (DE3) cells and purified in the presence of $CdCl_2$ using affinity and size exclusion chromatography. All purification procedures were performed at 4^oC either in an argon-filled environmental bag or under continuous argon flow for protection against oxidation.

Two main features distinguished this work from previous studies mentioned above. (1) It was the first report of systematic analyses for optimization of the purification procedure for recombinant plant MTs. (2) It was the first report where question of oligomerization state of the purified protein was directly addressed. Analyses were carried out on the fusion protein for the sake of ease and speed of purification, quantification and monitoring the oligomeric state but of course at the expense of working with a construct rather than the native protein. On the other hand the extent of applicability of the results to the native protein is also discussed and possibility of using GSTdMT as an accessible model system has been explored.

Optimization of the purification procedure was achieved through examining the effect of buffer system, reducing agent and $CdCl_2$ concentration on the quality of the purified protein. Protein quality, on the other hand, was monitored by checking yield, purity, monodispersity, oligomerization state and Cd content. Since determination of MT concentration is problematic due to lack of aromatic amino acids yield was measured in terms of GST concentration. Purity was monitored by SDS-PAGE where due to the GST component protein can bind SDS and migrate as expected on the gel and

can be readily visualized by Coomassie blue staining. Monodispersity and oligomerization state were analyzed by native-PAGE and DLS measurements. Cd content was determined by ICP-OES measurements on the purified samples.

Results presented in 4.1.2 show that a Tris based buffer with pH 7.5 was the most suitable for GSTdMT purification. These results also showed that when the protein needs to be stored over a period of time of about six days it is better preserved in a HEPES based buffer at pH 8.0. The best condition for storage appeared to be at 4^{o}C rather than freezing at -20 ^{o}C or at -80 ^{o}C. Results given in Figure 4.50 and Figure 4.53 showed that after six days the protein was still in intact form. It was not possible to compare these results with those given in the literature directly. In general MTs are reported to be stored in lyophilized form, however no analyses have been provided for the quality and oligomeric state of the resuspended proteins (Peroza and Freisinger, 2007, Domenech et al., 2005).

Effect of presence of Cd^{2+} ions at different concentrations in the growth medium and in purification buffers was also investigated. As mentioned above formation of metal-thiol clusters prevents proteolytic attack especially within the long spacer region (Kille et al., 1991). This is probably due to the Cys-rich domains that are folded together to participate in binding of metal (Rauser, 1999). Therefore, $CdCl_2$ was included for maintaining the stability of and proper folding of GSTdMT. Cd^{2+} concentration was varied between 0 and 0.2 mM and as results given in section 4.1.2 show that beyond 0.1 mM $CdCl_2$ caused aggregate formation. The optimum $CdCl_2$ for obtaining intact protein without formation of higher order oligomers was found to be about 0.1 mM. In addition, it was observed that including $CdCl_2$ during bacterial growth and only in the lysis buffer was sufficient to maintain stability of GSTdMT. In recent studies Domenech et al. (2005) had also included 0.5 mM CuSO4 or 0.3 mM ZnCl2 in the growth media to obtain holo Quercus suber MT and Akashi et al. (2004) have used 0.5 mM ZnSO4 in the growth media of bacteria expressing watermelon Type 2 metallothionein. These studies support the earlier observation that metals are required to achieve proper folding and protection of recombinantly synthesized MTs.

Similar to other cystein containing proteins the, sulfhydryl groups in dMT are susceptible to both oxidation and disulfide formation in solution. Reducing agents were

included in MT buffers to prevent disulfide formation and oxidation (Kagi, 1991). As results given in section 4.1.2 showed 1mM DTT was found to be sufficient for overcoming of the aggregation problem of GSTdMT due to the disulfide bond (i.e. Cys-S-S-Cys) formation.

Under the optimized conditions size exclusion chromatography of GSTdMT resulted in two peaks with elution volumes of 116 and 140 ml as shown in Figure 4.38. According to the column calibration the main peak (GII) at 140 ml corresponded to a molecular weight of about 77 kDa and contained the dimeric form of purified GSTdMT whereas the other peak (GI) at about 115 ml corresponded to a molecular weight of 188 kDa and contained highly aggregated forms of GSTdMT. These results were verified by native- and SDS-PAGE analysis of the purified fractions. A single band at about 35 kDa was visualized by SDS-PAGE analysis (Figure 4.39) and similarly native-PAGE analysis (Figure 4.40) yielded a single band corresponding to homogeneous species of GSTdMT in these fractions.

The monodispersity of the GII fractions were further monitored by DLS which provides information about the size distribution of particles in a solution. In particular distribution according to the intensity of scattered light is sensitive the large aggregates in solution. Measurements of fractions from the peak GII (Figure 4.41) resulted in one single peak centered around 10 nm in intensity distribution indicating that the GSTdMT solutions were monodisperse and the major species in solution was in dimeric form.

As expected GSTdMT yields were slightly lower than that for GST however one purification was sufficient for providing enough material for several biophysical characterizations.

One of the requirements for SAXS measurements for structural studies is high protein concentration (Svergun and Koch 2003). When GSTdMT was concentrated after size exclusion chromatography beyond 4 mg/ml higher order oligomers were observed. However re-dilution of concentrated solutions showed that the oligomerization of GSTdMT was a question of equilibrium and that it was reversible (Figure 4.57). This result is in agreement with those of Zhan et al., (2001) who observed that the stable form recombinant GST fusion protein is dimeric.

Results given in section 4.2 showed that the purification procedure, once optimized and established for GSTdMT, was readily applicable to dMT. Minor modifications, mainly due to the fact that yields were much lower, could be introduced without serious complications. As can be seen in Figure 4.64 dMT was eluted from the final size exclusion chromatography step at 74 ml corresponding to a molecular mass of about 17 kDa. It appeared that similar to GSTdMT, dMT was also eluted as a dimer. The expected molecular mass dMT dimer would be about 14 kDa. This apparent shift in the elution volume was observed for proteins with anisotropic shape (Garcia De La Torre et al., 2000). Analysis of purified dMT fractions by SDS-PAGE given in Figure 4.65 showed the anomalous electrophoretic mobility of this protein; more than one band was visualized by silver staining and the highest mobility band corresponded to a molecular mass of about 10 kDa which is higher than the 7 kDa expected from dMT. This behavior, reported by also by others including Sayers et al., (1999), Fresinger (2007), and Murphy et al., (1997) is due mainly to insufficient reduction of the protein during preparation for gels. In the presence of excess amount of DTT only a single band is detected (results not shown).

5.2 Biophysical Characterization of GSTdMT

UV-vis spectroscopy is a method commonly used for characterization MTs because absorption bands due to bound metals can be readily detected (Kagi and Vasak, 1984, Freisinger 2007, Peroza and Freisinger, 2007). As exemplified by Figure 4. 60 the absorption spectrum of GSTdMT has two prominent features, the shoulder at 280 nm arising from aromatic residues of GST and the charge transfer band at 250 nm. The charge transfer band is due to Cd-thiol interactions (Willner et al., 1987) and have been observed in other MTs such fruit-specific metallothionein MT3 (Freisinger, 2007), wheat seed MT (Peroza and Freisinger, 2007).

The binding ratio of Cd to GSTdMT was estimated using Cd concentration as measured by ICP-OES and protein concentration was directly calculated from A_{280} measurements. As shown in Table 4.5 the average Cd^{2+} to protein molar ratio was found to be 3.5 ± 0.6. Kille et al., (1991) found that recombinant Type 1 PsMTA, containing 12 Cys, bound about 6 g atoms of Cd per molecule. In a recent report Domenech et al., (2007) showed that Type 2 QsMT, with 14 Cys, bound 5.6 Cd per molecule. For Type 3

MTs, having 11 Cys, Freisinger (2007) reported 4 Cd^{2+} ions. Considering the number of Cys residues in GSTdMT the result given above is in agreement with the reports in the literature. Extinction coefficient at 250 nm/Cd^{2+} was found to be ~9000 M^{-1} cm^{-1}, which agrees well with ~11600 M^{-1} cm^{-1} given by Freisinger (2007) and ~12600 M^{-1} cm^{-1} (Willner et al., 1987). Metal coordination in GSTdMT was further probed by EXAFS and the spectra (Figure 4.81) are consistent with a tetrahedral structure for the metal center (see below).

5.3 Structural Analysis of GSTdMT and dMT

Circular dichroism (CD) is a technique sensitive to the secondary structure of polypeptides and proteins. The secondary structural features of GSTdMT were investigated by recording its CD spectra and comparing with that from GST. It was observed that, similar to the reports in the literature (Masino et al., 2002), CD spectrum of GST is dominated by the α-helical secondary structure of this protein (Figure 4.61). The GSTdMT spectrum, on the other hand, indicates a decrease in the α-helical content in the overall structure which could be achieved by incorporating more β structures or by having a less ordered structure superimposed on the main GST structure.

SAXS was used for determining shape of the GSTdMT fusion protein. Solutions of GSTdMT were measured at concentrations between 1.5 and 2.5 mg/ml and due to protein aggregation problem higher concentrations were avoided. SAXS measurements confirmed that GSTdMT protein solutions were homogeneous. The Rg values of GSTdMT and GST, 3.6 nm and 2.5 nm respectively, reflect the difference in the shapes of the two proteins. It was observed that presence of dMT introduces a significant anisotropy to the shape of the molecule. The calculated average molecular mass of GSTdMT and GST according to I (0) values indicated the dimeric state of these proteins in solution. But the experimental values for the molecular mass of GSTdMT and for GST were lower than those calculated. The main source for this difference is likely to be the inaccuracies in concentration measurements both for samples and reference protein. During data reduction the scattering curve is normalized according to the protein concentration which shifts the value of I (0).

GNOM analysis of the SAXS data indicated that the distance distribution function P(r) for GST and GSTdMT were different from each other and D_{max}; maximum macromolecular dimension was found to be 6.5 nm for GST and 13 nm for GSTdMT. These results further confirmed that GSTdMT is elongated.

The shape models developed for GSTdMT emphasized the asymmetric structure of the molecule and indicated that the fusion protein consisted of three sections; a dense globular region which is highly likely to correspond to GST, a still dense but elongated central section and a less dense tail.

The correspondence between GSTdMT domains and the models can be attempted by considering the complementary information obtained by different techniques in this study. The combination of EXAFS and ICP-OES results indicated that 3.5 ±0.5 Cd^{2+} ions were bound per molecule of protein and that the Cd-S distances were consistent with a tetrahedral arrangement with first coordination shell of about 2.5 Å. Furthermore the UV-vis spectrum of holo-GSTdMT showed a charge transfer band around 250 nm which indicates a tetrahedral arrangement of S ligands around Cd. Possible binding schemes that would lead to such arrangement are shown in Figure 5.1 (A) and (B).

In (A) dMT is depicted as a dumbbell, as proposed previously by Bilecen et al., (2005), Domenech et al., (2006) and Zhu et al., (2000), with two metal binding domains with Me_2S_6. Although the two clusters have the same metal binding stoichiometry the Cys-X-Cys motif distributions are not the same. The β domain has (Cys-X-Cys)-X3-(Cys-X-Cys)-X3-(Cys-X-Cys) whereas the α domain has (Cys-X-Cys)-X3-(Cys-X-Cys)-X2-(Cys-X-Cys). In one possible coordination pattern of for Cd ions C5 and C15 in the β domain would be bridging and C73 and C64 in the α domain would be bridging. This arrangement may result in different Cd binding affinities with β domain showing slightly lower affinity. In the scheme shown in (B) dMT is shown with a hairpin shape as was proposed by Kille et al., (1991) and Domenech et al., (2006). Here the protein consists of a single metal center with the stoichiometry of Me_4S_{12}. In this scheme a possible arrangement for binding four Cd ions would result in C5, C9, C70 and C73 to become bridging cysteins.

Models obtained from SAXS measurements can be interpreted in the light of the above discussion. The hairpin model appears to provide a better fit to the shape model in Figure 4.78. Accordingly the second electron dense region would correspond to the metal center and the tail region would represent the spacer domain.

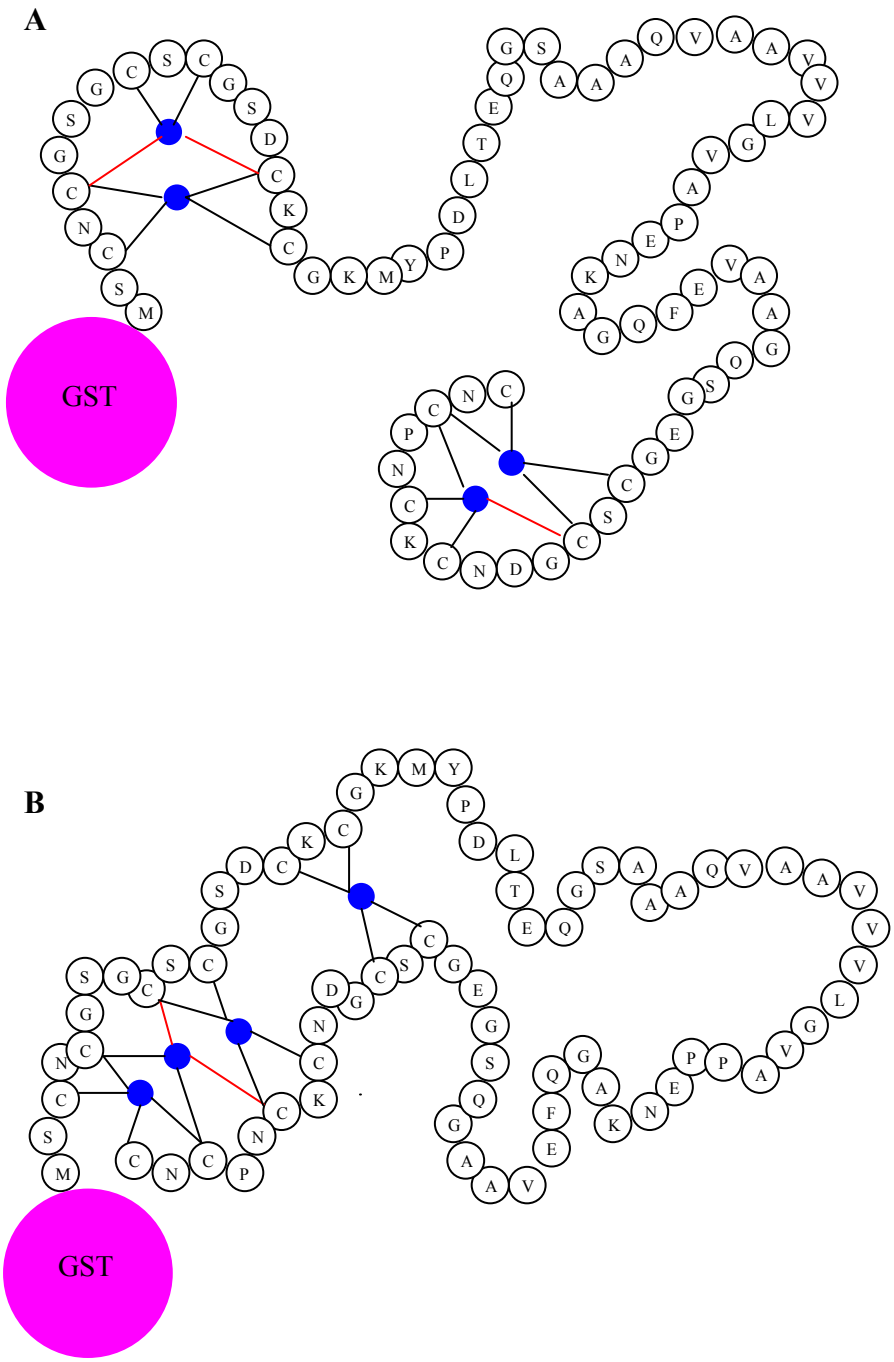

Figure 5.1: Possible Cd binding schemes of dMT. (A) dMT as a dumbbell. (B) dMT as a hairpin. The blue circles represent Cd^{2+} ions.

5.4 Functional Studies

Southern blot analysis resulted in a single band showing that *d-mt* gene exists as a single copy in the genome of *T. durum*. Similar result was obtained in rice MT; ricMT (Yu et al., 1998). But this differs from the other plant species; mt genes exist as a multigene family in pea (Evans et al., 1990), maize (de Framond, 1991), Arabidopsis (Zhou and Goldsbrough, 1995) and cotton (Hudspeth et al., 1996). However no information about the localization of *d-mt* gene could be obtained with southern blot analysis in *T. durum* genome.

The response of *T. durum* cv. Balcalı-85 cultivar to Cd stress was examined by treating Balcalı-85 plants with five different increasing Cd concentrations. This resulted in a significant decrease in growth and dry weights of both shoot and root tissue. Similar results were observed in the study of Köktürk (2006). Cadmium toxicity causes reduction in the concentrations of photosynthetic pigment and carotenoids, and as a result restricts activity of photosynthesis (Rai et. al., 2005). In general Cd affects root growth more severely than shoot growth. In addition, durum wheat cultivars generally accumulate more Cd than bread wheat cultivars (Greger and Löfstedt, 2004). In the present study, increasing Cd concentration showed that Cd was accumulated in the roots in much higher amounts than in the shoots in Balcalı-85 plants. Roots are the first site contacting with Cd therefore they have the greater capacity to accumulate Cd than shoots. As a result, generally it is observed that roots are more sensitive to Cd toxicity than shoots (Grant et. al. 1998).

The predicted structure for the hinge region shows similarity with a family that includes DNA binding proteins (Bilecen et al., 2005). DNA binding possibility of GSTdMT protein was tested with the whole genome PCR-based screening method. GST protein was also used in DNA-protein interaction studies as negative control.

During optimization of this method several difficulties were faced. The first one was the nonspecific binding of DNA to the protein and this was tried to overcome by the usage of nonspecific competitor poly-dIdC. However, it was shown clearly that poly-dIdC can be amplified with PCR with and without primers. This amplification was also observed by spectroscopic measurements at 260 nm and nondenaturing-PAGE.

These results showed more clearly that and the usage of poly-dIdC as nonspecific competitor was not suitable.

The second and most significant problem was amplification of primers themselves. Two different sets of linkers and primers were tried to avoid this problem. The first set of primers (f1 and f2) was designed according to the linker sequences which were reverse complementary to each other (Kinzler and Vogelstein 1989). It was thought that this reverse complementation led to amplification of f1 and f2 and to overcome this problem the second set of linkers and primers were designed according to Watson et al., (2000). In another strategy the selection and amplification of linker-ligated DNA fragments separately for each round of PCR was tried. According to results the primer amplification was still observed but also DNA samples from GST and GSTdMT were mostly eluted in wash steps. In the view of these observations it can be concluded that the WGPCR method was not suitable for the investigation of DNA binding possibility of GSTdMT.

Chapter 6

CONCLUSIONS

The general aim of the work presented in this thesis was to investigate the structure and related functional roles of dMT using GSTdMT as a model system.

A procedure was established to purify GSTdMT in highly homogeneous monodisperse solutions at high protein concentration. This is the first study in the literature where problems of protein quality and oligomerization state have been systematically addressed for plant MTs. GSTdMT could be purified in dimeric form with a yield of about 50 mg/1.5 L *E .coli* culture. As preliminary experiments showed this procedure is readily applicable to purification of dMT. Future work will focus on purification of dMT at high protein concentration and of defined oligomeric state.

Purified GSTdMT protein was shown to contain 3.5 ± 0.5 Cd^{2+}/protein with a tetrahedral arrangement of thiol groups in the first coordination shell of the metal. SAXS measurements revealed that GSTdMT has an elongated shape with a radius of gyration of 3.57 nm. *ab initio* models based on SAXS measurements resulted in a shape for the dimer in which the two GST molecules form an electron dense region at one end and the two dMT molecules extend from this region. dMT structure appears to be independent of GST in the GSTdMT fusion. Based on this model and possible schemes for the structure of the metal center(s) it can be proposed that dMT has a hairpin like structure in the GSTdMT. This model proposed for dMT structure needs to be experimentally verified.

DNA binding possibility of GSTdMT was also investigated. It was however not possible to reach a conclusion due to the artifacts involved in the Whole Genome PCR-based screening method. It appears that a better way to investigate the DNA binding possibility of dMT can be through development of antibodies against dMT and checking directly presence of dMT on DNA.

In part of this work response of *Triticum durum* cv. Balcalı-85 to environmental Cd was investigated. It was observed that reduction in dry weight matter occurred both in roots and shoots under increasing environmental Cd concentration. Balcalı-85 demonstrated high capacity to retain Cd in roots. These studies were carried out as a part of an investigation which will focus on the correlation between *mt-d* gene expression and Cd response.

Southern blot analysis revealed that the *mt-d* gene exists as a single copy in the *T. durum* genome.

Chapter 7

REFERENCES

Abdullah, S.N.A., Cheah, S.C., Murphy, D.J. (2002). Isolation and characterization of two divergent type 3 metallothioneins from the oil palm, *Elaeis guineensis*. *Plant Physiology and Biochemistry,* 40:255-263.

Akashi, K., Noriyuki, N., Ishida, Y., Yokota, A. (2004). Potent hydroxyl radical-scavenging activity of drought-induced type-2 metallothionein in wild watermelon Biochemical *and Biophysical Research Communications,* 323:72-78.

Bertini, I., Hartmann, H.J., Klein, T., Liu, G., Luchinat, C., Weser, U. (2000). High resolution solution structure of the protein part of Cu7 metallothionein. *European Journal of Biochemistry*, 267:1008-1018.

Bilecen, K., Öztürk, Ü.H., Duru, A.D., Sütlü, T., Petoukhov, M., Svergun, D. I. , Koch, M.H.J., Sezerman, U., Cakmak, I. and Sayers, Z. (2005). *Triticum durum* Metallothionein: Isolation of the gene and structural characterization of the proteins using solution scattering and Molecular Modeling. *The Journal of Biological Chemistry,* 280:13701-13711.

Binz, P.A., Kagi, J.H.R. (1999). Metallothionein: molecular evolution and classification. In *Metallothionein*, vol. IV (ed. C. Klaassen), pp. 7-13. Basel: Birkhauser.

Buchanan-Wollaston, V. (1994). Isolation of cDNA Clones for Genes That Are Expressed during Leaf Senescence in *Brassica napus*. *Plant Physiology,* 105:839-846.

Butt A., Mousley C., Morris K., Beynon J., Can C. (1998). Differential expression of a senescence-enhanced metallothionein gene in *Arabidopsis* in response to isolates of *Peronospora parasitica* and *Pseudomonas syringae*. *The Plant Journal,* 16:209-221.

Cai L., Klein J.B., Kang Y.J. (2000). Metallothionein inhibits peroxynitrite-induced DNA and lipoprotein damage. *Journal of Biological Chemistry,* 275:38957-38960.

Calderone, V., Dolderer, B., Hartmann, H-J., Echner, H., Luchinat, C., Del Bianco, C., Mangani, S. and Weser, U. (2005). The crystal structure of yeast copper thionein: The solution of a long-lasting enigma. Proc. Natl. Acad. Sci. U.S.A. (PNAS) 102(1):51-56.

Capdevilaa, M., Colsb, N., Romero-Isarta, N., Gonza`lez-Duarteb, R., Atrianb, S., Gonza`lez-Duarte, P. (1997). Recombinant synthesis of mouse Zn3-β and Zn4-α metallothionein 1 domains and characterization of their cadmium (II) binding capacity. *Cellular and Molecular Life Sciences,* 53:681-688.

Charbonnel-Campaa L., Lauga B., Combes D. (2000). Isolation of a type 2 metallothionein-like gene preferentially expressed in the tapetum in *Zea mays*. *Gene* 254:199-208.

Choi D., Kim H.M., Yun H.K., Park J.A., Kim W.T., Bok S.H. (1996). Molecular cloning of a metallothionein-like gene from *Nicotiana glutinosa* L. and Its lnduction by Wounding and Tobacco Mosaic Virus lnfection. *Plant Physiology,* 112: 353-359.

Cobbett, C., Goldsborugh, P. (2002). Phytochelatins and Metallothioneins: Roles in Heavy Metal Detoxification and Homeostasis. *Annual Reviews of Plant Biology*, 53:159-182.

Coyle, P., Philcox, J.C., Carey, L.C., Rofe, A.M. (2002). Metallothionein: the multipurpose protein. *Cellular and Molecular Life Sciences,* 59:627-647.

De Miranda J.R., Thomas M.A., Thurman D.A., Tomsett A.B. (1990). Metallothionein genes from the flowering plant *Mimulus guttatus*. *FEBS Letters*, 260:277-280.

Domènech J., Mir G., Huguet G., Capdevila M., Molinas M., Atrian S. (2006). Plant metallothionein domains: functional insight into physiological metal binding and protein folding. *Biochimie,* 88:583-593.

Domenech, J.; Tinti, A.; Capdevila, M.; Atrian, S. & Torreggiani, A. (2007). Structural study of the zinc and cadmium complexes of a type 2 plant (Quercus suber) metallothionein: insights by vibrational spectroscopy. *Biopolymers,* 86:240-248.

Duncan, K.E.R., Stillman, M.J. (2006). Metal-dependent protein folding: Metallation of metallothionein. *Journal of Inorganic Biochemistry,* 100:2101-2107.

Evans, K.M., Gatehouse, J.A., Lindsay, W.P., Shi, J., Tommey, A.M., Robinson, N.J. (1992). Expression of the pea metallothionein-like gene PsMTA in *Escherichia coli* and *Arabidopsis thaliana* and analysis of trace metal ion accumulation: implications for PsMTA function. *Plant Molecular Biology*, 20:1019-1028.

Fischer, E.H., Davie, E.W. (1998). Recent excitement regarding metallothionein. *Proc Natl Acad Sci USA* 95:3333-3334.

Foley, R.C., Liang, Z.M., Shing, K.B. (1997). Analysis of type 1 metallothionein cDNAs in Vicia faba. *Plant Molecular Biology,* 33:583–591.

Foley, R.C., Singh, K.B. (1994). Isolation of a *Vicia faba* metallothionein-like gene: expression in foliar trichomes. *Plant Molecular Biology,* 26: 435–444.

Fowler, B.A., Hildebrand, C.E., Kojima, *Y.,* & Webb, M. (1987). Nomenclature of metallothionein. *Experientia, Suppl.,* 52:19-22.

Freisinger E. (2007). Spectroscopic characterization of a fruit-specific metallothionein: *M. acuminata* MT3. *Inorganica Chimica Acta,* 360:369-380.

Garcia De La Torre, J., Huertas, M.L., Carrasco, B. (2000). Calculation of hydrodynamic properties of globular proteins from their atomic-level structure. *Biophysical Journal*, 78:719-730.

García-Hernández, M., Murphy, A. and Taiz, L. (1998). Metallothioneins 1 and 2 have distinct but overlapping expression patterns in Arabidopsis. *Plant Physiology,* 118:387-397.

Gehrig, P.M., You, C., Dallinger, R., Gruber C., Brouwer, M., Kagi J.H.R., Hunziker, P.E. (2000). Electrospray ionization mass spectrometry of zinc, cadmium, and copper metallothioneins: Evidence for metal-binding cooperativity. *Protein Science,* 9:395-402.

Greger, M., Löfstedt, M. (2004). Comparison of uptake and distribution of cadmium in different cultivars of bread and durum wheat. *Crop Science,* 44:501-507.

Guo, W-J., Bundithya, W., Goldsbrough, P.B. (2003). Characterization of the Arabidopsis metallothionein gene family: tissue-specific expression and induction during senescence and in response to copper. *New Phytologist,* 159:369-381.

Haq F., Mahoney M., Koropatnick J. (2003). Signaling events for metallothionein induction. *Mutation Research*, 533:211-226.

Kagi, J.H.R. (1991). Overview of metallothionein. *Methods Enzymology,* 205:613–26.

Willner, H., Vasak, M., Kagi, J.H.R. (1987). Cadmium-Thiolate Clusters in Metallaotionein: Spectrophotometric and Spectropolarimetric Features. *Biochemistry,* 26:6287-6292.

Kang, Y.J. (2006). Metallothionein redox cycle and function. *Experimental Biology and Medicine,* 231(9): 1459-1467.

Kille, P., Winge, D.R., Harwood, J.L., Kay, J. (1991). A plant metallothionein produced in *E. coli*. *FEBS Letters,* 295:171-175.

Kinzler, K.W., Vogelstein, B. (1989). Whole genome PCR: application to the identification of sequences bound by gene regulatory proteins. *Nucleic Acids Research,* 17:3645-3653.

Klaassen, C.D., Liu, J., Choudhuri, S. (1999). Metallothionein: an intracellular protein to protect against cadmium toxicity. *Annual review of pharmacology and toxicology,* 39:267-94.

Konarev, P. V., Volkv, V. V., Sokolova, A. V., Koch, M. H. J. and Svergun, D. I. (2003). PRIMUS: a Windows PC-based system for small-angle scattering data analysis. *Journal of Applied Crystallography,* 36:1277-1282.

Lane, B.G., Kajioka, R., Kennedy, T.D. (1987). The wheat germ Ec protein is a zinc containing metallothionein. *Biochemistry and Cell Biology,* 65:1001–1005.

Leszczyszyn O. I., Schmid R., Blindauer C.A. (2007). Toward a property/function relationship for metallothioneins: Histidine coordination and unusual cluster composition in a zinc-metallothionein from plants. *Proteins,* 68:922-935.

Loo, J.A. (1997). Studying noncovalent protein complexes by electrospray ionization mass spectrometry. *Mass Spectrom Rev 16*:1–23.

Maret, W. (2000). The Function of Zinc Metallothionein: A Link between Cellular Zinc and Redox State. *Journal of Nutrition,* 130:1455S-1458S.

Maret W., Larsen K.S., Vallee B.L. (1997). Coordination dynamics of biological zinc ‘‘clusters’’ in metallothioneins and in the DNA-binding domain of the transcription factor Gal4. *Proc Natl Acad Sci USA* 94:2233-2237.

Matsumura H., Nirasawa S., Terauchi R. (1999). Transcript profiling in rice (*Oryza sativa* L) seedlings using serial analysis of gene expression (SAGE). *Plant Journal,* 20:719-726.

Miller J.D., Arteca R.N., Pell E.J. (1999). Senescence-Associated Gene Expression during Ozone-Induced Leaf Senescence in Arabidopsis. *Plant Physiology,* 120:1015-1023.

Mir, G., Domènech, J., Huguet, G., Guo, W.J., Goldsbrough, P. (2004). A plant type 2 metallothionein (MT) from cork tissue responds to oxidative stress. Journal of Experimental Botany, 55:2483-2493.

Mosleh, Y.Y., Paris-Palacios, S., Ahmed, M.T., Mahmoud, F.M., Osman, M.A., Biagianti-Risbourg S. (2007). Effects of chitosan on oxidative stress and metallothioneins in aquatic worm *Tubifex tubifex* (Oligochaeta, Tubificidae). *Chemosphere*, 67:167-175.

Murphy, A., Zhou, J., Goldsbrough, P., Taiz, L. (1997). Purification and immunological identification of metallothioneins 1 and 2 from *Arabidopsis thaliana*. *Plant Physiology,* 113:1293–1301.

Navabpour S., Morris K., Allen R., Harrison E., A-H-Mackerness S., Buchanan-Wollaston V. (2003). Expression of Senescence-Enhanced Genes in Response to Oxidative stress. *Journal of Experimental Botany,* 54:2285-2292.

Nishiuchi S., Liu S., Takano T. (2007). Isolation and characterization of a metallothionein-1 protein in *Chloris virgata* Swartz that enhances stress tolerances to oxidative, salinity and carbonate stress in *Saccharomyces cerevisiae*. *Biotechnology Letters*, 29:1301-1305.

Palmiter, R.D. (1998). The elusive function of metallothioneins. *Proc Natl Acad Sci USA,* 95:8428–8430.

Penner-Hahn, J. E. (1999). X-ray absorption spectroscopy in coordination chemistry. *Coordination Chemistry Reviews*, 190-192:1101-1123.

Peroza E.A., Freisinger E. (2007). Metal ion binding properties of *Triticum aestivum* E_c-1 metallothionein: evidence supporting two separate metal-thiolate clusters. *Journal of Biological Inorganic Chemistry,* 12:377-391.

Peterson, C.W., Narula, S.S., Armitage, I.M. (1996). 3D solution structure of copper and silver-substituted yeast metallothioneins. *FEBS Letters,* 379:85-93.

Rai, V., Khatoon, S., Bisht S.S., Mehrotra, S. (2005). Effect of cadmium on growth, ultramorphology of leaf and secondary metabolites of *Phyllanthus amarus* Schum. and Thonn. *Chemosphere,* 61:1644-1650.

Rauser, W.E. (1999). Structure and function of metal chelators produced by plants: the case for organic acids, amino acids, phytin, and metallothioneins. *Cell Biochemistry and Biophysics,* 31:19-48.

Riek R., Prêcheur B., Wang Y., MacKay E.A., Wider G., Güntert P., Liu A., Kägi J.H.R., Wüthrich K. (1999). NMR structure of the sea urchin (*Strongylocentrotus purpuratus*) metallothioenein MTA. *Journal of Molecular Biology*, 291:417-428.

Rigby, K. E., Stillman, M. J. (2004). Structural studies of metal-free metallothionein. *Biochemical and Biophysical Research Communications*, 325:1271-1278.

Robbins, A.H., McRee, D.E., Williamson, M., Collett, S.A., Xuong, N.H., Furey, W.F., Wang, B.C., Stout, C.D. (1991). Refined crystal structure of Cd, Zn metallothionein at 2.0 Å resolution. *Journal of Molecular Biology*, 221:1269-1293.

Robinson, N.J., Tommey, A.M., Kuske, C., Jackson, P.J. (1993). Review article: Plant metallothionein. *Biochemical Journal*, 295:1-10.

Robinson, N.J., Wilson, J.R., Turner, J.S. (1996). Expression of the type 2 metallothionein-like gene MT2 from *Arabidopsis thaliana* in Zn2C-metallothionein-deficient *Synechococcus* PCC 7942: putative role for MT2 in Zn2C metabolism. *Plant Molecular Biology,* 30:1169–1179.

Romero-Isart, N., Vasak, M. (2002). Advances in the structure and chemistry of metallothioneins. *Journal of Inorganic Biochemistry,* 88:388–96.

Sayers, Z., Brouillon, P., Svergun, D.I., Zielenkiewicz, P. and Koch, M.H.J. (1999). Biochemical and Structural Characterization of Recombinant Copper-Metallothionein from *Saccharomyces Cerevisiae*. *European Journal of Biochemistry*, 262: 858-865.

Snowden K.C., Gardner R.C. (1993). Five Genes lnduced by Aluminum in Wheat (*Trificum aestivum* L.) Roots. *Plant Physiology,* 103:855-861.

Svergun, D.I. (1992). Determination of the regularization parameter in indirect-transform methods using perceptual criteria. *Journal of Applied Crystallography,* 25: 495-503.

Svergun, D.I., Koch, M.H.J. (2003). Small-angle scattering studies of biological macromolecules in solution, *Reports on Progress in Physics,* 66:1735–1782.

Tamai K.T., Gralla E.B., Ellerby L.M., Valentine J.S., Thiele D.J. (1993). Yeast and mammalian metallothioneins functionally substitute for yeast copper-zinc superoxide dismutase. *Proc Natl Acad Sci USA,* 90:8013-8017.

Tate, D., Miceli, M.V., Newsome, D.A. (2002). Expression of metallothionein in human chorioretinal complex. *Current Eye Research,* 24:12-25.

Thornalley P.J., Vasak M. (1985). Possible role for metallothionein in protection against radiation-induced oxidative stress. Kinetics and mechanism of its reaction with superoxide and hydroxyl radicals. *Biochimica et Biophysica Acta,* 827:36-44.

Tommey, A.M., Shi, J., Lindsay, W.P., Urwin, P.E., Robinson, N.J. (1991). Expression of the pea gene PsMTa in *E. coli* metalbinding properties of the expressed protein. *FEBS Letters,* 292:48–52.

Vasak, M. (2005). Advances in metallothionein structure and functions. *Journal of Trace Elements in Medicine and Biology,* 19:13-17.

Vasak, M., Hasler, D.W. (2000). Metallothioneins: new functional and structural insights. *Current Opinion in Chemical Biology,* 4:177-183.

Vasak, M., Kägi, J.H.R. (1994). In: Metallothioneins Encyclopedia of Inorganic Chemistry (King, R.B., Ed,) 4:2229–2241, J. Wiley and Sons, New York.

Watson D.K., Kitching R., Vary C., Kola I., Seth A. (2000). Isolation of Target Gene Promoter/Enhancer Sequences by Whole Genome PCR Method. *Methods in Molecular Biology*, 130:1-11.

Willner, H., Vasak, M., Kagi, H.R.J. (1987). Cadmium-Thiolate Clusters in Metallothionein: Spectrophotometric and Spectropolarimetric Features. *Biochemistry*, 26:6287-6292.

Wong H.L., Sakamoto T., Kawasaki T., Umemura K., Shimamoto K. (2004). Down-Regulation of Metallothionein, a Reactive Oxygen Scavenger, by the Small GTPase OsRac1 in Rice. *Plant Physiology,* 135:1447-1456.

Yu, L.H., Umeda, M., Liu, J.Y., Zhao, N.M., Uchimiya, H. (1998). A novel MT gene of rice plants is strongly expressed in the node portion of the stem. *Gene*, 206:29-35.

Yu, X., Wojciechowski, M., Fenselau, C. (1993). Assessment of metals in reconstituted metallothioneins by electrospray mass spectrometry. *Anal Chem, 65*:1355–1359.

Zhan, Y., Song, X., Zhou, G.W. (2001). Structural analysis of regulatory protein domains using GST-fusion proteins. *Gene*, 281:1-9.

Zhou, G. K., Xu, Y. F., Liu, J. Y. (2005). Characterization of a rice class II metallothionein gene: tissue expression patterns and induction in response to abiotic factors. *Journal of Plant Physiology*, 162: 686-696.

Zhou, G., Xu, Y., Li, J., Yang, L., Liu, J.Y. (2006). Molecular analyses of the metallothionein gene family in rice (Oryza sativa L.). *Journal of Biochemistry and Molecular Biology,* 39:595-606.

Zhou, J., Goldsbrough, P. (1994). Functional Homologs of Funga1 Metallothionein Genes from Arabidopsis. *The Plant Cell,* 6; 875-884.

Zhu C., Lü T., Zhang R., Zhao N., Liu J. (2000). Modeling of kiwi fruit metallothionein kiwi503. *Chinese Science Bulletin,* 45:1413–1417.

Zimeri, A. M., Dhankher, O. P., McCaig, B., Meagher, R.B. (2005). The plant MT1 metallothioneins are stabilized by binding cadmium and are required for cadmium tolerance and accumulation. *Plant Molecular Biology*, 58:839-855.

APPENDIX A

CHEMICALS

(in alphabetical order)

Acetic acid (glacial)	Riedel-de Häen, Germany	27225
30% Acrylamide-0.8% Biacrylamide	Sigma, Germany	A3699
Albumin (bovine serum)	Sigma, Germany	A7906
Ammonium persulphate	Carlo-Erba, Italy	420627
Bam HI	Fermentas	ER0051
Boric acid (99%)	Sigma, Germany	B6768
Bromophenol blue	Applichem, Germany	A3640
1-Butanol	Merck, Germany	100988
Cadmium (II) sulphate	Fluka, Switzerland	20920
Chloroform	Amresco	3566B066
Coomassie Brilliant Blue R-250	Fluka, Switzerland	27816
Complete Protease Inhibitor Cocktail Tablets	Roche	11 836 145 001
DNaseI	Fermentas	EN0521
dNTP mix	Fermentas	R0241
1,4-Dithiothreitol	Fluka, Switzerland	43815
DryEase mini cellophane	Invitrogen, Germany	NC2380
EcoRI	Fermentas	ER0271
Ethanol	Riedel-de Häen, Germany	32221
Ethylenediaminetetraaceticacid	Riedel-de Häen, Germany	27248
Glycerol (87%)	Riedel-de Häen, Germany	15523
Glycine	Amresco, USA	0167
Hind III	Fermentas	ER0501
HEPES	Fluka	54461

Hybond-P PVDF membranes	GE-Biosciences, Sweden	RPN2020F
Hydrochloric acid (37%)	Merck, Germany	100314
Hydrogen peroxide (30%)	Merck, Germany	107209
IPTG	Fermentas	R0392
Klenow fragment	Fermentas	EP0051
MassRuler DNA Ladder Mix	Fermentas	SM0403
MassRuler DNA Ladder Low Range	Fermentas	SM0383
2-Mercaptoethanol	Aldrich, Germany	M370-1
Methanol	Riedel-de Häen, Germany	24229
Nytran SPC nylon membrane	Whatman, USA	10416085
Omniscript RT kit	Qiagen	205111
PageRuler protein ladder	Fermentas, Germany	SM0661
Phenol: Chloroform:Isoamylalcohol	Amresco	3255B47
Phenylmethylsulphonylfluoride	Amresco, USA	0754
PolydI-dC	GE-Biosciences, Sweden	27-7880
Prestained protein MW marker	Fermentas, Germany	SM0441
1-Propanol	Merck, Germany	100996
Protein Prestained Ladder	Fermentas	SM0671
Protein Molecular Weight Marker	Fermentas	SM0431
Reduced Glutathione	Merck	K33271590522
Shrimp Alkaline Phosphatase	Fermentas	EF0511
Silver staining plus kit	BioRad	161-0449
Sodium chloride	Riedel-de Häen, Germany	13423
Sodium dodecyl sulphate	Sigma, Germany	L-4390
T4 DNA ligase	Fermentas	EL0016
TaqI	Fermentas	ER0671
Taq polymerase	Fermentas	EP0401
Tetramethylethylenediamine	Sigma, Germany	T-7029
Thrombin	GE-Biosciences, Sweden	27-0846-01
Tris	Fluka, Switzerland	93349
Triton X-100	Applichem, Germany	A1388

APPENDIX B

BUFFERS AND SOLUTIONS

Tris Borate EDTA Buffer (TBE) (5X): 54g Tris base, 27.5g Boric Acid, 20ml 0.5 M EDTA pH 8.0, completed to 500ml.

Tris Acetate EDTA Buffer (TAE) (50X): 121.1g Tris base, 28.55ml Glacial Acetic acid, 7.3g EDTA, completed to 500ml.

CTAB Extraction Buffer (2%): 10g CTAB, 75mM Tris HCl pH 8.0, 100mM EDTA pH 8.0, 5M NaCl, completed to 500ml.

20xSSC: 0.3 M Na_3citrate, 3 M NaCl, pH adjusted to 7.0, completed to 1L.

10 X Tris EDTA (TE) Buffer: 0.1M Tris-HCl, 10mM EDTA, pH adjusted to 7.5.

2x SDS Sample Buffer: 4% (w/v) SDS, 20% (v/v) Glycerol, 0.004% (w/v) Bromophenol blue, 10% (v/v) 2-mercaptoethanol, 0.125M Tris-HCl, pH 6.8 in ddH_2O.

2x Native Sample Buffer: 200mM Tris-HCl pH 7.5, 20% (v/v) Glycerol, 0.05% (w/v) Bromophenol blue in ddH_2O.

SDS-PAGE Running Buffer: 25mM Tris, 192mM Glycine, 0.1% (w/v) SDS in ddH_2O.

Native-PAGE Running Buffer: 25mM Tris, 192mM Glycine in ddH_2O.

Coomassie Staining Solution: 0.1% (w/v) Coomassie Brilliant Blue R-250, 40% (v/v) Methanol, 10% (v/v) Acetic acid in ddH_2O.

Destaining Solution: 4 % (v/v) Methanol, 7.5 % (v/v) Acetic acid completed to 1L.

Transfer Buffer: 96 mM Glycine, 12 mM Tris-base, and 20% Methanol in ddH_2O.

Blocking Solution: 5% Non-fat dry milk, in PBS-T (80 mM Na_2HPO4, 20 mM NaH_2PO4, 100 mM NaCl, 0.2% Tween-20, pH 7.4).

APPENDIX C

EQUIPMENTS

AKTA FPLC:	GE-Biosciences, SWEDEN
Autoclave:	Hirayama, Hiclave HV-110, JAPAN
	Certoclav, Table Top Autoclave CV-EL-12L, AUSTRIA
Balance:	Sartorius, BP211D, GERMANY
	Sartorius, BP221S, GERMANY
	Sartorius, BP610, GERMANY
	Schimadzu, Libror EB-3200 HU, JAPAN
Centrifuge:	Eppendorf, 5415C, GERMANY
	Eppendorf, 5415D, GERMANY
	Eppendorf, 5415R, GERMANY
	Kendro Lab. Prod., Heraeus Multifuge 3L, GERMANY
	Hitachi, Sorvall RC5C Plus, USA
	Hitachi, Sorvall Discovery 100 SE, USA
Circular Dichroism:	Jasco, J-810, USA
Dynamic Light Scattering:	Malvern, Zetasizer Nano-ZS, UK
Deepfreeze:	-80^{o}C, Kendro Lab. Prod., Heraeus Hfu486, GERMANY
	-20^{o}C, Bosch, TURKEY
Distilled Water:	Millipore, Elix-S, FRANCE
	Millipore, MilliQ Academic, FRANCE

Electrophoresis:	Biogen Inc., USA
	Biorad Inc., USA
Gel Documentation:	UVITEC, UVIdoc Gel Documentation System, UK
	Biorad, UV-Transilluminator 2000, USA
Ice Machine:	Scotsman Inc., AF20, USA
ICP-OES:	Varian, Vista-Pro CCD, AUSTRALIA
Incubator:	Memmert, Modell 300, GERMANY
	Memmert, Modell 600, GERMANY
Laminar Flow:	Kendro Lab. Prod., Heraeus, HeraSafe HS12, GERMANY
Magnetic Stirrer:	VELP Scientifica, ARE Heating Magnetic Stirrer, ITALY
	VELP Scientifica, Microstirrer, ITALY
Microliter Pipette:	Gilson, Pipetman, FRANCE
	Mettler Toledo, Volumate, USA
Microwave Oven:	Bosch, TURKEY
pH meter:	WTW, pH540 GLP MultiCal®, GERMANY
Power Supply:	Biorad, PowerPac 300, USA
	Wealtec, Elite 300, USA
Refrigerator:	+4^{o}C, Bosch, TURKEY
Shaker:	Forma Scientific, Orbital Shaker 4520, USA
	GFL, Shaker 3011, USA
	New Brunswick Sci., Innova™ 4330, USA
Sonicator:	BioBlock Scientific, Vibracell 7504, FRANCE
Spectrophotometer:	Schimadzu, UV-1208, JAPAN
	Schimadzu, UV-3150, JAPAN
	Secoman, Anthelie Advanced, ITALY
	Nanodrop, ND-1000, USA.

Speed Vacuum:	Savant, Speed Vac® Plus Sc100A, USA
	Savant, Refrigerated Vapor Trap RVT 400, USA
Thermocycler:	Eppendorf, Mastercycler Gradient, GERMANY
Vacuum:	Heto, MasterJet Sue 300Q, DENMARK
Water bath:	Huber, Polystat cc1, GERMANY